The role of interneurons in sensory processing in the primary visual cortex

James C. H. Cottam

University College London

Thesis submitted for the degree of

Doctor of Philosophy

2013

Declaration

I, James C. H. Cottam, confirm that the work presented in this thesis is my own. Where information has been derived from other sources, this has been indicated .

Abstract

Cortical networks are comprised of a multitude of cell types. To understand sensory processing, the function and interaction of these cell types must be investigated. Neurons can be separated into two main groups: excitatory pyramidal (Pyr) cells and inhibitory interneurons. Inhibitory interneurons make up 20% of the total cortical neuronal population and they exhibit a striking array of molecular, morphological and electrophysiological characteristics. The most numerous are the parvalbumin-expressing (PV^+) interneurons, accounting for 35-40% of the interneuron population in adult mouse visual cortex. Somatostatin-expressing (SOM^+) neurons are another significant group, comprising 20-25% of the interneuron population. In this thesis I examine the functional role of PV^+ and SOM^+ interneurons in visual processing.

The visual responses of SOM^+ and PV^+ interneurons were measured using 2-photon targeted cell-attached recordings and compared with Pyr cells in the primary visual cortex of anaesthetized mice. These interneuron populations exhibited higher firing rates than Pyr cells in response to oriented gratings, but were less orientation selective, with PV^+ interneurons exhibiting the lowest orientation selectivity. In terms of response latency, PV^+ interneurons were the first to respond to the onset of a visual stimulus, followed by Pyr cells, with SOM^+ interneurons responding last.

Next, SOM^+ interneurons were stimulated optogenetically using channelrhodopsin to measure their effect on Pyr cell and PV^+ interneuron responses to visual stimuli. Activating small numbers of SOM^+ interneurons *in vivo* inhibited stimulus-evoked firing in PV^+ interneurons but not in Pyr cells. Stimulating a large number of SOM^+ interneurons confirmed this differential effect, inhibiting PV^+ interneurons twice as effectively as Pyr cells. Moreover, the remaining responses to oriented gratings in PV^+ cells were more orientation-tuned and time-

modulated. In short, inhibitory SOM^+ cell activity does not summate with PV^+ cell activity, but suppresses it, reconfiguring the inhibitory input to Pyr cells. These results suggest a new role for SOM^+ cells, which are activated more slowly and provide dendritic inhibition to Pyr cells while strongly antagonizing PV^+ cells, thereby shifting inhibitory input to Pyr cells from somatic to dendritic inhibition throughout the course of the network's visual response.

Acknowledgements

I am deeply indebted to Spencer L. Smith for the support he has given me throughout this thesis. He has guided me through this work in all of its aspects and taught me a great amount about experimentation, data interpretation and how science should be done. He managed to do all this while keeping his temper despite my mistakes and making science fun and inspiring. My great thanks also go to Michael Häusser for giving me the opportunity to study in his lab, for creating an exciting environment in which to do science and for keeping this project on the straight and narrow.

Many people in the lab gave particular help at various stages during this project. Thanks to Martha Havenith for lots of visual neuroscience chats, Ben Judkewitz for help with single cell electroporation and Matteo Rizzi for help with 2-photon imaging. Thanks to Ikuko Smith for help designing plasmids, Arifa Naeem for help with genetics and technical assistance and to Christian Wilms for advice on imaging. Thanks also go to Duncan Farquharson and his team of lads in the works department and to Rich Pugh for all his help in the animal house.

This project wouldn't have been nearly as fun without the support and friendship of all the members of the lab, who provided help, both encouragement and discouragement and the occasional beer. Particularly thanks go to the PhD students: Ben Judkewitz, Matteo Rizzi, Kate Powell, Jan Gruendemann, Sara Ho, Sarah Rieubland, Alex Mathy, Gabija Toleikyte, Han Langeslag, Charlotte Arlt, Yuya Kanemoto, Matej Macak and Salpie Nowinski.

Special thanks go to my friends and family who were at times unsure of what I was doing and why I was doing it but supported me anyway, and to Dara for all her support especially during the final stages. Final thanks go to Russell Brand and Matt Morgan, John Oliver and Andy Zaltzman, and Dan Savage for keeping me entertained throughout.

Table of contents

List of figures

1 Introduction

This thesis will examine the responses and functions of specific cell types in visual cortex. Work in recent decades has deepened our understanding of the diversity of cellular and synaptic physiology in cortex (Kawaguchi, 1993; Macdonald and Olsen, 1994; Larkum et al., 1999; Hausser et al., 2000; London et al., 2002; Douglas and Martin, 2004; Markram et al., 2004), but only very recently have we started making significant progress towards understanding the roles of this diversity in cortical function *in vivo* (Liu et al., 2009; Gentet et al., 2010; Ma et al., 2010; Hofer et al., 2011; Ko et al., 2011; Letzkus et al., 2011; Adesnik et al., 2012). In this introduction I will outline the methods for investigating how the computations carried out by the brain can be attributed to components within its microcircuits. I will describe the diversity of cell types involved, discuss which brain regions are the most favourable to study and which techniques are required to unravel the mapping of brain function onto its structure.

1.1 Brain function, microcircuits and cortex

1.1.1 Brain function and how to investigate it

Before selecting an approach for investigating brain function, it is necessary to define what would constitute ultimate success in understanding it. Neuroscientists, being a diverse group including psychologists, physiologists, and cell biologists, differ in what they believe would constitute such a complete understanding. For this thesis, the working definition will be: "Brain function is fully discovered and understood when any behaviour or internal state can be explained by a mathematical model that accounts for cell-type specific neural activity at every point in a defined circuit, and which makes predictions that are supported by experimental manipulations." This means that the behavioural and neuronal coding outcomes of any input stimulus, should be predictable within the bounds of stochastic variability. Neuroscientists have long used two main techniques to study brain function: recording and manipulation of neural activity.

Recording measurements of brain connectivity and activity are made in a range of different areas and contexts to establish how the 'normal' brain reacts to immediate stimuli. Longer term changes can also be studied, such as plasticity of connections that may be associated with memory or adaptations to particular stimulus sets.

Methods for manipulating neural activity can be split into stimulation methods and lesion methods. Stimulation increases the activity of the brain in some way, or adds additional patterns of activity. This goes beyond sensory stimuli and typically consist of direct neuronal stimulation, whether electrical (Penfield, 1937; Meliza and Dan, 2006), chemical (Pettit et al., 1997) or optogenetic (Boyden et al., 2005; Zhang et al., 2007). Lesion methods are the opposite manipulation that reduce neuronal activity, chemically (Naik et al., 1976) and optogenetically (Zhang et al., 2007; Chow et al., 2010). Traditionally structural disruption has been widely used, from where the term lesion derives, which involved the

destruction of part or all of a brain region to examine the deficits produced. Though still useful in some studies, structural lesions have decreased in popularity as they are suitable only for rather coarse investigations, and post lesion plasticity may make the data difficult to interpret. Of all of these methods, optogenetics is the newest and most powerful as it allows the expression of light activated channels/pumps derived from single celled organisms in specific cells or cell classes that can then be controlled remotely with light (Nagel et al., 2003; Boyden et al., 2005). The most widely used are channelrhodopsin (ChR2) and halorhodopsin (NpHR)/archaerhodopsin (Arch). ChR2 and its variants drive spiking in transfected cells in a pattern dictated by the blue light used (Nagel et al., 2003; Boyden et al., 2005). NpHR/Arch can be used to hyperpolarized the neuron or neurons targeted, and shut down spiking (Zhang et al., 2007; Chow et al., 2010). In this study ChR2 has been used both at the single-cell level (Chapter 4) and over wide populations of neurons (Chapter 5) to manipulate the activity of specific cell types.

Having established the ultimate level of understanding that is the goal, and the suite of tools available to get us there, it is also important to select where on the path from sensory input to motor output this study will be set. Many of the tools best suited to analysing the activity in networks require a high level of genetic control of our model organism, making mouse the natural choice. The complexity of the mouse brain means that when attempting to map function onto particular cell types it is prudent to start in a brain region whose responses are understood. In the cortex of mice and other animals, these areas are close to the sensory input or motor output. There is a rich canon of work in primary sensory processing regions of cortex that provides an excellent basis to explore the contribution of different cell types. Knowledge about the receptive fields of principal cells in these regions should allow the different receptive field properties to be characterized and the role in creating each feature to be apportioned amongst the cell types within that cortical region.

1.1.2 The importance of the microcircuit level

The brain is being studied across a huge range of scales. From the level of individual atoms and molecules, making up its membrane channels and other component parts (Doyle et al., 1998), to studying the entire brain at once through a range of large scale imaging (Corbetta and Shulman, 2002), electrophysiological (O'Keefe and Recce, 1993) and MRI techniques (Maess et al., 2001). Our goal is to have a full understanding of the brain as defined earlier. The question then is which level or scale of study is the most rich in this information. It is likely that there is a scale below which the processes operating are not crucially affecting the neuronal information being transferred, for example the stochastic motion of phospholipid molecules in each neuron's lipid bilayer. Likewise there is a scale above which the resolution, to be able to achieve the goal of complete understanding, is lost, such as fMRI imaging of an entire brain area. This is not to say that important information cannot be gleaned from studying either of those scales, rather that to meet our definition of understanding one can be simplified while the other fails to capture lots of the necessary fine-scale detail. To explain this concept a little further, it is true to say at the physical level that no two NMDA receptors are exactly the same, each is in a slightly different configuration from every other in the universe, but this level of distinction is not very important in defining the behaviour of individual neurons or populations of neurons, so NMDA receptors of the same subunit composition are thought of as being the same (Monyer et al., 1992). In the same way, single neurons with the same genetic makeup and inputs can be thought of as operating in a similar way. Ultimately all information about how a biological system works may be very useful. For the sake of targeting our specific goal, a level should be found which treats some lower level processes as a black box, but captures the requisite details for a full understanding.

The appropriate level remains, to some extent, a matter of taste. It predominantly ranges from single dendrite electrophysiology to population imaging of large areas of the network, but crucially at the single-cell level. This range of scales is the realm of the microcircuit and, as recent funding investment confirms

(Markram, 2006; Abbott and Schiermeier, 2013; Alivisatos et al., 2013; Markof, 2013), is an area that is thought likely to produce a lot of the crucial discoveries that will allow the understanding of the brain in a full and practically useful way.

1.1.3 Focus on the cerebral cortex

Now that the scale for the study has been specified as the microcircuit level, which brain region would be optimal for studying the link between different components in the network and the computations they are involved in? As specified earlier it should be somewhere reasonably close to the sensory input or motor output to ensure more chance of linking the neural spiking code to something meaningful in the outside world. In theory then, there are many cortical and subcortical regions of the brain that would fulfill these criteria. There is one practical constraint that limits this choice, which is that, as it will be important to distinguish different cell types within the network in these experiments, it will be necessary to image the cells of the microcircuit *in vivo*. This requires 2-photon microscopy and is restricted to a depth of 400-600 μm below the brain surface (Denk et al., 1990). This practical point essentially limits the brain area choice to either cerebral cortex or cerebellum. Both areas receive sensory information; in cerebral cortex the sensory modalities are separated into different regions while in cerebellum, they often overlap. Individual granule cells can receive inputs from multiple modalities (Snider and Stowell, 1944; Arenz et al., 2009). This varies across the cerebellum but for this thesis the simplicity of a dedicated brain region for a single modality makes cerebral cortex preferable.

Based on those constraints it appears wise to focus on the microcircuits of the cerebral cortex to attempt to establish how the different components of the circuit interact together to achieve computations. The neocortex is a six layered structure that is evolutionarily the most recent addition to the vertebrate brain with its origins in the earliest mammals (Northcutt and Kaas, 1995; Kaas, 2011). The layers contain a range of different cell types that can be separated into two main groups excitatory and inhibitory cells. The excitatory cells appear more

homogenous although they vary in size across neocortical layers while the inhibitory interneurons are highly diverse in morphology, electrophysiology and the genes they express (more detail in section 1.2). Much data on these cell types has already been collected in slice and some *in vivo,* providing useful information to allow grouping of these components so they can be studied separately. The six layer structure and diversity of cell types are grossly similar across all cortical regions, with local variations (Brodmann, 1994). This means that although different parts of the cortex have different functions whether processing different sensory modalities, implementing motor sequences or carrying out higher cognitive processes, a similar network structure is being used. This gives investigators hope that by understanding the primary sensory areas or primary motor areas unifying cortical principles will be discovered that will accelerate the understanding of higher areas with their more abstracted and generalized functions.

1.2 Cell-type diversity in cerebral cortex

As mentioned above there is a diversity of cortical cell types. Excitatory cells make up around 80% of cortical cells while inhibitory interneurons make up the remaining 20% (Markram et al., 2004). Both cell types show some diversity but interneurons are significantly more diverse. This suggests interneurons may have a role in cortex beyond merely preventing the amount of somatic action potentials from exceeding a certain level. Inhibitory interneurons in cerebral cortex exhibit diversity in many characteristics, from their morphology, to the molecules they express, to their excitability (Markram et al., 2004). This diversity arises from their developmental trajectories including their birthplace, route of migration and how they integrate into the circuit (Xu et al., 2004; Yuste, 2005). There are ongoing efforts to organize this diversity and establish to what extent clear grouping can ever be achieved (Ascoli et al., 2008; Battaglia et al., 2013). Ultimately function is the best arbiter of which differences between cells matter (Maccaferri and Lacaille, 2003; Defelipe et al., 2013). In the absence of a functional grouping scheme for interneurons, sensible interneuron groupings based on their characteristics are used to allow progress towards discovering their functional roles in cortex.

1.2.1 The diversity of cortical interneurons

1.2.1.1 Features that vary amongst interneurons

The first and most striking feature of inhibitory interneurons is their range of morphologies (Figure 1.1 A). From the earliest days of cellular neurophysiology the "short axon cells" or interneurons were noted for the differences in arrangement of their axons and dendrites (No, 1938; Fairen, 2007). It has been suggested that the variety of axonal patterns are more informative when discriminating between different inhibitory cell types (McGarry et al., 2010;

Defelipe et al., 2013), because the dendrites are less extensive and less distinctive (Figure 1.1 B).

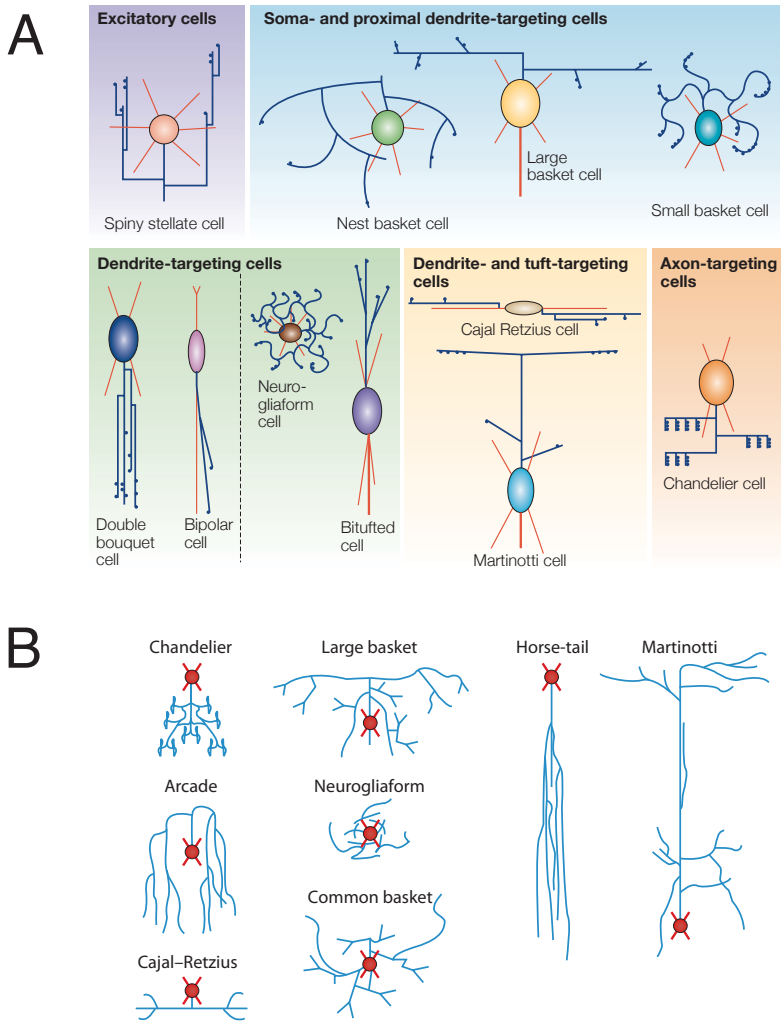

Figure 1.1 Interneuron diversity

A, The range of interneuron, dendritic and axonal morphologies and their Pyr cell target regions (adapted from Markram et al., 2007). **B**, Interneuron diversity focusing on axonal morphology (adapted from DeFelipe at al., 2013).

Chandelier cells are probably the most clearly distinct group of interneurons (Somogyi, 1977). These cells have a complex local cluster of axons that are composed of many shallowly branching axons with short columns of boutons extending from them giving the appearance of a chandelier. The boutons of the

interneurons specifically target the axon initial segment of pyramidal (Pyr) cells and it is this targeting that results in the distinctive morphological features that identify these cells. Basket cells have a thick local mesh of axons like chandelier cells but, in their case, this lacks the bouton columns (Marin-Padilla, 1969). Their name derives from the basket-like appearance that their axons make around Pyr cell somata, which they innervate heavily. This group can be broken down into 3 main subtypes: large basket cells, small basket cells and nest basket cells. Large basket cells have longer ranging axonal projections spreading over large lateral distances (across columns in the case of barrel cortex) and often innervating multiple cortical layers (Cajal, 1909). Small basket cells have more localized axonal projections that are noted for being curvy and highly branching (Kisvarday et al., 1985). Nest basket cells have been compared to bird's nests and share some properties with large and small basket cells (Wang et al., 2002). Within these cell type classes, it may be possible to further classify them into smaller and smaller subgroups. The point at which to stop splitting groups is a subjective decision taken by the experimenter. Another large class of interneuron groups are those that target the dendrites of Pyr cells. These include Martinotti cells which project their axons upwards towards layer 1 (Wang et al., 2004) and also cover long distances laterally and double bouquet cells with columnar axon bundles resembling "horse-tails" (Somogyi and Cowey, 1981; DeFelipe et al., 1990). This is not an exhaustive survey of all possible cell types which have been reviewed in detail (Cajal, 1909; Houser et al., 1984; Jones, 1984; Peters, 1984; White, 1989; Somogyi et al., 1998; McBain and Fisahn, 2001; DeFelipe, 2002; Silberberg et al., 2002; Toledo-Rodriguez et al., 2003; Markram et al., 2004) but gives a flavour of the range of possible morphological variability. Dendrites do also vary between cells such as in the distinctive bitufted dendrites in bipolar cells that contrast with the multipolar dendrites often seen in basket cells (Markram et al., 2004). Although the descriptions given here are qualitative, many studies have quantified a range of different morphological features in order to establish a more objective comparison between cell types (Ascoli et al., 2008). It is also interesting to consider that these cell types vary between layers and to ask the question whether or not this layer variability could be enough to merit novel classification.

The second characteristic that differs greatly across cells is their electrophysiology. There are many different properties that can be measured to compare between cells, one study used 32 separate measures without using every possible metric (Battaglia et al., 2013). These measures extend from subthreshold properties, such as input resistance and resting membrane potential, to spiking metrics, such as steady state firing frequency (for a given level of current injection) and spike adaptation, to measures of the spikes themselves, particularly spike amplitude and spike width. Some of these metrics segregate with previously established morphological cell types. For example, a large proportion of basket cells are fast spiking, meaning that they have short lasting spikes (less than 0.5 ms) while most other interneurons have longer spikes with many being indistinguishable from Pyr cells (McCormick et al., 1985; Connors and Gutnick, 1990; Kawaguchi, 1993; Kawaguchi and Kubota, 1993, 1996; Porter et al., 1998). Many fast spiking basket cells also do not accommodate during a long pulse of current injection meaning that their spikes do not become less frequent during the injection. Other cell types, including many Martinotti cells, do accommodate, decreasing their firing during the long current injection (Kawaguchi, 1993). There is not a perfect match between the morphological and electrophysiological data, cells in a given morphological group can express a range of electrophysiological properties. Likewise cells with particular electrophysiological feature can display a range of morphologies. The examples of electrophysiology/morphology combinations that I have given here have also been ones that segregated together particularly well, when it comes to properties like stuttered firing (firing high frequency spike clusters separated by unpredictable periods of silence (Markram et al., 2004)) a wide range of cells from different morphological groups can express this property.

Cortical interneurons can also be distinguished by the molecules they express. There are some marker molecules that are used particularly frequently, but any molecule expressed by the cell can be used if it is differentially expressed across the inhibitory interneuron population (Nelson et al., 2006). The main markers used are a selection of calcium binding proteins: parvalbumin (PV), calbindin (CB) and calretinin (CR) (Demeulemeester et al., 1989; Rogers and Resibois,

1992; Kawaguchi and Kubota, 1993; Kubota et al., 1994; Cauli et al., 1997; Parra et al., 1998; DeFelipe, 1999; Cauli et al., 2000; Wang et al., 2002; Toledo-Rodriguez et al., 2004; Blatow et al., 2005) and neuropeptides: somatostatin (SOM), vasoactive intestinal peptide (VIP), cholecystokinin (CCK) and neuropeptide Y (NPY) (Hendry et al., 1984b; Hendry et al., 1984a; Morrison et al., 1984; Somogyi and Cowey, 1984; Meinecke and Peters, 1986; Demeulemeester et al., 1989; Rogers and Resibois, 1992; Wahle, 1993; Kawaguchi and Kubota, 1998). These markers are very useful as they can be identified readily using immunohistochemistry and so can be used to assign a cell to a small number of categories. A single cell may express many of these markers but there is some structure to the expression. PV, SOM, and VIP are expressed in a mutually exclusive pattern that immediately splits inhibitory cells into three groups, plus the small proportion that express none of these (Kawaguchi and Kubota, 1997). A similar, more recent, classification has split nearly 100% of interneurons into three groups, using ionotropic serotonin receptor 5HT3a as a label rather than VIP (Rudy et al., 2011). When compared with other interneuron classifiers such as morphology and electrophysiology the same problem occurs with cells expressing a particular marker often having a range of morphologies and electrophysiologies. Other proteins expressed by a cell can be taken into account such as ion channels or membrane proteins (Llinas, 1988; Martina et al., 1998; Erisir et al., 1999; Rudy and McBain, 2001; Toledo-Rodriguez et al., 2004). Large scale gene expression screens have attempted to identify other markers that may cosegregate more clearly with the other characteristics of the cell and to test if looking over the expression of many genes a higher order pattern will emerge. So far this has not clarified the situation (Monyer and Markram, 2004; Nelson et al., 2006). Ultimately, the expression of all proteins are controlled by the interaction of a cell specific sets of transcription factors with the genetic code (and some mechanisms of transcriptional and post-transcriptional modulation), so it may be possible, in future, to obtain a full genetic signature for each cell type and then see if they group neatly into categories or not.

Another characteristic of cortical neurons is the position of their soma, with respect to cortical layer. Many of the main cell types, such as basket cells, appear

across layers 2-6 (Marin-Padilla, 1969; Kisvarday et al., 1985; Wang et al., 2002), while some cell types are limited to a single layer such as cell types in layer 1 like Cajal-Retzius cells (Anderson et al., 1992; Hestrin and Armstrong, 1996; Zhou and Hablitz, 1996).

Connectivity was already mentioned in the morphology section but it is important to know which cells are innervated by which interneuron groups and where on those cells the inhibition is delivered. Basket cells tend to innervate the soma and proximal dendrites of Pyr cells while other cell types such as Martinotti cells and double bouquet cells focus their inhibition onto the dendrites, and in the case of Martinotti cells also the apical tuft. The nature of connections can vary as well as the target. This is most obvious for some types of interneurons in terms of the short term plasticity of the excitatory inputs they receive, with some cell types receiving highly depressing excitatory inputs while others receive facilitating inputs (Thomson et al., 1993; Thomson, 1997; Thomson and Deuchars, 1997; Markram et al., 1998; Reyes et al., 1998; Wang et al., 1999; Silberberg, 2008).

Finally interneuron cell types can be distinguished by their activity patterns *in vivo* in response to different brain states, sensory stimuli or motor activity. This is a product of many of the other properties discussed above but it is hard to predict from morphology, slice electrophysiology and connectivity how a cell will respond in vivo. These responses may more closely reflect the function of an interneuron in the network and so may be a better guide to grouping cells. An interesting study of temporal patterns of activity in the hippocampus was one of the inspirations for this thesis and shows that interneurons respond very differently to each other in a range of brain states, allowing them to be separated (Klausberger et al., 2003).

All of this diversity in inhibitory interneurons is thought to arise from their developmental history, with their birthplace and genetics having a large role to play alongside some probable influences from activity within the circuit that they arrive in. The overwhelming factor appears to be genetics, however, and once the cell type is defined, which occurs early in development, transplanting it into a different environment does not change its assigned fate (Xu et al., 2004). Mapping

the fates of cells from different embryonic locations consistently produce particular cell types (Butt et al., 2005).

1.2.1.2 Organising interneuron diversity

Organising the overlapping diversity along multiple axes is not trivial (Figure 1.2) (Somogyi et al., 1998; Markram et al., 2004; Monyer and Markram, 2004; Blatow et al., 2005; Foldy et al., 2005; Nelson et al., 2006; Bota and Swanson, 2007; Ascoli et al., 2008).

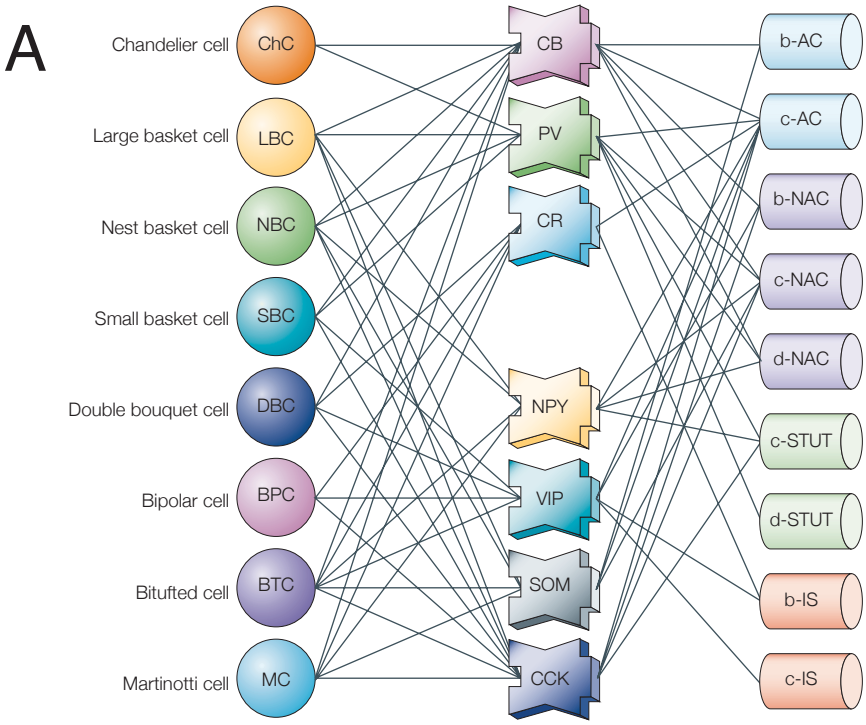

Figure 1.2 The overlap between interneuron properties

A, A chart showing the range of possible sets of interneuron properties, morphologies (left), molecules they express (centre) and spiking patterns they show (right). AC, accommodating; b, burst subtype; c, classic subtype; d, delay subtype; IS, irregular spiking; NAC, non-accommodating; STUT, stuttering (adapted from Markram et al., 2004).

A range of supervised and non-supervised clustering approaches have been used which guarantee the division of groups into subgroups (Guerra et al., 2011). The possible number of combinations of all of the electrophysiologies, morphologies

and molecular profiles is very large. Is there structure to this diversity or are there an equal number of cells of all types producing, effectively, a continuum? Some have argued for continua as the organizing principal of interneuron diversity but often only having taken into account a small proportion of the possible characteristics listed above; two characteristics in the examples I reference here (Parra et al., 1998; Battaglia et al., 2013). In Battaglia et al. 2013 there does appear to be a lot of clustering within the continua, with cells clustering towards being purely of one class or another rather than equally filling the whole fuzzy parameter space. In a simpler way we see the exclusive expression of some markers such as PV, SOM and VIP/serotonin and the broad matching of PV with basket cell or chandelier morphology and often with fast spiking properties too (Kawaguchi and Kubota, 1997; Markram et al., 2004; Rudy et al., 2011). It seems there is structure but the level of clarity of grouping varies across the population. When selecting groups to compare in an experiment aiming to test for different functional diversity it is important to select groups carefully. Selecting those that are the most different and the most tightly grouped in terms of their intragroup identity should be the best strategy for detecting clear distinctions in function.

Ultimately we are interested in how interneurons contribute to how the brain works, so function should be the primary arbiter of cell-type. Quoting Albert Einstein via Maccaferri et al. (Maccaferri and Lacaille, 2003) “make everything as simple as possible but not any simpler”. In this way we should group interneurons according to the aspects of their diversity that affect the type of function they carry out and ignore those aspects that don’t. It also should be borne in mind that a degree of diversity amongst interneurons might be an important part of the way they function in the network (Battaglia et al., 2013). It may be incorrect to presume that as soon as we find the organizing principle all the interneuron diversity will resolve itself, and neat highly separate groups will fall out. In reality it could be that single functions do not map simply onto single cells. Each cell may be involved in a range of overlapping functions, therefore they may also share many of the properties we currently measure. The optimum solution for inhibition in cortex may not be to have multiple exact copies of a few archetypal cell types but an integrated circuit of inhibition that arises through the interaction

of components. Changes in some components could be compensated by changes in others, broadening the array of cell-type characters away from the 'pure form' Platonic cell types (Battaglia et al., 2013).

For the sake of practicality and progress the current solution is to take two or more sensibly distinct interneuron cell types and compare them in terms of a particular function, or test the outcome of perturbing one or more of them on different cells within the network. As the mapping between function and diversity is explored further we will be able to evaluate how well diversity of function maps onto diversity of interneuron properties. This initial work should also allow us to gain a better understanding of what we mean by interneuron function and the distribution of function across the cortical network. This in turn will aid us with the original question of how function relates to interneuron diversity.

In this study various GFP and Cre lines are used. These transgenic mouse lines group cells by their expression of various genes. As these lines become increasingly widely used in the community and referred to as relating to different cell types it is worth bearing in mind the cell-type marker mismatches detailed above. Any one marker of cell type is currently insufficient to fully delineate a functional interneuron type.

1.2.2 SOM$^+$ and PV$^+$ interneurons

For this study, we focused on two interneuron cell types that are highly distinct in their properties, and account for a large portion of the cortical interneuron population: PV$^+$ interneurons and SOM$^+$ interneurons, which represent 35-40% and 20-25% respectively of the total interneuron population (Gonchar et al., 2007).

They differ on every dimension discussed above: morphology, molecular diversity, and electrophysiologically. Morphologically, PV$^+$ cells include the different types of basket cell which, although they differ in size, primarily target the somata of Pyr cells (Kawaguchi, 1993; Chow et al., 1999; Toledo-Rodriguez

et al., 2004). PV^+ interneurons also include chandelier cells which have a unique morphology and target the axon initial segment but these cells are relatively rare in the population (DeFelipe et al., 1989; DeFelipe, 1999). SOM^+ cells predominantly target the dendrites of Pyr cells, although in higher cortical layers (layer 2/3) the vertical dimension is more compact so the separation of targeting to different Pyr regions is less distinct. A large proportion of SOM^+ cells are Martinotti cells which have a distinct vertically directed axonal projection, targeting upper layer 2 and layer 1, and have some extensive lateral branching (Wang et al., 2004).

In terms of the molecules they express, various studies have found the expression of SOM and PV to be mutually exclusive. These molecular markers, discussed previously in more detail, are the main molecules chosen, when making the comparison between these two cell types, and are definitive, though there are undoubtedly others such as different receptors and ion channels (Kawaguchi and Kubota, 1997; Markram et al., 2004; Rudy et al., 2011).

Electrophysiologically, again, these two cell types are strikingly different. The resting membrane potential of SOM^+ cells is significantly depolarized in comparison with PV^+ cells which led to their original classification as low threshold cells. PV^+ cells have the lowest input resistance of any interneuron group, notably lower than SOM^+ cells, which is linked to their ability to respond only within a small time window around a given input (Kawaguchi and Kubota, 1993). SOM^+ cells might also be expected to respond quickly due to being near spike threshold but they receive facilitating excitatory inputs that have a low initial EPSP amplitude and so often require multiple inputs over time to reach action potential threshold (Reyes et al., 1998; Kapfer et al., 2007; Silberberg, 2008). PV^+ cells in contrast receive depressing excitatory inputs with a large initial EPSP amplitude and so are likely to respond quickly to the start of a train of stimuli but then reduce their responsiveness over time (Reyes et al., 1998). In terms of inhibitory output both cells provide inhibition onto Pyr cells that depressed by around 50% during a 40 Hz stimulus train and less during lower frequencies (Beierlein et al., 2003; Fanselow et al., 2008), although these studies

disagree somewhat as to the SOM^+ cell output onto Pyr cells, with one saying it is less consistently depressing (Beierlein et al., 2003). Both cell types make promiscuous connections with the surrounding Pyr cells that tail off with distance (Fino and Yuste, 2011; Packer and Yuste, 2011) and both cell types also connect to each other, although less data has been collected for this connection (Gibson et al., 1999). Both cell types appear throughout all layers except layer 1.

The diversity within these groups has already been described with PV^+ neurons comprising a range of different basket cells and chandelier cells. SOM^+ cells are diverse as well; despite the dominance of Martinotti cells, new transgenic lines have revealed morphological and electrophysiological variants in layer 4 and 5 (Ma et al., 2006). A clustering study has also split the SOM^+ cells within layer 2/3 into 3 separate groups, although there are some questions over whether the young age of the animals used in this study means that some of the interneurons had not achieved their final mature state (McGarry et al., 2010).

1.2.3 Are excitatory cells in cortex also diverse?

Excitatory cells are often considered to be a uniform group contrasting with the exuberant diversity of inhibitory interneurons. However it has long been known that there are different types of excitatory cells and knowledge of these distinctions has become more sophisticated and nuanced over time. To start with, as you scan down through the cortical layers, it is clear that there are size differences between Pyr cells. Those with cell bodies in layer 5 have dendrites spanning almost the entire vertical depth of the cortex, while those in layer 2/3 are much smaller, with less extreme separation between apical dendrites and soma. In addition there are excitatory cells that are stellate rather than pyramidal which reside in layer 4, the target for the majority of the thalamic input.

Amongst Pyr cells there appears to be a high degree of uniformity but over the last few decades and particularly within the last 5 to 10 years a surprising amount of previously hidden diversity has been unearthed (Molnar and Cheung, 2006;

Krook-Magnuson et al., 2011). This diversity is primarily in the non-random connectivity of subnetworks of Pyr cells but also includes some morphological variability, and is underlain by genetic and molecular variability.

Pyr cells that resemble each other in a given layer may project to very different cortical and/or subcortical locations. Layer 5 Pyr cells are known to fall into at least three classes as they can project to the striatum, the tectum and other cortical areas (Jones, 1984). In a similar way, layer 6 Pyr cells also vary in their targets with some projecting to their primary relay nuclei and others projecting to higher order thalamic nuclei and primary relay nuclei (Bourassa et al., 1995; Zhang and Deschenes, 1998). As well as their projection identities, these Pyr cells also have specific intracortical connectivity patterns. Pyr cells that project to the same distant locus may preferentially connect to each other (such as layer 5 corticostriatal projecting cells (Brown and Hestrin, 2009)), or preferentially target a different layer 5 subnetwork as corticocortical projecting cells do onto corticotectal cells (Brown and Hestrin, 2009). These subnetworks of Pyr cells in layer 5 are also specifically connected to subnetworks that have been shown to exist in layer 2/3 (Yoshimura and Callaway, 2005; Kampa et al., 2006; Morishima and Kawaguchi, 2006; Otsuka and Kawaguchi, 2008; Anderson et al., 2010; Sato and Svoboda, 2010; Morishima et al., 2011; Otsuka and Kawaguchi, 2011). This complex wiring of layers 2/3 and 5 give rise to a complexity of cell types identified by their position in different subcircuits. These different groups may qualify as different cell types as they are likely to have different functional roles even though they may look very similar on the surface. The structured connectivity from layer 2/3 onto layer 5 shows that Pyr cells differ in the inputs they receive as well as where they project and how they connect to each other within a cortical layer. This reflects a finding in the hippocampus showing that excitatory cells within the same region can be separated on the basis of the inputs they receive (Beed et al., 2010).

As well as a range of Pyr cell groups based on connectivity there are morphological differences between Pyr cells in cortex. Admittedly these morphological variants are much more similar to each other than the inhibitory

cells are but the differences are real and likely to be of functional significance. The most famous of these is the difference between type 1 and type 2 layer 5 Pyr cells. Type 1 cells have thick dendrites that are highly branched and extend into layer one with an apical tuft that branches there. Type 2 cells have thinner dendrites and an apical dendrite that rarely extends as far as layer 2 and does not possess an apical tuft (Molnar and Cheung, 2006; Le Be et al., 2007). Not only do these layer 5 cells differ in their morphology but also in their long range projections (type 1 – spinal cord, superior colliculus, pons, striatum; type 2 – contralateral cortex, striatum), their electrophysiology (type 1 – bursting, type 2 – non-bursting) and the molecules they express (type 1 – OTX-1, N200, SMI-32, Ctip2; type 2 – calretinin, lmo4) (Molnar and Cheung, 2006; Le Be et al., 2007; Krook-Magnuson et al., 2011). This clear separation of the two Pyr cell types over a large range of cellular properties is very likely to meet the strictest criteria for dividing them into different cell types. The similarities in the basic Pyr cell morphology and electrophysiology have obscured differences likely to be crucial for their separate roles in cortical processing.

It is interesting to consider the mechanisms that drive this diversity which is no doubt set up early in development and has a strong genetic component. Recent developmental discoveries found that clonally related sister cells in cortex are more likely to synapse with each other than with non-sister cells (Yu et al., 2009). More recently this preferential connectivity has been shown to have important functional correlates as the sister cells are also more likely to share similar stimulus response properties than cells that are less closely related (Li et al., 2012; Ohtsuki et al., 2012).

1.3 Dendritic inhibition

In this thesis SOM^+ dendritic targeting interneurons will be manipulated, therefore it is important to review what is known about the special properties of dendritic inhibition. One of the main reasons for requiring an independent group of interneurons to target the dendrites is that Pyr cells have excitable dendrites that are able to produce their own *N*-methyl-D-aspartate (NMDA) and calcium (Ca^{2+}) dependent spiking activity when stimulated sufficiently or in the correct pattern.

1.3.1 Excitable dendrites

It has been shown in visual cortex that regenerative $Ca2^+$ spikes can be produced in Pyr cell dendrites visual cortex when sodium (Na^+) conductances were blocked (Hirsch et al., 1995). These Ca^{2+} transients have been identified *in vivo* and i*n vitro* using electrophysiological and imaging methods (Helmchen et al., 1999; Svoboda et al., 1999; Larkum and Zhu, 2002; Kitamura et al., 2008; Murayama et al., 2009; Chen et al., 2011; Rochefort et al., 2011; Varga et al., 2011). There is a spatially restricted low threshold zone at the base of the dendritic tuft, that is responsible for these regenerative Ca^{2+} spikes produced by the opening of voltage gated calcium channels (Larkum and Zhu, 2002). Later, it was shown that input into the finer more distal dendrites within the tuft itself could lead to NMDA spikes that, if sufficient, could trigger spiking in the Ca^{2+} spike activation zone at the base of the tuft (Larkum et al., 2009). Ca^{2+} spikes produced in the tuft can interact with backpropagating action potentials from the soma to switch the Pyr cell firing into a burst firing mode (Larkum et al., 1999). This functions to change spike output but is also likely to have a role in promoting Ca^{2+} dependent plasticity (Cavazzini et al., 2005).

The input arriving at the Pyr cell tuft in layer 1 comes predominantly not from the local cortical circuit but from feedback projections from higher cortical areas and other brain regions (Rockland and Pandya, 1979; Coogan and Burkhalter, 1990;

Felleman and Van Essen, 1991; Cauller et al., 1998; Shipp, 2007). This arrangement of projections with 90% coming from outside the local area was described by David Hubel as the "crowning mystery" of cortex (Hubel, 1982). This suggests that the tuft may be a functionally separated region of the pyramidal cell, receiving different inputs and able to spike independently of the somatic compartment (Petreanu et al., 2009). A recent study showed that these feedback projections are likely to be crucial for associative learning in auditory cortex (Letzkus et al., 2011). The projections via layer 1 inhibit layer 2/3 interneurons in this case allowing more pyramidal cell spiking (Letzkus et al., 2011; Jiang et al., 2013).

It is important to note that dendritic excitability can be affected by anaesthesia (Potez and Larkum, 2008) suggesting that ideally, in future, awake experiments will be carried out. Almost all anaesthetics also interfere with inhibitory signaling giving a second reason that the awake preparation may be needed to confirm findings from intact anaesthetized animals (Franks and Lieb, 1994).

1.3.2 Dendritic inhibition regulates excitability in different ways

Around the same time that dendritic Ca^{2+} excitability began to be studied intensively with new imaging methods it was demonstrated that inhibition was able to curtail and eliminate Ca^{2+} spikes (Kim et al., 1995). Two main circuits responsible for dendritic inhibition have been identified. The first relies on SOM^{+} Martinotti cells which have cell bodies that reside in the same layer as the Pyr cells and project axons upwards into higher layers where they form inhibitory synapses onto Pyr cells (Figure 1.3 A, B) (Kapfer et al., 2007; Silberberg and Markram, 2007; Murayama et al., 2009). These interneurons inhibit the dendrites via fast and short acting $GABA_A$ receptors and are able to greatly reduce the Ca^{2+} excitability of the apical dendrites in the awake animal that are produced by sensory stimulation (Murayama et al., 2009). The second inhibitory circuit acts via neugliaform cells in layer 1 (Figure 1.3 A, B) (Olah et al., 2007; Palmer et al., 2012a; Palmer et al., 2012b; Jiang et al., 2013). When these neurogliaform

interneurons are activated they inhibit distal pyramidal dendrites predominantly via slower, longer lasting $GABA_B$ receptors (Perez-Garci et al., 2006; Olah et al., 2007; Palmer et al., 2012b). It has been shown that the neurogliaform cells can be activated by callosal excitatory axons projecting from the opposite hemisphere, suggesting this circuit may have a role in longer time-scale coordination between the sensory cortices on different sides of the brain (Palmer et al., 2012b).

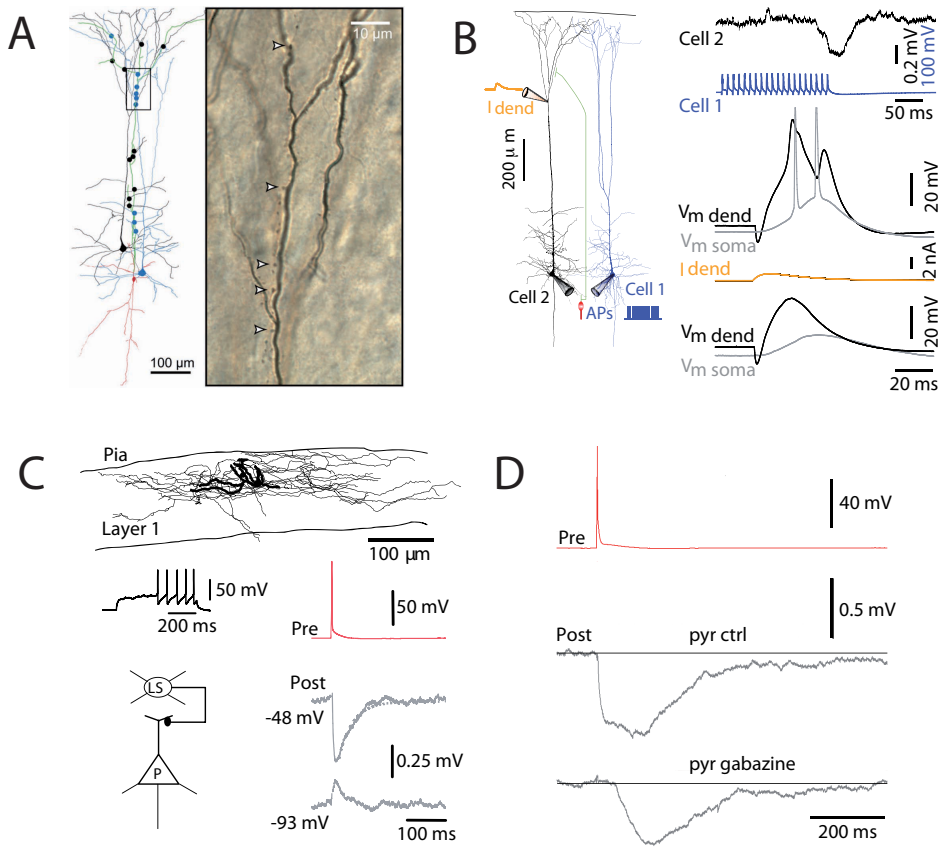

Figure 1.3 Two circuits for dendritic inhibition

A, A reconstruction of putative Martinotti cell connections onto Pyr cell dendrites (adapted from (Silberberg and Markram, 2007)). **B**, Disynaptic Martinotti cell inhibition of Pyr cells measured intracellularly (adapted from (Murayama et al., 2009)). **C**, Layer 1 neurogliaform cells target inhibition to Pyr cell apical dendrites (adapted from (Chu et al., 2003)). **D**, Neurogliaform cells deliver their inhibition predominantly via $GABA_B$ receptors (adapted from (Olah et al., 2007)).

1.3.3 Modelling dendritic inhibition

The excitatory to inhibitory ratio of synapses on the dendrites of hippocampal cells was found to be 4:1 (Liu, 2004). This ratio was found locally throughout the tree and a simple Poisson model suggests that is highly unlikely to occur by random recruitment of excitatory and inhibitory synapses. What is more, perturbations that changed the level of one of the synaptic types were balanced by a change in the number of the other type to maintain the 4:1 ratio (Liu, 2004). Despite making up only 20% of the dendritic synapses inhibitory synapses are able to closely regulate dendritic excitation. Different models have been devised to explain the effectiveness of inhibition in regulating dendritic excitation and what the optimal spatial arrangement is between excitatory and inhibitory synapses to ensure the highest suppression of excitation. Classically, on-path inhibition, in which the inhibitory synapses lies on the dendrite between the soma and the excitatory synapse, was thought to be the most effective (Koch et al., 1983; Hao et al., 2009). Hao et al. published a study recently summarizing inhibitory/excitatory interactions as an arithmetic sum including a shunting term. However they tended not to push their inhibitory synapses very far out into the dendrites and their rule broke down when their inhibitory and excitatory inputs were located together on the same branch. Since then Gidon et al. have published a study that disagrees with the classical view. They take what they describe as a more "dendrocentric" approach and solve Rall's cable equations for their measure of shunt, called shunt level, throughout the dendrites (Gidon and Segev, 2012). They find distal off-path inhibition to be stronger than on-path inhibition and show that this distal shunt can spread over large distances ~100 μm. Due to this strength and spread of shunting, as few as 15 inhibitory synapses can regulate the excitability of the whole dendritic tree. This may help explain why there are so many fewer inhibitory synapses in the dendrites than excitatory synapses. This distal off-path effect relies on increasing input resistance as you move further down the dendrite away from the soma. Arguing against this trend is the fact that some cells have been shown to have lower specific membrane resistivity in the more distal dendrites that would decrease input resistance (Magee, 1998; Stuart and Spruston, 1998; Ledergerber and Larkum, 2010). The Gidon et al. model

counters this by showing that due to tapering of the dendrites reducing dendritic diameter, and the powerful sealed end effect, input resistance still increases more distally rather than decreasing. It is important to note that in all of the studies discussed here passive models were used. These models are of great use as they can be solved analytically and capture many of the properties of the dendrites, however ultimately experimental confirmation is needed. This could come in the form of uncaging GABA (although a method not as developed as glutamate uncaging (Wang and Augustine, 1995; Kanemoto et al., 2011)) at different synapses during synaptic excitatory stimulation, to confirm the spatial predictions that have been made.

1.3.4 Comparison between dendritic and somatic inhibition

Somatic and dendritic inhibition differ in terms of the spatial location of their inhibitory synapses on Pyr cells and the type of input they regulate, whether feedforward or feedback. In addition some studies have attempted to separate somatic and dendritic inhibition by the way in which they affect the Pyr cell's input/output function. A study in the electric brown ghost knife fish found that dendritic versus somatic inhibition had differential effects on spiking output. Dendritic inhibition caused divisive inhibition of cell output while somatic inhibition caused a subtractive change (Mehaffey et al., 2005). The differences between the two types of inhibition were stark but have not been so easy to separate in visual cortex (Lee et al., 2012; Wilson et al., 2012). This may be because the visual cortex experiments activate the dendritic and somatic targeting interneurons directly rather than using focal application of muscimol as was used in the fish study. It could also be due to the idiosyncratic morphology of the fish Pyr cell that provides a very clear separation between dendrites and soma and has multiple long extending dendrites oriented in the same direction (Mehaffey et al., 2005).

The fast acting somatic inhibition located close to the spike initiation zone has long been thought to be linked to close control of spike timing both in normal and

pathological states (Freund and Katona, 2007; Trevelyan, 2009; Menendez de la Prida and Trevelyan, 2011). In contrast the slower onset of dendritic inhibition, requiring multiple spikes to bring Martinotti cells to threshold (Kapfer et al., 2007; Silberberg and Markram, 2007), is thought to be less involved with regulating exact timing of spikes and more with controlling sensitivity and dynamic range (Kapfer et al., 2007; Murayama et al., 2009) of Pyr cells and synchronizing cells over longer timescales (Berger et al., 2010). However some suggestions for the involvement of dendritic inhibition in a timing role have been made when considering the control of theta oscillations in the hippocampus (Tamas et al., 2003; Klausberger, 2009).

It is important to highlight that much of the work on the separation between dendritic and somatic inhibition in cortex has been carried out on layer 5 Pyr cells. These cells span almost the entire vertical distance of the cortex and therefore have the largest separation between apical tuft and soma in cortex. Although it is known that layer 2/3 Pyr cells do express Ca^{2+} based excitability in their dendrites (Hirsch et al., 1995; Svoboda et al., 1999) their vertical axis is much compacted compared to layer 5 Pyr cells. This means that it is not currently clear to what extent the separation of roles between somatic and dendritic inhibition also applies in layer 2/3 Pyr cells.

1.4 Visual Cortex

The mammalian visual cortex is one of the most studied regions of the brain (Chalupa and Werner, 2004; Chalupa and Williams, 2008). This section highlights the features of visual cortex that made it the brain region of choice in which to study interneuron function. Important properties of the receptive field of visual cortical neurons are reviewed, and subsequently, progress in understanding the responses and effects of inhibitory interneurons in visual cortex is summarized.

The fact that it is a heavily studied area is one of its great strengths. To understand the function of a particular cell type in visual cortex you must first have a good idea of what the area does and the details of how this is achieved. The extensive body of work carried out in cats and monkeys is an excellent foundation on which to build, and it is fortunate that many of the basic principles discovered in those organisms also apply to other mammals. Mice are one such group, and have the benefit of the genetic tools and transgenic lines that have been developed since their genome was sequenced, that allow access to a range of cell types (Waterston et al., 2002; Luo et al., 2008). A further practical point is that the position of cortex above the subcortical regions makes studying it easier. Its superficial location also access to cells in layer 2/3 with 2-photon imaging. This allows *in vivo* visualization of cells and identification of cell types with fluorescent labels (Oliva et al., 2000; Meyer et al., 2002; Luo et al., 2008). Since the few years before the start of this project, mouse visual cortex has hugely expanded as an area of research (Hubener, 2003).

1.4.1 Receptive field responses

Visual cortex is an excellent brain region in which to investigate cell type function. It has tuned responses to a large range of stimuli with many dimensions (Bair, 2005). This range of tuning properties, with cells that have narrow selectivities that vary across the population, is important, as it allow cell types to

be compared in a large parameter space, to look for differences in response. It also means that when manipulating the activity of particular cell types there are many dimensions of readout from Pyr cells that can be measured, to look for changes.

Our knowledge of receptive field responses in visual cortex began in earnest with a set of seminal discoveries made by Hubel and Wiesel (Hubel and Wiesel, 1959, 1962). These showed that neurons respond preferentially to particular orientations of black or white bars, the direction these bars are moving in, and their size (Figure 1.4).

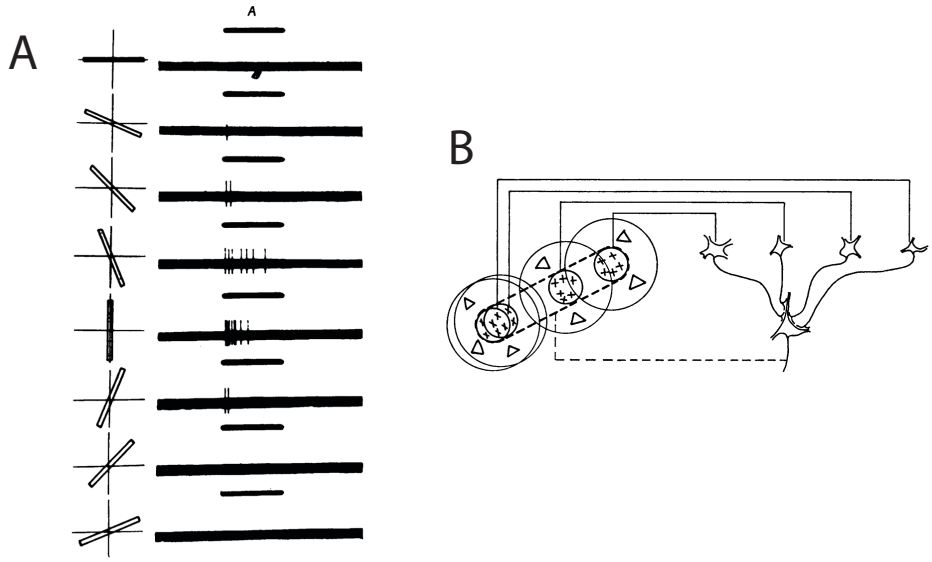

Figure 1.4 Orientation selectivity

A, An orientation selective cell that fires (right) for selective orientations of a bar of light (left) (adapted from Hubel and Wiesel, 1959). **B**, A hypothesis for the formation of an orientation selective simple cell, multiple circular on/off receptive fields arranged geometrically feedforward onto a simple cell (adapted from Hubel and Wiesel, 1962).

The prediction of single cell responses has been improved with the demonstration that Pyr cells can be well fit by Gaussian curves (Campbell et al., 1968; Carandini and Ferster, 2000). From the mean spiking responses at each orientation, and the fit, a large number of different parameters can be extracted. The simplest metric is the mean firing rate in response to visual stimuli. Following that, peak firing rate

which is the highest firing rate across all orientations of visual stimuli. Using the Gaussian fit, the size of the tuned component and the untuned component can be calculated. The tuned component is the peak to trough amplitude of the Gaussian, while the untuned component is the amplitude from the baseline to the trough of the Gaussian. The fit can then be used to calculate metrics of orientation selectivity, preferred orientation, direction selectivity and tuning width. Different cell types may differ from each other in any one or a combination of these metrics. Likewise manipulating a cell type will produce an unknown effect but it can be precisely quantified using this highly parameterised visual response space.

These discoveries were mainly made in cats, the traditional model for visual neuroscience. Receptive fields in mouse visual cortex do differ in some ways from the previous work carried out mainly in cats and monkeys (Hubener, 2003). Fortunately these changes are mainly quantitative rather than qualitative in character (Drager, 1975; Mangini and Pearlman, 1980; Metin et al., 1988). Mice have much larger receptive fields than the cat or monkeys. Comparing receptive fields from the central, non-foveal, visual field, cats have receptive fields of around 1 degree of visual space (monkeys even smaller) whereas mouse receptive fields are around 14 degrees in size (Hubel and Wiesel, 1974a; Wilson and Sherman, 1976; Metin et al., 1988). The second main difference is that mice, being a prey species, have sideways facing eyes rather than the forward facing eyes of cats and monkeys. This means they have a reduced degree of binocularity compared to previously studied species, although around a third of mouse visual cortex does receive visual input from both eyes (Drager, 1978; Gordon and Stryker, 1996). A final difference is at the population organisation level. Cats and monkeys have the orientation tuning properties of their cells separated on a large scale into tuning columns around pinwheel centres. This means as you move over the cortex there are graded changes in orientation tuning across the cell population, with occasional singularities as you cross a pinwheel centre (Hubel and Wiesel, 1974b; Blasdel and Salama, 1986). In the mouse visual cortex the orientation preference organization is less structured and can better be described as being “salt and pepper” (Ohki et al., 2005). This difference may affect the expected outcome of changing the activities of interneurons in the population as

in cats and monkeys they are generally well orientation tuned, while in mice they are not.

Significant work has also been carried out studying how these receptive fields are produced. The original hypothesis from Hubel and Wiesel shows a hierarchical organization of receptive fields to produce orientation tuning (Figure 1.4 B) (Hubel and Wiesel, 1962; Alonso and Martinez, 1998). This hypothesis is still important today with many groups advocating it as the most important component of orientation tuning (Priebe and Ferster, 2008, 2012). As well as the hierarchical organization of Pyr cells the cortical circuit also contains inhibitory interneurons. Their role is yet to be fully understood but a range of recording and manipulation studies have been performed in an attempt answer this fill this gap.

1.4.2 Inhibition data from visual cortex

The difference between glutamatergic excitatory neurons and GABAergic inhibitory interneurons was established a number of decades ago (Dreifuss et al., 1969). In the past it was difficult to study these cell types separately as interneurons are relatively rare and can be hard to distinguish (although see (Swadlow, 1988)). Often access to information on inhibition in the cortex was gained either through intracellular recordings, or pharmacological manipulations that interfered with inhibition, alongside models which aimed to summarise the findings and test them for accuracy of fit.

As described above there are many different interneuron types in cortex, so it has been the aim for a long time to bring the role of these cells which are activated by visual stimulation into the models of visual cortical function. It was understood that interneuron activity had to have a role in cortex, but it was not known where this role might be, and how large an influence it would play in any given computational function. One of the main potential roles for inhibition that created a large amount of controversy in the literature was to what extent cortical inhibition was involved in the emergence of orientation tuning in the cortex from the non-orientation tuned lateral geniculate nucleus inputs. An early provocative

study was carried out using bicuculline to manipulate the level of inhibition in the cortex (Sillito, 1975). Bicuculline is a competitive antagonist of $GABA_A$ receptors and when applied iontophoretically greatly reduces the amount of $GABA_A$ driven inhibition in the circuit. This study showed that alongside an increase in firing rate orientation tuning became broader. This prompted the suggestion that inhibition was necessary to reign in and sharpen the relatively non-specific excitation. A few years later a similar study, also using bicuculline, confirmed this result although did not see quite as large an effect (Tsumoto et al., 1979). This tempered the conclusion slightly, suggesting that while inhibition played an important role in producing orientation tuning it was not the sole element. Much later a different pharmacological approach was taken (Nelson et al., 1994). The aim was to block $GABA_A$ receptor mediated inhibition but this time intracellularly in a single cell rather than across the whole network. Picrotoxin or DIDS (4,4' diisothiocyanatostilbene-2,2'-disulfonic acid) were used alongside a caesium based internal solution to measure excitatory inputs to Pyr cells. It was found that excitatory inputs to all of the cells tested remained orientation tuned, arguing against the previous findings that GABAergic input is necessary for tuning. Both of these pharmacological methods have since been questioned. Bicuculline applied on a large scale may have such a major effect on the network that it brings into question the validity of the results. At the same time bicuculline is known to not be as specific as originally thought: it is now known to block Ca^{2+}-activated K^+ (SK) channels that cause non-specific excitation (Khawaled et al., 1999). Both of these factors have led the bicuculline results to be questioned. Likewise the specificity of DIDS has been called into question, although its ability to reveal some excitatory tuning while likely blocking a large amount of inhibition makes it the more convincing tool.

Running simultaneously to the pharmacological studies were a large number of recording studies some of which were focused specifically on how orientation tuning arose in a single cortical cell. These experiments relied on intracellular recordings measuring the subthreshold activity in an attempt to explain the spiking patterns of various phenomena particularly orientation tuning. Initially experiments were carried out using sharp electrodes which make it impossible to

distinguish between inhibition and excitation with any level of certainty, and therefore make it hard to conclude what inhibition is doing (Ferster, 1988). Later, the use of whole cell patch clamp recordings allowed for better separation between excitation and inhibition, showing that shunting is an important part of the inhibitory activity in Pyr cells (Borg-Graham et al., 1998), something which had previously been thought not to be the case (Douglas et al., 1988). The potential roles of this shunting inhibition were then compared to see whether it could be used to influence orientation tuning (Anderson et al., 2000a). The original feedforward model devised by Hubel and Wiesel suggested that orientation tuning arose from the biased selection of on- and off-centered thalamic afferents meaning that the input into a given cells would be larger for visual inputs at certain orientations rather than others. Studies had shown that a cell's orientation tuning in terms of spike output was matched by it's broader subthreshold tuning (Priebe and Ferster, 2008) so the question became: could some transform of the subthreshold input explain the tuning without a need for inhibition (Carandini and Ferster, 2000)? Subthreshold tuning is around three times broader than spike tuning and linear transformations could not account for the extra sharpening leaving space for an inhibitory role. This seemed unlikely however as the patterns of inhibitory input required to achieve this sharpening did not appear to match those that were recorded experimentally (Anderson et al., 2000a). A rectification model with an offset linear fit proved a much better match with the data and provided the nonlinear element necessary to produce a more sharply tuned spiking pattern from the broader subthreshold activity (Carandini and Ferster, 2000). Although this model failed to deal completely with contrast invariance, it provided an economical model that explained orientation tuning and did not require inhibition to contribute in a specific way other than to balance inhibition to prevent overexcitation. Contrast invariance is the maintenance of orientation tuning width across different levels of excitatory input produced by different contrast levels. Since the original rectifying iceberg model was proposed, suggestions have been made to more fully explain contrast invariance that also do not require inhibition. A particularly interesting suggestion is the idea that trial to trial membrane potential variability and contrast are correlated, with

variability increasing with decreasing contrast (Anderson et al., 2000b; Finn et al., 2007). This increased variability at lower contrast means that, although less spikes are being produced, the likelihood of crossing threshold on a given trial is increased. This compensates for the reduction in tuning width that would otherwise occur from the iceberg effect alone (Finn et al., 2007).

In the case of orientation tuning, both experiments and models have played down the role of inhibition in defining it. Many in the field believe this exclusion of inhibition should extend to many of the well-known response properties that emerge in visual cortex such as direction selectivity and cross-orientation suppression (Priebe and Ferster, 2012). This still leaves inhibition with potential roles in surround suppression and gain control. It is also possible that some of the other receptive field properties that seem not to require inhibition actually do. Just because a plausible minimum model can operate well without a specific role for inhibition does not always mean that it is how the brain functions. Also, since the vast majority of these experiments were carried out in anaesthetized animals it is possible the data was collected under very different regimes of inhibition than occur in the awake animal.

Finally, as well as recording from Pyr cells and looking at the total inhibition they receive it is necessary to record from the interneurons themselves. This will allow the refining of models once we know how interneurons truly respond, and also allow the exploration of their diversity to test whether their physical diversity matches with a visual response diversity. Interneurons are rare in cortex and therefore present a problem for targeting them in vivo, particularly before the advent of transgenic animals and 2-photon microscopy. An early set of recordings included recordings from fast spiking cells (Swadlow, 1988) and identified them using the information that some interneurons have thin spikes (McCormick et al., 1985). These experiments were carried out in awake rabbits and it was found that none of the putative interneurons were orientation selective and that they had larger receptive fields than other cell types (Swadlow, 1988). Another study carried out blind recordings in a similar way to Swadlow, but also morphologically reconstructed the recorded cells to give more certainty that they

were interneurons by their lack of spines (Hirsch et al., 2003). These recordings showed that the interneurons in layer 4 of cat visual cortex could be separated into two groups based on their response properties. Some interneurons were simple cells and their activity was therefore modulated at the frequency of a grating stimulus while other interneurons were complex and therefore unmodulated. This is an important demonstration that interneurons can have different responses to the same visual stimuli. Other identifiers of interneuron type such as molecular markers were not looked at to see if the different response types segregated into different cell types. The authors used these differences to suggest that each interneuron type might have a different role in shaping the visual response in Pyr cells within layer 4.

Since it is relatively laborious to reconstruct the morphology of every single cell recorded from, another way of categorizing cells is by their spiking patterns. A recent study in cat used current injection and analysis of the resulting firing patterns to separate recorded cells into four groups: regular spiking, chattering, intrinsically bursting and fast spiking (Nowak et al., 2008). The first three classes are associated mainly with excitatory cells (though they can also be interneurons), while the fast spiking cells (defined in this case by their high spike rate and lack of adaptation, not just spike width) are very likely to be interneurons. In cat visual cortex many interneurons are tuned, as they fall within orientation columns but here they found that a subgroup of fast spiking cells had very little orientation selectivity which they hypothesized to be due to the broad subthreshold tuning of these cells and their lower than average spike threshold (Nowak et al., 2008). Recordings of interneuron visual response properties have also been made in mouse visual cortex (Sohya et al., 2007). As mentioned previously mice have the benefit of being one of the earliest animals to have had their genome sequenced and, as a popular model organism, have a range of genetic tools and transgenic modifications that can be used (Luo et al., 2008). One class of these transgenics useful in neuroscience are those that express GFP in a genetically specified subset of neurons. These cells can then be visualised using 2-photon microscopy and targeted for either electrophysiological or imaging recordings. In this study a mouse expressing GFP under the control of the GAD-67 promoter was used,

which had previously been shown to express in the majority of interneurons (Tamamaki et al., 2003). Ca^{2+} imaging (Stosiek et al., 2003) was used to measure the responses of interneurons in layer 2/3 to drifting gratings. The responses of GFP^+ and GFP^- cells were then compared to test if Pyr cells and interneurons showed different orientation tuning (Sohya et al., 2007). They found GFP^+ interneurons to be less orientation tuned than Pyr cells. GFP^+ cells did not completely lack selectivity for orientation as shown by the population histogram and some average responses of individual cells in the supplementary figures (Sohya et al., 2007). Unlike in cat visual cortex the mouse visual cortex has the distinctive 'salt and pepper' structure of orientation tuning so interneurons are less likely to become tuned purely by taking on the tuning of their neighbours (Ohki et al., 2005). There are some questions about how accurate a reflection of spike rates Ca^{2+} imaging is in interneurons. Interneurons tend to fire at high rates and have different Ca^{2+} buffering dynamics to Pyr cells (hence the use of the different Ca^{2+} buffers such as parvalbumin to identify them). This has been controlled for by carrying out electrophysiological recordings during Ca^{2+} imaging in a sample of cells to rule out dye saturation or sensitivity problems and that the Ca^{2+} transients in the imaging data correlated in a broadly linear pattern with spiking output (Hofer et al., 2011).

Visual interneuron data collected by other experimenters during this project will be dealt with in the data chapter discussions and in the final discussion section. It is useful to talk about it alongside the data I have collected as a lot of it is highly relevant.

1.5 Optogenetic molecules and their delivery

The recent discovery and development of light activated ion channels and pumps has revolutionized our ability to control neural activity (Nagel et al., 2003; Boyden et al., 2005). The ability to shine light on a region of the brain and stimulate only the neurons expressing the light-activated proteins allows for the targeting of subsets of cells. This is not possible with electrical stimulation and is only possible on much longer timescales with pharmacological methods. Channelrhodopsin (ChR2) was the first of these optogenetic proteins used in neurons and is still the most widely used today. It is a cation channel activated by blue light (470 nm) that allows positive ions into the neuron depolarizing it and causing it to fire action potentials (Figure 1.5) (Nagel et al., 2003; Boyden et al., 2005; Bamann et al., 2008). Its ability to trigger firing in selected cells in a population at the millisecond timescale means that it is ideally suited to investigating neural networks at the same timescales at which they operate in the intact animal. Part of a growing trend of using biological molecules as tools in the study of biology, it is derived from the green alga *Chlamydomonas reinhardtii* (Nagel et al., 2003). It does require the cofactor retinal, to be able to progress through its photocycle, but fortunately this is produced by mammalian neurons and so does not need to be added or supplemented (Boyden et al., 2005; Bamann et al., 2008). As this is a genetically targeted system, expression levels need to be within the correct bounds to ensure spikes are produced, but also that the protein is not overexpressed to the level where it interferes with normal cellular processes. The use of ChR2 in a variety of different cell types mean that controls need to be carried out in each case to ensure reliable manipulation of cell activity and cell health (Kuhlman and Huang, 2008; Ivanova and Pan, 2009; Schultheis et al., 2011; Lovett-Barron et al., 2012; Madisen et al., 2012).

Since the discovery of ChR2 the range of optogenetic proteins has vastly expanded and the properties of particular proteins has been tuned for optimum function and expression (Gradinaru et al., 2008; Zhang et al., 2008; Zhao et al.,

2008; Airan et al., 2009; Berndt et al., 2009; Lin et al., 2009; Chow et al., 2010; Gunaydin et al., 2010). One of the first additions to the optogenetic arsenal was halorhodopsin (NpHR) a yellow light-activated chloride pump that hyperpolarizes cells it is expressed in and acts as the opposite of ChR2 (Figure 1.5).

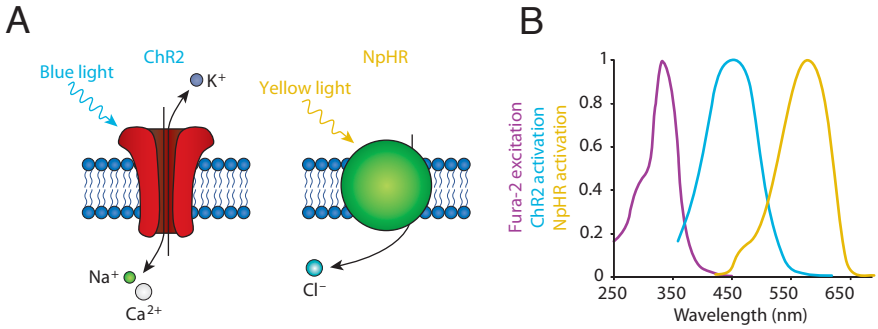

Figure 1.5 Optogenetic membrane proteins

A, Channelrhodopsin (left) is activated by blue light and depolarises the neuron by allowing Na^+ and Ca^{2+} ions in and K^+ ions out, Halorhodopsin (right) is activated by yellow light and hyperpolarises the neuron by pumping Cl^- ions in. **B**, The activation spectra for ChR2, NpHR and the Ca^{2+} imaging dye Fura-2 (adapted from (Hausser and Smith, 2007)).

NpHR had expression problems that were gradually addressed in newer versions (Zhao et al., 2008). The problems occurred during its transport through the ER and the Golgi where it tended to aggregate causing unnatural and likely damaging swellings. NpHR has since been superceded by a more problem free spike inhibitor known as Arch which pumps protons out of the neuron when driven with yellow light (Chow et al., 2010). Optogenetic proteins have been discovered and optimized to work on different timescales both faster (Gunaydin et al., 2010) and much slower (Berndt et al., 2009). It is now possible to shop around for a variant that suits your experimental design and then work out how to target it to your cell type of interest.

This targeting stage also has a large range of options. The most commonly used are viruses to transfect large groups of cells or, more recently, transgenic lines expressing ChR2, or other optogenetic variants, in specific cell types have become

available (Luo et al., 2008; Madisen et al., 2012). In terms of interneuron targeting, the promoters of marker molecules such as somatostatin or parvalbumin did not prove strong enough to produce enough ChR2 when placed directly into viruses (Luo et al., 2008). As more Cre lines became available the virus could simply contain a loxed/flexed version of the chosen optogenetic protein and this would be expressed only in the cells in the animal that express Cre (Atasoy et al., 2008; Cardin et al., 2009; Sohal et al., 2009; Cardin et al., 2010). Likewise for the transgenic lines expressing ChR2 a line expressing loxed ChR2 could be crossed with a Cre line to produce offspring with specific ChR2 expression. The catch about the crosses rather than viral injection into an adult animal is that many cell types may transiently express Cre during development that would not normally be identified as being part of the targeted cell group. This may lead to some level of incorrect expression. This can be avoided by viral expression which normally occurs once the neurons have finished developing and have taken on their adult gene expression profile. As will be seen later in this project other more specialized transfection methods can also be used such as single cell electroporation (discussed in more detail later), or in utero electroporation (Tabata and Nakajima, 2001).

1.6 Introduction summary

The brain is made up of many neurons that work together to process sensory information and coordinate behavioural responses. Studying the microcircuit level is crucial to understanding how these cells work together to carry out these processes.

The cerebral cortex is accessible to the latest, deep, *in vivo*, imaging techniques and has well-defined regions corresponding to particular sensory modalities. Cerebral cortex consists of a number of different cell types, both excitatory and inhibitory. Inhibitory interneurons are highly diverse, but their function in the microcircuit is poorly understood.

Visual cortex is a highly studied area which provides an excellent platform from which to investigate the function of inhibitory interneurons. To understand their role, interneuron visual responses need to be characterized, in addition to evaluating the effects of manipulating their activity. New tools allow identification of interneuron cell types for recording and cell type specific methods of manipulation at the large or small scale.

Bringing together these latest tools and the large amount of information that exists about the response properties of visual cortex, this study aims to discover new features of the relationship between different cell types in visual cortex and their function.

1.7 Aims of this thesis

1. To record from Pyr, SOM^+ and PV^+ cells *in vivo*, while presenting visual stimuli, and compare the structure and timing of their responses.

2. To stimulate small numbers of interneurons from the SOM^+ group and establish if an effect is detectable in other cells of the circuit *in vivo* during visual stimulation.

3. To stimulate large numbers of SOM^+ cells in vivo during visual stimulation and assess the effect on Pyr cells and PV^+ cells. Do these effects match with the small scale stimulation?

2 Materials and Methods

In this section, as well as the usual details, I have included small practical details which I found particularly important in the execution of these techniques. These are included in a Pro-tips section at the relevant junctures.

2.1 Animals

All experiments were carried out in accordance with UK Home Office regulations. Electrophysiological recordings were performed on adult (P30 – 65) mice, viral injections were carried out on mice aged P18 – P32 and single cell electroporation was carried out on mice aged P28 – P40. Mouse genotypes used were: C57-Bl6 wildtype, GAD65 (Lopez-Bendito et al., 2004), PV-GFP heterozygotes (Meyer et al., 2002), SOM-GFP heterozygotes (Oliva et al., 2000), Jackson lab number: 003718), SOM-ires-Cre homozygotes ((Taniguchi et al., 2011), Jackson lab number: 013044). All transgenic lines were backcrossed with C57-Bl6 for at least 10 generations so all mice had a similar genetic background. For some experiments animals positive for Cre and GFP were produced by crossing the PV-GFP with the SOM-Cre lines. To identify animals positive for GFP in heterozygote offspring, blue excitation/green emission goggles from BLS ltd. were used. In *SOM-GFP* animals goggles needed to be used in animals < P6, the GFP fluorescence could be particularly well visualized in the olfactory bulb and halfway down the spinal column. The *PV-GFP* animals could be easily identified by detecting GFP in their musculature or tail at any age from P8.

2.2 Visual Stimulation

2.2.1 Equipment

Visual stimulation was presented on a 20 inch Dell UltraSharp 2009WFP LCD Monitor which was supported in front of the microscopy setup on an ErgoMounts VisionPro 500 extending LCD arm mounted on an ErgoMounts stand. Visual stimulation software was run on a 2008 Apple Macbook. A USB 1208FS Daq board from Measurement Computing was used to coordinate triggering and a photodiode and TTL adaptor from RS electronics was used to record visual stimulus state.

2.2.2 Visual Stimuli

At the beginning of the project a range of visual stimuli were experimented with including checkerboards, grating and manual mapping stimuli. Quickly, square wave gratings were converged upon as they produced strong visual responses in many cells in visual cortex and had parameters such as orientation and spatial frequency that could be altered to provide a range of responses and optimized to produce maximum firing in a particular cell. Square wave gratings with a spatial frequency of 0.04 cyc/deg or 0.16 cyc/deg, drifting at 2 cyc/sec in 16 directions (from 0^o to 337.5^o) were presented in a random order for 2 s each with no blanks, with control and ChR2 stimulation conditions interleaved. Visual stimulus routines were written and presented using Matlab and the psychophysics toolbox (Brainard, 1997). Images were presented on a Dell 2009WFP LCD screen with 60 Hz refresh rate, 1280 x 800 resolution, extending in visual space from +30 to +110 in azimuth and from -10 to +40 in elevation. Brightness values ranged from 73.3 cd m^{-2} for the white bar, to 0.2 cd m^{-2} for the black bar, with the grey screen at 30.2 cd m^{-2}.

2.2.3 Triggering and synchronisation

Visual stimulus triggering was implemented by sending a TTL pulse from the electrophysiology software to the visual stimulus computer via the Measurement Computing Daq board. Once the visual stimulus had started alongside the electrophysiology recording, synchronisation was ensured by programming a small square in the bottom right hand corner of the screen to turn either black or white with each alternating grating orientation. This square was monitored using a photodiode that was fed into the electrophysiology software so the beginning an end of each different 2 s stimulus epoch could be precisely recorded next to the accompanying electrophysiological trace by the presence or absence of a voltage signal from the photodiode.

2.3 2-photon Imaging

2.3.1 Imaging setup

A custom *in vivo* microscope made by Prairie technologies was used in combination with a Nikon 16x, 0.8 numerical aperture water immersion objective and a MaiTai Ti:Sapphire laser from Spectra-Physics. Images were acquired using Scanimage in conjunction with Matlab and later using Prairie's own Prairie View software.

2.4 Electrophysiology

2.4.1 Cell-attached recording

For early experiments mice were anaesthetized with ketamine (100 mg/kg)/xylazine (15 mg/kg) and topped up with ketamine as necessary. In later experiments animals were anaesthetized first with chlorprothixene (2 mg/kg), then after 20 minutes with urethane (1 g/kg). Surgery began when the animal became

unresponsive to foot pinch, usually after an additional 20 minutes. The animals were topped up as necessary with urethane.

Lacrilube (Allergan) was used to keep the eyes moist. A 1 mm by 0.5 mm craniotomy was opened over monocular visual cortex and the dura mater was removed. The craniotomy was then covered with 1.5% agar and ACSF (NaCl 150 mM, KCl 2.5 mM, Hepes 2.5 mM, $CaCl_2$ 2 mM, $MgCl_2$ 1 mM). Cell-attached recordings were made using 6 MΩ pipettes filled with ACSF and 50 μM Alexa 594 from Invitrogen. Signals were acquired at 50 kHz in voltage clamp and filtered at 4 kHz. Shadowpatching was used to approach Pyr cells and to aid visualization of the formation of loose cell-attached seals of hundreds of MOhms. In many cases the Pyr cell body and apical dendrite could be clearly identified.

2.4.2 Intracellular recording

Surgery and anaesthesia were the same as for extracellular recordings above. Intracellular recordings used 6 MOhm pipettes filled with internal solution (K-gluconate 135 mM, KCl 4 mM, Hepes 10mM, disodium-phosphocreatine 10 mM, Mg-ATP 4 mM, Na_2-GTP 0.3 mM, pH 7.2, 291-293 mOsm) and 50 μM Alexa 594 from Invitrogen. Signals were acquired in current clamp at 50 kHz and filtered at 4 kHz. After approaching the cell using shadow patching or fluorescent visualisation a gigaOhm seal was formed by releasing the pressure, putting on a -70 mV holding potential in voltage clamp mode and the application of gently negative pressure. Stronger negative pressure was later applied to break in.

2.4.3 Recording Pro-tips

The key to good cell attached or intracellular recording was shown over time to be due to 4 main factors. Firstly, creation of a clean and stable craniotomy. It is very hard to record from cells that are moving too much or in conditions in which the optical quality of the tissue has been too highly degraded and visualization of the

cells is poor. Secondly, selection of the target cell or area for recording before entering the brain to ensure it is visually clear. This means choosing an area that is accessible to the pipette (not too close to the sides or back of the craniotomy) and that is not obscured by surface or intracortical blood vessels. Thirdly, using smooth, fast movement down to the cell while ensuring continuously that the pipette is unblocked is important. This requires continuous control of pressure while navigating around cell bodies, blood vessels and other obstructions on the way down. Fourthly, the final approach to the cell is crucial for getting a good seal (whether giga or otherwise). Scan up and down in z having aligned the tip with the cell and make sure you are not shooting over the top or underneath the cell.

2.5 Single Cell Electroporation

2.5.1 Plasmid genetics

A range of plasmids were electroporated into cells during this project. Fluorescent protein plasmids to label cells were pCAG-EGFP and pCAG-Turbo were used for green and red labeling respectively. Red labeling was necessary for targeted electroporation of interneurons as the interneurons already expressed GFP to allow them to be targeted in the first place. pCAG-EGFP was obtained from Addgene while pCAG-Turbo (originally named Katushka, (Shcherbo et al., 2007)) was obtained from Evrogen. For the ChR2 plasmid we used a version kindly donated by Juan Burrone that expressed wildtype ChR2 on a pCI-neo vector originally from Promega. We also produced a pCAG version of the ChR2 plasmid in our laboratory in order to get a higher level of ChR2 expression but, in interneurons, both worked well and so the pCI-neo version was used for all experiments. The pCAG-ChR2 plasmid was produced by cloning the wildtype ChR2 from the pCI-neo vector, and then cutting the clone and the plasmid with complementary restriction enzymes, before ligating the ChR2 into the pCAG vector.

2.5.2 Electroporation methods

The animals were anaesthetized with ketamine (100 mg/kg)/xylazine (15 mg/kg). An area of scalp was removed and a head plate fixed to the skull over monocular visual cortex. Using a dental drill from NSF a 1 mm by 0.5 mm craniotomy was made inside the headplate. The skull was soaked for 5-10 mins in ACSF (NaCl 150 mM, KCl 2.5 mM, HEPES 2.5 mM, $CaCl_2$ 2m M, $MgCl_2$ 1 mM) before removal of the small bone cap, exposing the dura. The animal was placed under the microscope and a glass pipette (12-15 MΩ) was filled with ACSF, 50 µM Alexa 594 dye from Invitrogen and the plasmids (100 ng/µl) to be transfected into the interneurons. Despite the fact that two separate plasmids were used we never found a case of an interneuron that expressed RFP but did not respond to blue light stimulation, suggesting that both plasmids always entered the cell upon electroporation. Pressure was put on the pipette (100 mbar) and it was advanced through the dura into the brain, at which point the pressure was then reduced (to 40 mbar). GFP^+ cells were approached, the pressure released, and a train of voltage pulses (1 second train of 1 ms, -10 V pulses at 100 Hz) delivered with an Axoporator 800A from Axon instruments. Once a number of interneurons had been electroporated the craniotomy was resealed using Kwik-Sil from World Precision Instruments and the mouse was allowed to recover for 48 hours before recording. A recovery cocktail of 100 µl carprofen (5%) and 600 µl baytril (2.5%) was added to 150 ml of drinking water. When recordings were made from electroporated animals the recorded cells were always within 100 µm of an electroporated cell. Recorded cells were classed as either Pyr cells or PV^+ interneurons based on their average firing rates and orientation selectivity index. We set an orientation selectivity threshold of 0.5 and an average firing frequency threshold of 5 Hz to separate the cells. In addition spike shape was taken into account with cells selected as PV^+ interneurons having a distinct upward deflection in their spikes, recorded in cell attached voltage clamp recordings that was not present in cells selected to be pyramidal.

2.5.3 Electroporation Pro-tips

The Pro-tips above in the recording section all also apply here. Detailed here are the tips that are particular to electroporation. Firstly as the dura is still on, this needs to be penetrated by the pipette. Put on a high pressure (180 mbar) and move quickly through the dura using a coarse manipulator setting. Once through the dura ensure that there is a large plume of dye leaving the pipette as blocked pipettes do not give good results. Secondly on the final approach to the cell let the seal resistance increase (it is useful to monitor this with a variable tone played over a speaker) and then hit the electroporation button before is gets too high and you form a strong seal with the cell. Thirdly to get some immediate feedback as to the quality of electroporation of a given cell the speed and brightness of the fill should be monitored. A good fill is very quick, filling the soma and the early parts of the proximal dendrites with bright Alexa. A poor fill is slow, the dye appears to leak gradually into the cell or the final fill is not particularly bright indicating not much of the plasmid entered the cell.

2.6 Viral Injections

2.6.1 Viral injections

Animals were anaesthetized with ketamine (100 mg/kg)/xylazine (15 mg/kg) and a 1.5 mm craniotomy was opened over monocular visual cortex. A cre-inducible ChR2 construct housed within an adeno-associated virus expression vector (sequence: http://www.everyvector.com/sequences/show_public/2491, produced by the UNC viral vector core, Supplementary Figure 1a) was used that contained the hChR2(H134R) version of ChR2 that is optimized for mammalian expression and large light activated currents. 0.5 µl of this virus at a titre of 2 x 10^{12} viral genomes/ml, was injected at a tip depth of 200-400 µm. The injection capillary tube (Blaubrand, Intramark) was held in a stereotax (Narishige) and manual pressure was applied using a 1 ml syringe connected via plastic tubing. Post-injection the scalp was sutured and animals were allowed to recover. A recovery

cocktail of 100 µl carprofen (5%) and 600 µl baytril (2.5%) was added to 150 ml of drinking water. Experiments began between 2 and 4 weeks after virus injection.

2.6.2 Viral injections Pro-tips

The injection capillary tube was pulled on a pipette puller using the same heat settings used to pull 6 MOhm pipettes for electrophysiology. After pulling, the tip was broken manually with forceps to allow it to be tip-filled with virus using manual negative pressure. The tip should not be so large that the virus is ejected too quickly during injection. The injection of viral solution into the brain should be done very slowly. It should take between 10 and 20 minutes to inject the 0.5 µl.

2.7 ChR2 stimulation

2.7.1 Equipment

ChR2-expressing cells were stimulated with blue light produced by a royal blue LED from Luxeon with peak output at 455 nm (LXHL-NRR8). This LED was built into a small circuit containing an integrated circuit (ULN2003AN, Texas Instruments) a TTL adaptor from RS electronics, a 9 V power adaptor from RS electronics, a 15 Ohm resistor (between the intergrated circuit and the LED) and a potentiometer from Maplin electronics (JM69A). An Arduino Duemilanove was used to coordinate the timing of blue light pulses. The LED was attached to the camera port on top of the 2-photon microscope that is aligned vertically with the objective. The light it produced was focused through the Nikon objective onto the craniotomy.

2.7.2 Timing

The TTL input to the LED circuit triggered the blue light to be switched on. This input came from a preprogrammed Arduino which produced 1 ms pulse trains at the required frequency (usually 40 Hz). The Arduino received input from the visual stimulus screen via a photodiode that monitored the bottom right hand corner where a small box flashed black or white to signal the start or end of each visual stimulus. This fast closed loop between the screen, the Arduino and the LED meant that fast, accurate pulses could be sent to the LED circuit and were regulated directly by the visual stimulus on the screen. ChR2 stimulation during visual stimulation was arranged so that alternating 2 s visual stimulus epochs had blue light pulses. This was controlled by the box of pixels in the bottom left hand corner of the screen that was programmed into the visual stimulus and dictated when the Arduino drove ChR2 stimulation.

2.7.3 Different stimulation intensities

The maximum power output of the blue LED was 220 mW measured directly from the LED. A large fraction of this power was lost due to the imperfect coupling with the Nikon objective. Two different stimulus intensities were used in this study using the potentiometer to control the power. The first of these, used in the vast majority of the ChR2 experiments, was 13 mW as measured immediately after the objective. For the stronger stimulation used in some experiments brighter blue light was used (25 mW immediately after the objective) and cells were recorded close to the center of the virally injected area (< 100 μm), as opposed to in most experiments in which cells were located >100 μm from the center of viral injection.

2.8 Immunohistochemistry

2.8.1 Antibodies

Target	Host	Concentration	Company	Code
Primary Antibodies				
Somatostatin	Rabbit	1:800	Bachem	T4103.0050
Parvalbumin	Goat	1:1000	Swant	PVG 214
eGFP/eYFP	Mouse	1:500	Abcam	ab1218
Secondary Antibodies				
anti-rabbit - Alexa 405	Goat	1:400	Invitrogen	A31556
anti-Goat - Alexa 647	Donkey	1:400	Invitrogen	A21447
anti-Mouse - Alexa 488	Chicken	1:400	Invitrogen	A21200

2.8.2 Staining protocol

Animals were taken post-experiment already under urethane anaesthesia and were further anaesthetized with ketamine (100 mg/kg)/xylazine (15 mg/kg). They were then perfused first with 1X phosphate buffered saline (PBS), then with 4% paraformaldehyde. After fixing overnight 100 μm sections were cut and washed three times for 10 minutes in 1X PBS. The following protocol was adapted from Xu et al., 2010. After the washes the slices were incubated for 2 hours at room temperature in 0.4% Triton X-100 then washed once in 1X PBS for 10 minutes. Primary antibody solutions were prepared in 1X PBS using rabbit anti-somatostatin (Bachem, T-4103.0050, 1:800), goat anti-parvalbumin (Swant, PVG 214, 1:1000) and monoclonal mouse anti-eYFP/GFP (Abchem, ab1218, 1:500). Primary antibodies solutions were added to the slices and incubated overnight in at 4^{o}C then washed three times for 10 minutes in 1X PBS. Secondary antibody solutions were prepared using goat anti-rabbit (Invitrogen, A31556, 1:400), donkey anti-goat (Invitrogen, A21447, 1:400), chicken anti-mouse (Invitrogen, A21200, 1:400) and were added to the slices for three hours. A final three 10

minute washes in 1X PBS were carried out before the slices were mounted onto slides.

2.8.3 Confocal imaging

Images were collected using a Perkin Elmer Ultra*VIEW* confocal system and Volocity software. This system allowed for fast imaging of large 3D volumes and accurate stitching offline in Volocity software. Images from the volume that were selected as representative regions of interest were coloured and overlaid in ImageJ.

2.9 Data analysis

2.9.1 From raw electrophysiology to Gaussian fits

Raw cell-attached electrophysiological recordings were first filtered at 3 kHz and then thresholded at an appropriate level calculated for each trace to isolate the spike times. This long series of spike time-stamps was then split into sections corresponding to each 2 s visual stimulus epoch corresponding to a different grating orientation using the photodiode screen recording taken simultaneously with the electrophysiology data. A similar procedure was carried out for intracellular recordings but with an opposite direction of threshold and 5 kHz filtering. This spiking data could then be summed for each orientation and averaged across the number of repeats to produce the points used to create an orientation tuning plot with the mean spike frequency responses plotted against the orientation of the visual stimulus grating. To obtain tuning curves, visual responses were fit with 2 summed Gaussians separated by 180^{o}. The fitting routine used a least squares method to minimize the Cartesian distance between the model and the data (Carandini and Ferster, 2000). Cells were used that met these criteria: > 2 Hz firing at the peak response in the raw data, visually

responsive above spontaneous firing rate, at least 5 repeats of each orientation, and the sum of squared residuals normalized by maximum value of the proposed Gaussian fit must be below a 0.125 threshold. The last criterion was used for Pyr cells only as interneurons are not necessarily expected to be fit well by two summed Gaussians separated by 180 ^{o} (Liu et al., 2009). The spike timing information was thrown out when making Gaussian tuning curves but was used for separate analysis detailed in section 2.9.5.

2.9.2 Calculating visual response parameters

Peak firing rates were extrapolated from the raw data using these Gaussian fits. Orientation selectivity index (OSI) was calculated by comparing the maximum amplitude of the preferred orientation (Rp) with the minimum value of the Gaussian fit (Ro):

$$OSI = \frac{(Rp - Ro)}{(Rp + Ro)}$$

Circular variance (CV) is another measure of orientation tuning. It takes into account the average response at each orientation. Zero circular variance would be a perfect circle, while a circular variance score of one would mean a highly tuned cell responding to only one orientation. Circular variance is calculated using the following equation (r = visual responses, o = grating orientations):

$$CV = \frac{\sum_k \left(r_k - \bar{r}\right) e^{2\pi i \left(\frac{o_k}{180}\right)}}{\sum_k r_k}$$

Half width at half height (HWHH) is a measure of tuning width in degrees calculated from the Gaussian sigma obtained from the fitting process. Sigma is converted to HWHH using the following equation:

$$HWHH = \sigma \times \sqrt{(2 \times \ln 2)}$$

The direction selectivity index (DSI) was used to measure to what extent a cell had a preference for the direction of movement of an oriented grating. If both directions (e.g. for a horizontal grating moving upwards (90^o) or downwards (270^o) are preferred equally then direction selectivity index equals zero whereas if only one direction produces a response then direction selectivity index equals one. Some PV^+ cells were excluded from this analysis as they were not well fit by two summed Gaussians and so were not able to provide the preferred and non-preferred direction measurements. The equation is as follows (Rp = responses to the preferred direction, Rn = responses to the non-preferred direction):

$$Direction\ selectivity = \frac{(Rp - Rn)}{(Rp + Rn)}$$

Visually responsive cells in this study were those that increased their firing in response to drifting gratings. Some cells respond to the drifting grating with phasic activity at the frequency of grating drift (2 Hz) known as simple cells (Hubel and Wiesel, 1962). Others called complex cells (Hubel and Wiesel, 1962) respond more uniformly, lacking the 2 Hz modulation. To quantify the proportion of 2 Hz modulated activity versus non-modulated activity for the preferred direction of a given cell we used the F1/F0 measure. F1 is the amplitude of the 2 Hz modulation and F0 is the mean firing rate. F1 was calculated by carrying out a Fourier transform on the 2 second grating response histogram binned at 100 ms and taking the amplitude at 2 Hz from the discrete Fourier transform. Cells used for the F1/F0 analysis had to meet three criteria: Firstly they must have a measurement of the spontaneous rate taken as this needs be subtracted before the

calculation, secondly the cells must fire above a minimum threshold in the ChR2 condition (mean firing rate must be above 1 spike/s) as very low spike rates give spurious results, thirdly the tuning curves must be sufficiently well fit by the standard Gaussian model as measured by their residuals from the Gaussian fit.

The untuned component is equal to Ro (see the orientation selectivity index) the minimum value of the Gaussian fit. The tuned component is the difference between Rp (see above) and Ro (see above) to show how large the modulated part of the Gaussian fit is that lies above the untuned component.

2.9.3 Least mean square fits

Least mean squares fitting to compare subtractive with divisive inhibition, was carried out using an algorithm written in Matlab. The Gaussian fits for visual responses in the control and ChR2 conditions were compared while the control Gaussian was altered either by pure subtraction or pure division until it converged on the least mean squares fit (i.e. the least average mean squared error between the control Gaussian and the ChR2 Gaussian). Each cell was fit individually and then population mean ± SEM was calculated for each form of inhibition.

2.9.4 Statistics

InStat software was used to help make the correct selection between statistical tests. Data being compared were tested that they met the assumptions of parametric tests such as normality using the Kolmogorov-Smirnov or similar standard deviations across groups using the Bartlett test. If the data met these assumptions a parametric test was used such as the ttest or an ANOVA if not then a nonparametric test was used for example the Wilcoxon signed rank test or the Kruskal Wallis test.

3 Visual responses of identified interneurons in cortical layer 2/3

3.1 Introduction

Visual neuroscience aims to understand how visual information entering the eye from the outside world is represented and processed in the brain. A set of seminal discoveries made in visual cortex by Hubel and Wiesel were pivotal in defining some of the main properties of these representations (Hubel and Wiesel, 1959, 1962). Cells in visual cortex have been shown to be selective for orientation, direction and size of visual stimuli (Bair, 2005). Following these discoveries, the literature describing many different parameters of the visual receptive fields of cortical neurons has grown dramatically uncovering many new features (Bair, 2005). The majority of these recordings did not include the morphological recovery of the recorded cells after the experiment or assessment of their electrophysiology and the molecules they express. This meant that it was difficult to correctly attribute the responses to a particular cell type, as the cortex is known to have a diverse array of cell types (Markram et al., 2004). Much of this diversity, whether morphological, genetic or electrophysiological, occurs within the inhibitory interneuron group that makes up a small fraction of the total cell population (Markram et al., 2004). This means that blind recordings will by default undersample this diverse group. Ultimately to establish how interneurons respond to visual stimuli, which in turn should give many clues as to their function within the circuit, it is necessary to be able to reliably identify them: ideally by visually targeting them allowing both for unambiguous identification and an increase in yield of recordings of these rarer cells.

3.2 Results

Visual targeting of recordings to specific interneuron types was achieved using 2-photon microscopy to guide intracellular and extracellular recordings to cells expressing GFP under cell-type specific promoters. In each mouse line a different set of interneurons express GFP therefore the appropriate line must be selected (Oliva et al., 2000; Meyer et al., 2002; Taniguchi et al., 2011). Over time our ability to produce transgenic mouse lines has greatly improved, and interest in distinguishing between interneuron cell types has increased (Luo et al., 2008). This has led to a large recent growth in the number of mouse lines specifically targeted at allowing access to the full range of interneuron diversity (Jackson, 2013b). Many of these lines became available during the course of this study and the most useful of these have been incorporated (Taniguchi et al., 2011). Initially in this project the GAD65 mouse line was used. This labels a large number of interneurons across different groups (Lopez-Bendito et al., 2004). Later the use of different lines allowed the more refined targeting of specific morphological and electrophysiological groups.

It was also important to focus on choosing the correct anaesthesia and visual stimulation protocols to use in mice. Although recordings have been made in mouse visual cortex for many decades (Drager, 1975), it is only recently that it has become a widely used visual model and so a range of anaesthetic protocols are still being used (Mrsic-Flogel et al., 2007; Niell and Stryker, 2008; Smith and Hausser, 2010). Recording time was limited, so a stimulus that provided an array of different visual response parameters was required. Square wave drifting gratings were used as they give information about a range of orientation tuning parameters, direction selectivity and firing rates. They also produce large responses in anaesthetized animals. The visual stimulus protocol was refined during the GAD65 experiments to get the best results from the comparison between the visual responses of Pyr cells, SOM^+ interneurons and PV^+ interneurons.

3.2.1 GAD65 mouse line recordings, optimizing visual stimulation and anaesthesia

A 2-photon imaging setup was used that allowed the recording pipette to be moved under visual guidance to target labeled cells (Figure 3.1 A). This setup was used to target and record from GFP^+ interneurons in the GAD65 mouse line both extracellularly and intracellularly under ketamine/xylazine anaesthesia (Figure 3.1 B,C). Recordings were also made from Pyr cells both to confirm that these mice responded as predicted from the existing visual literature and as a reference to compare with the tuning of the interneurons (Figure 3.1 D).

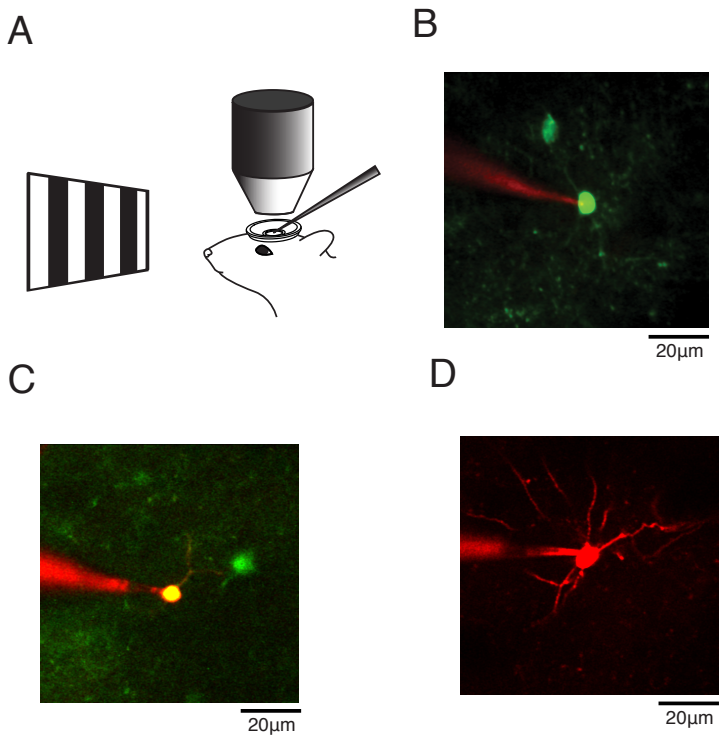

Figure 3.1 Targeted recordings

A, Schematic showing the experimental configuration that allows 2-photon targeting of GFP^+ cells and presentation of visual stimuli. **B**, A 2-photon image showing a cell-attached recording from a GFP+ interneuron from the GAD65 mouse line. **C**, A 2-photon image showing an intracellular recording from a GFP+ interneuron from the GAD65 mouse line. **D**, A 2-photon image showing an intracellular recording from a Pyr cell having used shadowpatching to visualise it.

Figure 3.2 shows radial plots and orientation tuning curves for some representative cells. The Pyr cells tended to be well tuned for orientation, only responding strongly to a small number of grating orientations, and often exhibited some direction selectivity, firing more strongly when the grating for a given orientation moved in one direction rather than the other (Figure 3.2 A,B). GFP^+ interneurons from GAD65 animals showed a much larger range of tuning properties from quite high levels of tuning (Figure 3.2 C) to being visually responsive but non-orientation selective, firing strongly in response to gratings of all orientations (Figure 3.2 D,E). Although the Pyr cell tuning matched the literature well, the Pyr cell firing rates were often low (for example, peak firing rates of 4.9 and 1.4 spikes/s respectively in Figure 3.2 A,B) suggesting a possible non-optimal choice of anaesthetic.

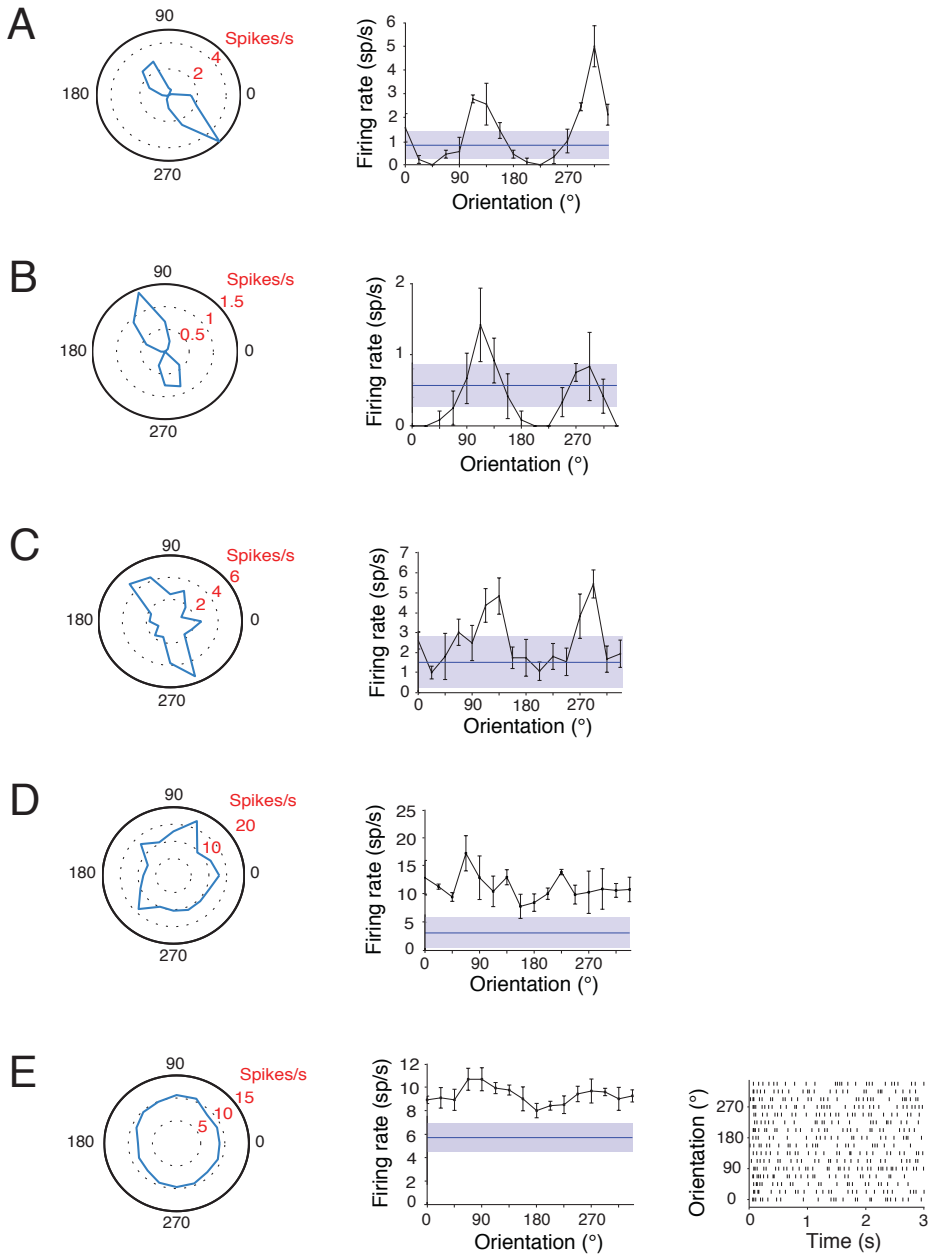

Figure 3.2 Targeted cell-attached recordings from Pyr cells and interneurons

A and B, Radial plots and tuning curves recorded from putative pyramidal cells showing tuning for grating orientation and a degree of direction selectivity. Error bars on the tuning curve are SEM, the horizontal blue line shows the average spontaneous firing frequency, the region shaded blue around it is its SEM **C**, A GFP⁺ interneuron from the GAD65 mouse line showing orientation tuning, layout as in A and B. **D and E**, Two relatively untuned GFP⁺ interneurons from the GAD65 mouse line, layout as in A and B. E also shows the spike raster for one repeat at each orientation.

As well as showing variability in orientation tuning amongst the population, the GAD65 GFP^+ interneurons also varied in their responses to grating onset. The visual stimulus drifting grating protocol had 16 directions of 3 second drifting grating each separated by 1 second of grey screen. Some GFP^+ interneurons responded strongly to the first stimulus presentation in the train but then less strongly throughout the rest of the train (Figure 3.3 A). This occurred in these two example cells despite the shuffling of the orientations across trials. Other GFP^+ interneurons showed a different form of onset response where they responded strongly to each grey to grating transition (Figure 3.3 B). Here the majority of the spikes triggered by the visual stimulus occurred within 200 ms of its onset and occurred across a wide range of stimulus orientations. Pyr neurons also responded strongly to visual stimulus onset from a grey screen. This was most obvious when intracellular recordings were made as the cells tended to have a relatively low spike rate under ketamine/xylazine anaesthesia. The current clamp voltage traces showed that despite not spiking on every stimulus presentation the cell was very often driven into an upstate as defined by an elevated transient plateau potential close to spike threshold (Figure 3.3 C). This can be seen clearly when the averages of multiple trials at each of 8 orientations is shown. The onset of visual stimulus drives the Pyr cell shown here into an upstate regardless of the orientation of the visual stimulus grating (Figure 3.3 D).

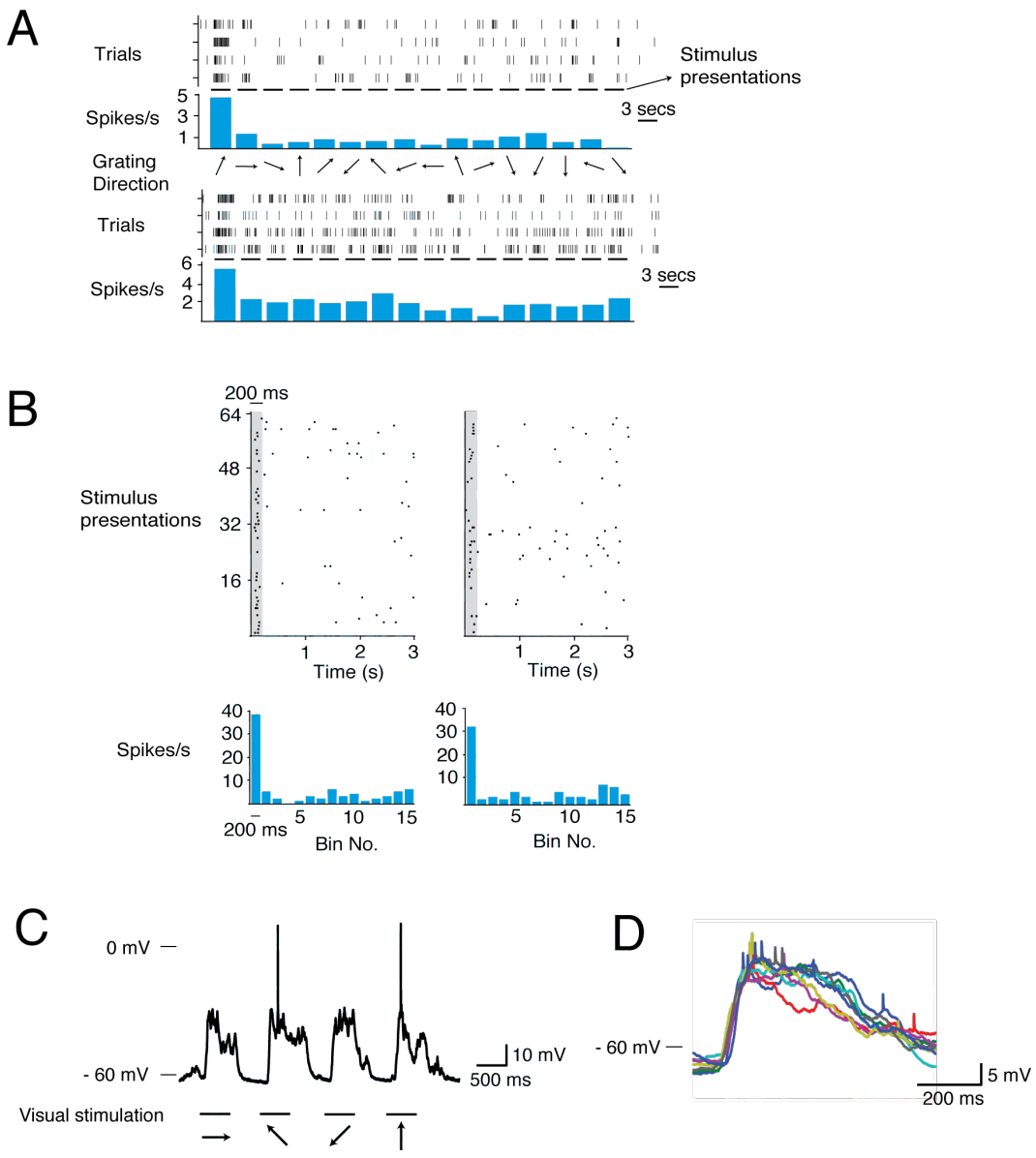

Figure 3.3 Onset effects amongst interneurons and upstate synchronisation

A, Spike rasters and histograms for two GFP⁺ interneurons that responded strongly to the first stimulus in the train but did not respond strongly to the other stimuli despite one second of grey screen in between each stimulus direction. **B**, Spike rasters and histograms for two different GFP⁺ interneurons that respond to each stimulus onset with spiking biased towards the first 200 ms of the stimulus. **C**, A section of intracellular recording from a putative pyramidal cell with short periods of drifting grating visual stimulation, the black arrows denote the direction of grating drift. **D**, Averages of six repeats for the 8 different directions used, all are aligned to visual stimulus onset showing a high degree of synchronisation of upstate onset.

3.2.2 Comparing the visual responses of Pyr, SOM$^+$ and PV$^+$ cells

Following the initial experiments using the GAD65 animals, new mouse lines were used that expressed GFP$^+$ in more distinct interneuron subtypes. The GIN mouse line from Professor Swann's lab expressed GFP in Layer 2/3 Martinotti cells that are defined by their morphology and electrophysiology and their expression of somatostatin (1.2.2, (Oliva et al., 2000)). This line was created by random insertion of a vector (GAD67-eGFP) into the mouse genome via pronuclear injection. By chance the insertion location in one of the mouse lines led GFP to be expressed only in cells also expressing somatostatin. The second transgenic mouse line used was the PV-GFP line created by Professor Monyer's lab using BAC technology to integrate the parvalbumin promoter driving GFP expression into the genome (Meyer et al., 2002). More details on the differences in properties and potential functions of the SOM$^+$ and PV$^+$ interneurons labeled by these two lines can be found in the introduction (1.2.2).

Pyr cells were recorded from both transgenic mouse lines during experiments in which interneurons were also recorded, so that recordings from different cell types were matched, originating from the same circuits and background genetics. The visual stimuli used in these experiments were 17 periods of 2 second drifting gratings in a random sequence that varied with each repeat. There were no periods of grey separating each orientation and of the 16 orientations shown the first was repeated at the end of the series allowing the first drifting grating presentation to be ignored. This lack of grey gaps between stimuli and the throwing out of the first stimulus presentation was based on the data collected from GAD65 animals that showed large increases in spiking at the onset of visual stimulation. The anaesthetic regime used for these recordings was urethane and chlorprothixene as used by Niell and Stryker (Niell and Stryker, 2008). This produced better visual responses both in terms of firing rate amplitude and sharper tuning. An additional benefit of using the same anaesthesia as Niell and Stryker was that data collected could be compared with their extensive survey of Pyr cell firing properties. Recordings were made from Pyr cells, PV$^+$ interneurons and SOM$^+$ interneurons

to determine whether the differences in their morphology, electrophysiology and connectivity were reflected as differences in their responses to visual stimuli.

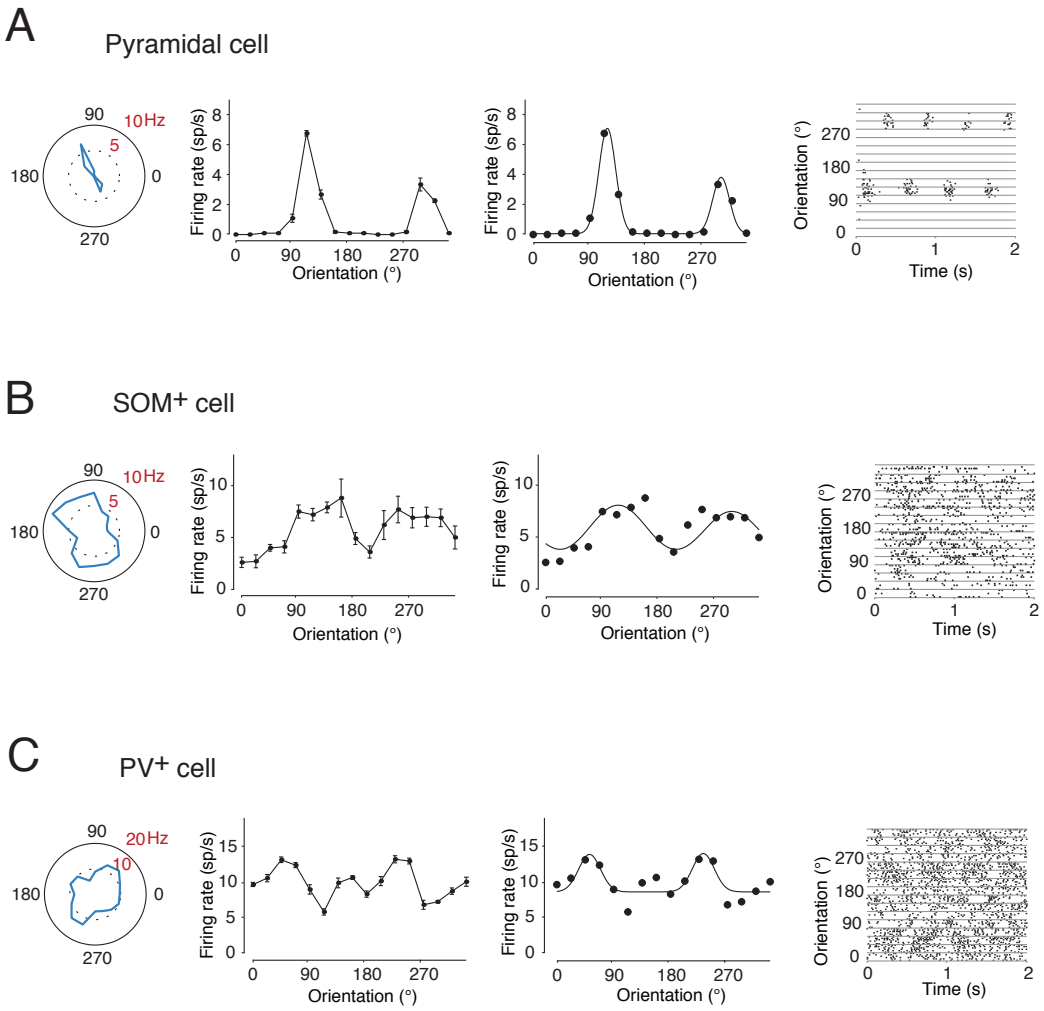

Figure 3.4 Representative Pyr cells, SOM$^+$ interneurons and PV$^+$ interneurons

A, Radial plot, average firing rates with SEM, Gaussian fit to average firing rates and spiking raster showing the visual responses of a representative pyramidal cell. **B**, Visual responses of a representative SOM$^+$ cell. **C**, Visual responses of a representative PV$^+$ cell.

Figure 3.4 A-C shows representative visual responses from each of the cell types. A range of values can be extracted from these raw responses to quantify the differences in response properties between the three cell types. Firstly and most simply, the mean firing rate across all orientations and repeats was calculated (Figure 3.4 Pyr cell: 1.05 spike/s, SOM^+ cell: 5.8 spikes/s, PV^+ cell: 9.8 spikes/s). The Pyr cell has a much lower firing rate than the two interneuron examples. The main reason for this is the fact that being orientation tuned, it only responds to certain orientations and therefore when averaged across all stimuli comes to much less than the example interneurons, which fire to some extent across all orientations. Secondly the peak firing rate can be obtained by taking the highest value from the Gaussian fit (Figure 3.4 Pyr cell: 6.81 spike/s, SOM^+ cell: 8.10 spikes/s, PV^+ cell: 13.96 spikes/s). There are lower percentage differences between the three example neurons on this measure but the PV^+ cell still has a higher value than the other groups. The Gaussian fit can also be used to separate responses into tuned and untuned components. The untuned component is defined as the firing rate at the lowest part of the Gaussian curve, i.e. the amount of activity that is present across all stimuli. This represents spiking that has no orientation tuning and is effectively an offset from baseline of the Gaussian (tuned) component. The untuned component is much larger in the two interneurons while it approaches zero in the Pyr cell (Figure 3.4 Pyr cell: 0.06 spike/s, SOM^+ cell: 3.75 spikes/s, PV^+ cell: 8.56 spikes/s). The amplitude of the tuned component (peak to trough of the Gaussian fit) varies less between these cells (Figure 3.4 Pyr cell: 6.75 spike/s, SOM^+ cell: 7.85 spikes/s, PV^+ cell: 5.34 spikes/s).

The orientation selectivity index is a measure of orientation tuning that compares Gaussian peak amplitude with Gaussian trough amplitude to produce a score between zero and one, with zero being the least orientation tuned and one being the most tuned (see methods section for more details). As is obvious from visual inspection, the Pyr cell is more orientation tuned than the example interneurons although the interneurons, especially the SOM^+ interneuron, also show a level of orientation selectivity (Figure 3.4 Pyr cell: 0.98, SOM^+ cell: 0.35, PV^+ cell: 0.24). Circular variance is another measure of orientation tuning. In contrast to the OSI,

it takes the firing rate at all orientations into account (see methods section for more details). It is also scored between zero and one and shows similar results to the orientation selectivity index although shifted to lower values due to the differences in the calculation of the two indices (Figure 3.4 Pyr cell: 0.86, SOM^+ cell: 0.17, PV^+ cell: 0.12). The preferred orientation of these cells can be calculated by measuring the orientation that corresponds to the peak of the Gaussian fit (Figure 3.4 Pyr cell: 118^o, SOM^+ cell: 116^o, PV^+ cell: 53^o). The expectation is that when looking at populations of cells of any cell type they should be distributed largely randomly in terms of orientation (but see Drager 1975). As well as orientation measures, direction selectivity indicates whether a grating oriented at the preferred orientation produces higher responses when moving in one direction versus the other. This can be visualized on the Gaussian fit of the Pyr cell (Fig. 3.4 A) by comparing the height of the two peaks of the Pyr cell response. As the orientation is measured from 0 to 360 degrees, 180^o and 360^o represent a grating of the same orientation drifting in opposite directions. In the example Pyr cell there is some direction tuning since the peak response at 118^o is higher than the peak response at the opposite direction at 298^o. The two interneurons both show hardly any direction selectivity with their peaks being almost the same amplitude in both directions (Figure 3.4 Pyr cell: 0.29, SOM^+ cell: 0.05, PV^+ cell: 0.04). A final useful metric is the half width at half height (HWHH) of the Gaussian fits, which provides a measure of tuning sharpness. The Pyr cell being more orientation tuned in this example has a lower HWHH than the two interneurons (Figure 3.4 Pyr cell: 16.08, SOM^+ cell: 58.56, PV^+ cell: 31.14).

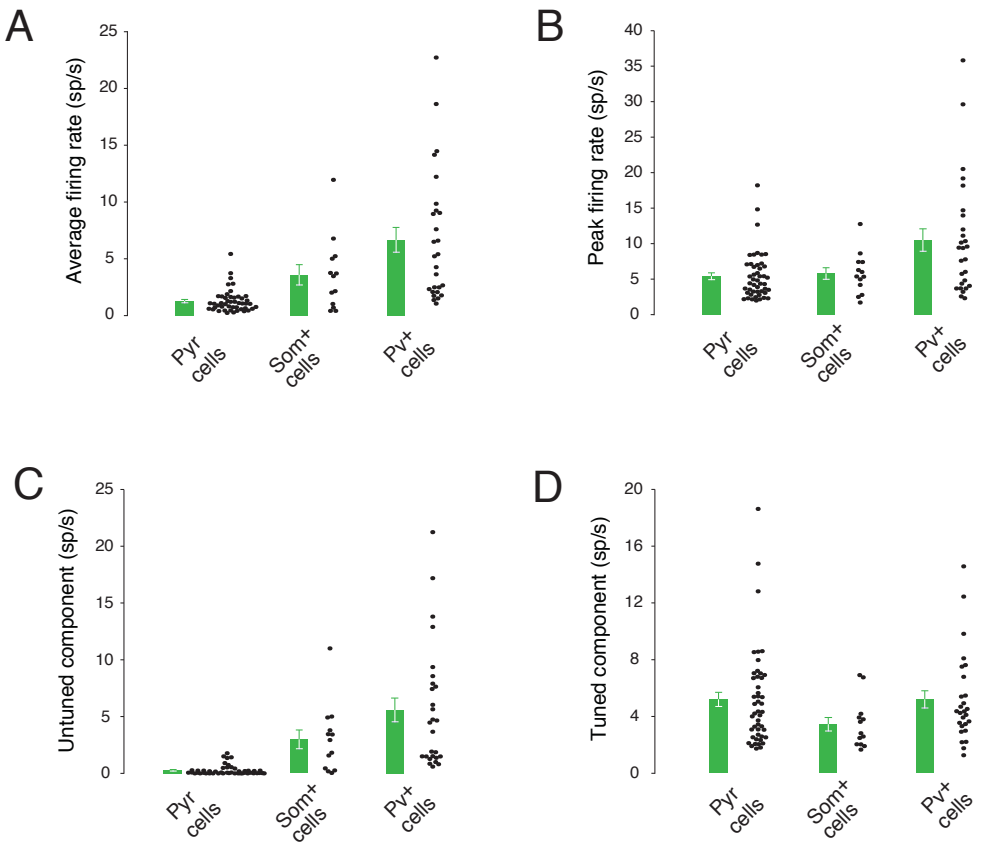

Figure 3.5 Firing frequency measures in Pyr, SOM$^+$ and PV$^+$ cells

A, Average firing rate differs significantly between pyramidal cells, SOM$^+$ interneurons and PV$^+$ interneurons (n = 47, 13, 27 Kruskal-Wallis test $P < 0.0001$, Dunn's multiple comparison test finds that: Pyr cells and SOM$^+$ cells are significantly different $P < 0.05$, Pyr and PV$^+$ cells are significantly different $P < 0.001$ but SOM$^+$ cells and PV cells are not significantly different). **B**, Peak firing rate differs significantly between pyramidal cells, SOM$^+$ interneurons and PV$^+$ interneurons (n = 47, 13, 27 Kruskal-Wallis test $P < 0.004$, Dunn's multiple comparison test finds that: Pyr cells and SOM$^+$ cells not significantly different, Pyr and PV$^+$ cells are significantly different $P < 0.01$, SOM$^+$ cells and PV cells are not significantly different). **C**, The untuned component differs significantly between pyramidal cells, SOM$^+$ interneurons and PV$^+$ interneurons (n = 47, 13, 27 Kruskal-Wallis test $P < 0.0001$, Dunn's multiple comparison test finds that: Pyr cells and SOM$^+$ cells are significantly different $P < 0.001$, Pyr and PV$^+$ cells are significantly different $P < 0.001$ but SOM$^+$ cells and PV cells are not significantly different). **D**, The tuned component does not differ significantly between pyramidal cells, SOM$^+$ interneurons and PV$^+$ interneurons (n = 47, 13, 27 Kruskal-Wallis test $P = 0.086$).

Having introduced these measures of visual tuning it is now time to look at how they compare between populations of the three different cell types. The previous example cells are a good indication of the properties but do not tell the whole story. Figure 3.5 summarises the four firing rate based metrics for populations of cells from the three cell types (Pyr cells n = 47, SOM^+ cells n = 13, PV^+ cells n = 27). Average firing rate differed significantly across the three cell types ($P < 0.0001$). A Kruskal-Wallis test was used in this case as not all of the data passed a normality test, which precluded the use of one-way ANOVAs. Pyr cells had the lowest mean firing rate while PV^+ interneurons had the highest (Pyr cells: 1.28 +/- 0.14 spikes/s, SOM^+ cells: 3.59 +/- 0.89 spikes/s, PV^+ cells: 6.67 +/- 1.10 spikes/s, all shown as mean +/- SEM, Figure 3.5 A). A Dunn's multiple comparison test showed the mean firing rate of Pyr cells to be significantly different from both SOM^+ ($P<0.05$) cells and PV^+ ($P<0.001$) cells, but the interneurons are not significantly different from each other, although the mean firing rate of SOM^+ cells is lower. For the peak firing rate, PV^+ are still the highest whereas Pyr cells and SOM^+ cells are similar (Pyr cells: 5.40 +/- 0.49 spikes/s, SOM^+ cells: 5.79 +/- 0.81 spikes/s, PV^+ cells: 10.50 +/- 1.59 spikes/s, Figure 3.5 B). Overall peak firing rate does differ significantly across the groups ($P = 0.004$) but only the Pyr cell versus PV^+ cell comparison is significant in the Dunn multiple comparison test ($P<0.01$). The untuned component representing the DC offset of the Gaussian from zero follows a similar pattern to the average firing rate (Pyr cells: 0.26 +/- 0.06 spikes/s, SOM^+ cells: 2.99 +/- 0.83 spikes/s, PV^+ cells: 5.58 +/- 1.04 spikes/s, Figure 3.5 C). This parameter differs significantly between cell types ($P<0.0001$) and Pyr cells are significantly different from SOM^+ ($P<0.001$) and PV^+ ($P<0.001$) cells in the Dunn's multiple comparison tests without the interneuron types being significantly different from each other. The tuned component, the amplitude of the Gaussian from peak to trough, is the only firing frequency parameter that is not significantly different between cell types ($P = 0.086$), with Pyr cells have a similar sized mean tuned component to PV^+ cells (Pyr cells: 5.19 +/- 0.50 spikes/s, SOM^+ cells: 3.44 +/- 0.48 spikes/s, PV^+ cells: 5.19 +/- 0.60 spikes/s, Figure 3.5 D). In summary Pyr cell tuning for orientation means that they differ from the interneurons in average firing and in their level of untuned component as they

tend to fire at low rates when the stimulus is at a non-preferred orientation. Although they fire at much higher rates when stimulated optimally their peak firing rate is not as high as PV^+ interneurons though it cannot be distinguished statistically from SOM^+ cell peak firing. The amplitude of the tuned component is similar across Pyr and PV^+ cells though lower in SOM^+ cells.

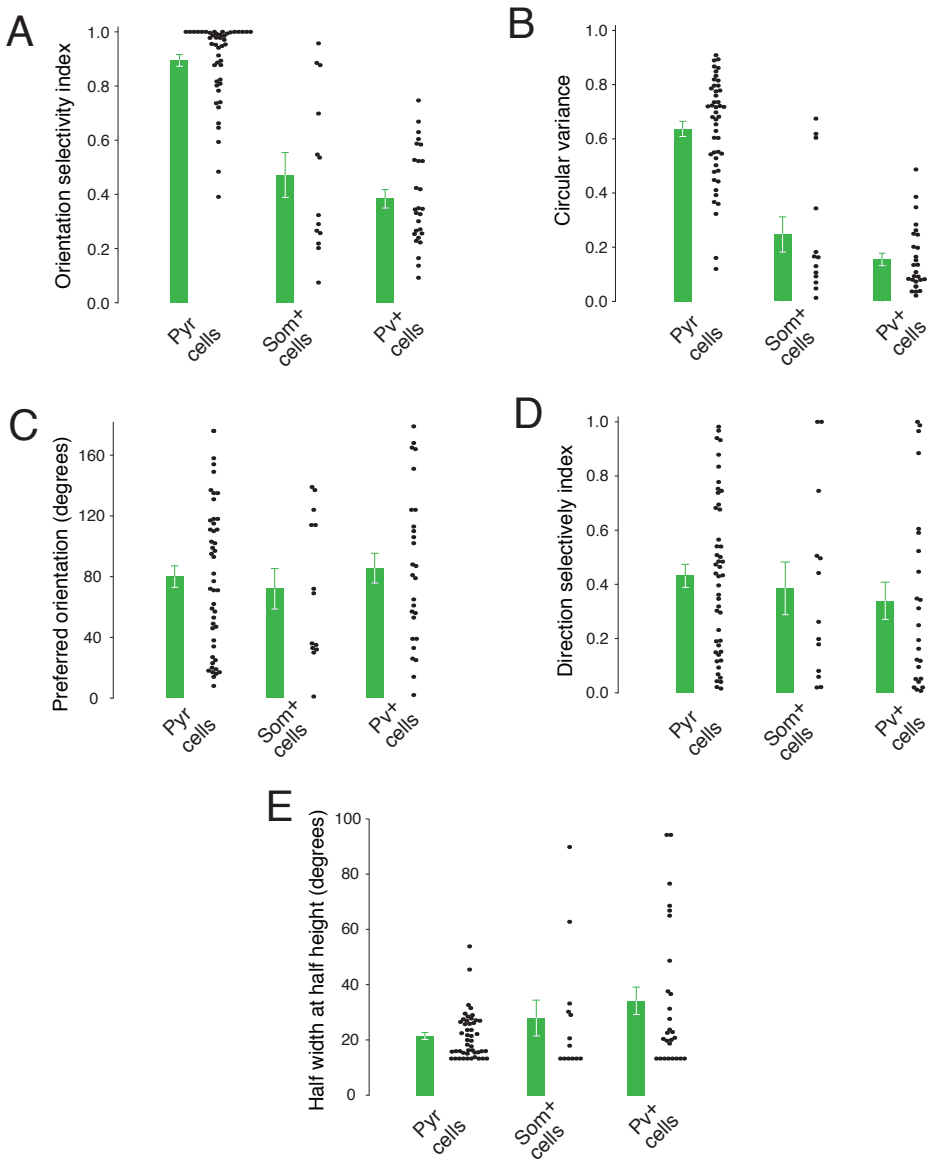

Figure 3.6 Further tuning measures for Pyr, SOM^+, PV^+ cells

A, The orientation selectivity index differs significantly between pyramidal cells, SOM^+ interneurons and PV^+ interneurons (n = 47, 13, 27 Kruskal-Wallis test $P < 0.0001$, Dunn's multiple comparison test finds that: Pyr cells and SOM^+ cells are significantly different $P < 0.001$, Pyr and PV^+ cells are significantly different $P < 0.001$ but SOM^+ cells and PV cells are

not significantly different). **B**, The circular variance differs significantly between pyramidal cells, SOM+ interneurons and PV+ interneurons (n = 47, 13, 27 Kruskal-Wallis test P < 0.0001, Dunn's multiple comparison test finds that: Pyr cells and SOM+ cells are significantly different P < 0.001, Pyr and PV+ cells are significantly different P < 0.001 but SOM+ cells and PV cells are not significantly different). **C**, Preferred orientation does not differ significantly between pyramidal cells, SOM+ interneurons and PV+ interneurons (n = 47, 13, 27 Kruskal-Wallis test P = 0.802). **D**, Direction selectivity does not differ significantly between pyramidal cells, SOM+ interneurons and PV+ interneurons (n = 47, 13, 27 One-way ANOVA P = 0.500). **E**, Half width at half height does not differ significantly between pyramidal cells, SOM+ interneurons and PV+ interneurons (n = 47, 13, 27 Kruskal-Wallis test P = 0.345).

Figure 3.6 compares tuning properties across the three cell types. The orientation selectivity index shows Pyr cells to be highly tuned in many cases though with some tapering spread towards lower levels of tuning. SOM^+ cells span the range from cells that approach the highest levels of Pyr cell tuning to almost completely untuned cells responding equally to all orientations. PV^+ cells are biased towards lower orientation selectivity indices but still have some cells that reach above an OSI of 0.6 (Pyr cells: 0.89 +/- 0.02, SOM^+ cells: 0.47 +/- 0.08, PV^+ cells: 0.38 +/- 0.03, Figure 3.6 A). There is a clear significant difference across groups with Pyr cells being significantly different from SOM^+ cells ($P<0.001$) and PV^+ cells ($P<0.001$, Dunn's multiple comparison test). Though they span different ranges the PV^+ cells and SOM^+ cells are not significantly different from each other. Circular variance is a similar measure, but it takes into account data from all orientations. Results are similar: As with OSI the Pyr cells are significantly different from the interneuron groups but not the interneurons from each other (Pyr cells: 0.64 +/- 0.03, SOM^+ cells: 0.25 +/- 0.06, PV^+ cells: 0.15 +/- 0.02, Figure 3.6 B).

Preferred orientation is expected to be distributed randomly over all possible orientations. This should be most easily measured for the Pyr cells and PV^+ interneurons which have the highest number of samples. The mean therefore would be expected to be around 90^o for all cell types (Pyr cells: 80.04 +/- 7.07 degrees, SOM^+ cells: 72.00 +/- 13.29 degrees, PV^+ cells: 86.56 +/- 9.62 degrees,

Figure 3.6 C) and these cell types would not be expected to be significantly different from each other, which is the case. Direction selectivity varies widely within each group. All groups have cells that are highly directionally selective with scores around one and cells that respond equally to both directions with scores around zero. The means of the different cell types (Pyr cells: 0.43 +/- 0.04, SOM^+ cells: 0.39 +/- 0.10, PV^+ cells: 0.34 +/- 0.07, Figure 3.6 D) are not significantly different from each other (P = 0.500). It is however important to note that direction selectivity is taken from the Gaussian fit and while in Pyr cells this makes up the vast majority of the response (Figure 3.5 C) in the interneurons the untuned component is much more prominent (Figure 3.5 C) so that the Gaussian tuned portion of the response can be a much smaller part of the total response. In addition the interneurons, especially PV^+ cells, tend not to be as well fit by Gaussians as the Pyr cells.

The final tuning property is the HWHH of the Gaussian fits. From the OSI and CV measurements, one might expect the tuning of the interneurons, and especially the PV^+ cells, to have much wider Gaussians. However this is not the case, often the Gaussian response components of interneurons are narrow but ride on a large untuned component (see for example PV^+ cell in Figure 3.4 C). The mean HWHHs for the different cell types (Pyr cells: 21.44 +/- 1.24 degrees, SOM^+ cells: 27.91 +/- 6.47 degrees, PV^+ cells: 34.14 +/- 4.97 degrees, Figure 3.6 E) do not differ significantly (P = 0.345). The cluster of identical values at the low end of the HWHH distribution across cell types is the minimum HWHH value attainable from the spacing of grating orientations we presented (22.5^o between orientations). In summary, both interneuron types differ significantly from Pyr cells in OSI and CV, but not from each other. For the measures of preferred orientation, direction selectivity and HWHH there are no significant differences across the three groups.

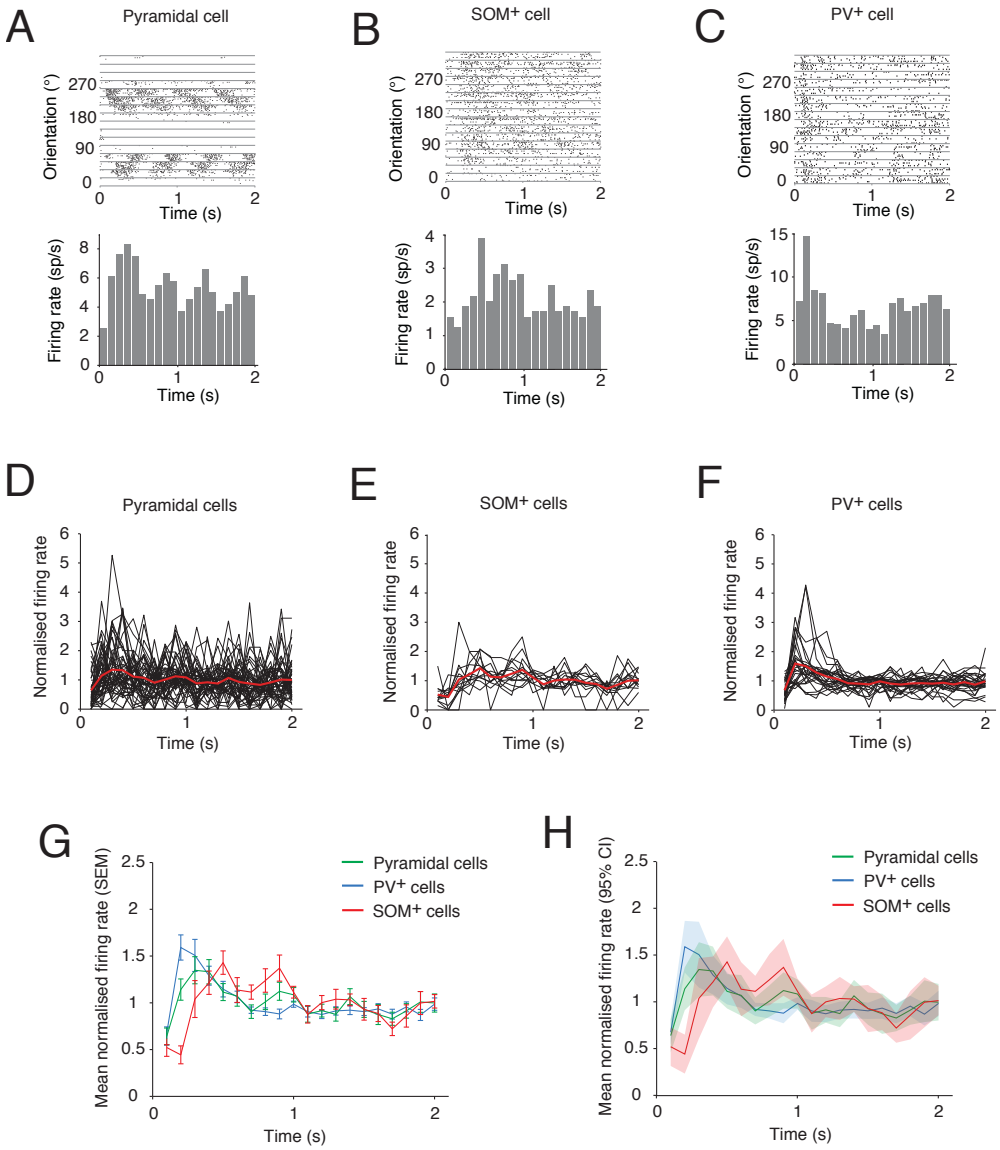

Figure 3.7 Spike timing across cell types during 2 seconds of visual stimulus

A, An example pyramidal cell spike raster and histogram. **B**, An example SOM⁺ cell. **C**, An example PV⁺ cell. **D**, All pyramidal cells (n = 47) normalised by dividing each cell by its mean firing rate plotted as black lines with the population mean in red. **E**, All SOM⁺ interneurons (n = 13), same layout as D. **F**, All PV⁺ interneurons (n = 27), same layout as D. **G**, Mean normalised firing rates for all cell types with SEM error bars (Pyramidal cells - green, SOM⁺ cells - red, PV⁺ cells - blue). **H**, Layout is the same as G but with 95% confidence interval as the error envelope.

Having compared the three cell types in terms of their firing rates and tuning it is also important to look at the time course of these responses during the two seconds of stimulus presentation. Figure 3.7 A-C shows the firing patterns of three example cells across all stimulus presentations in raster form, then summarized as a histogram. Histograms were produced for all cells and then each one was normalized by its mean firing rate, so that cells of different firing rates could be compared in terms of the timing of changes in spike rate. These normalized data are plotted as black lines in Figure 3.7 D-F. The population means of the normalized histograms for the three cell types are plotted for comparison with SEM and 95% confidence interval respectively (Figure 3.7 G-H). These summary plots show that PV^+ cells reach their maximum firing within 200 ms of stimulus onset with Pyr cells peaking next, followed by SOM^+ interneurons. To examine these early response components further, Figure 3.8 shows the first 500 ms after stimulus onset, and responses are binned in 50 ms rather then 100 ms bins (Figure 3.8 G,H).

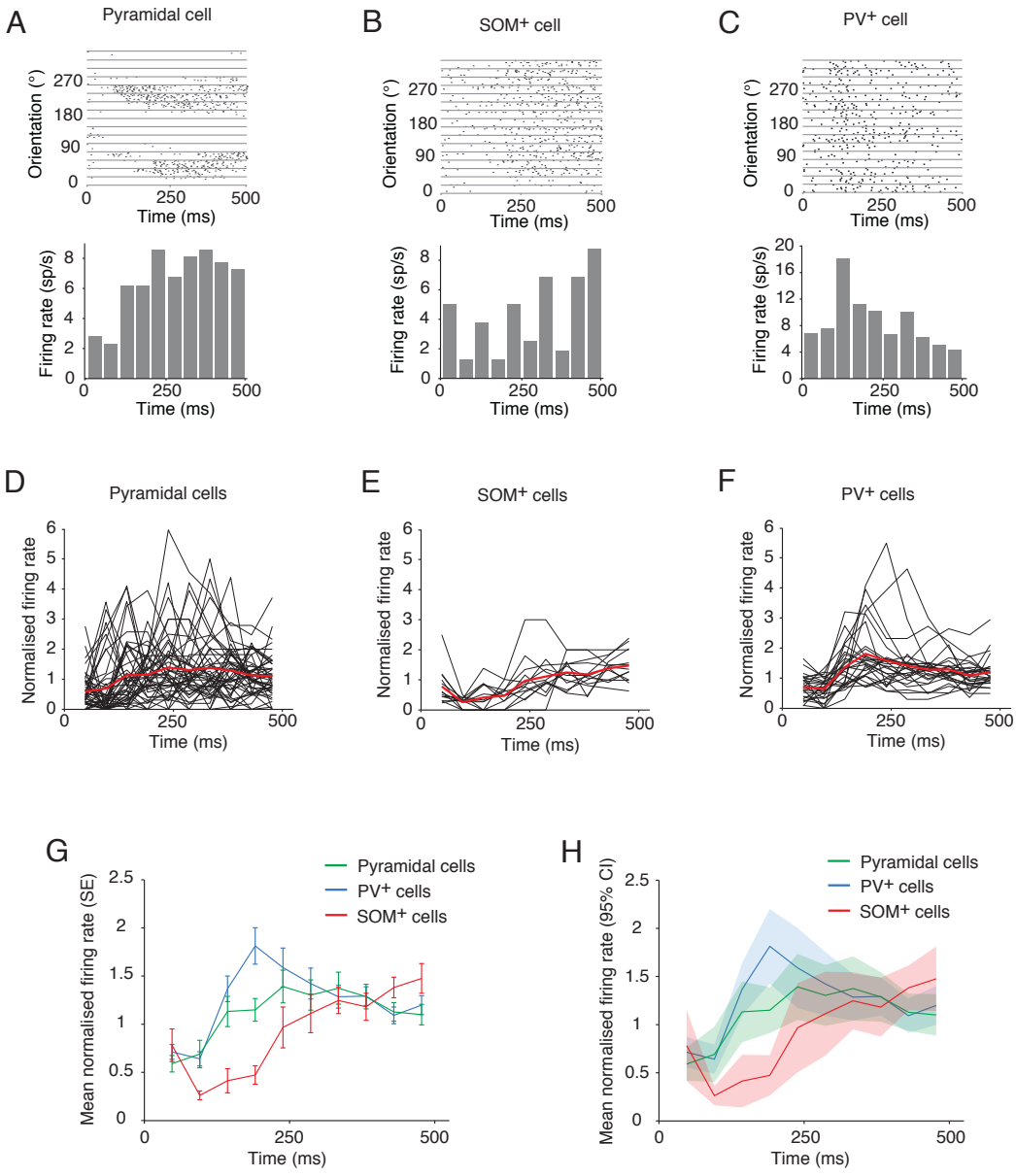

Figure 3.8 Spike timing across cell types during the first 500 ms of visual stimulus

A, An example pyramidal cell spike raster and histogram. **B**, An example SOM⁺ cell. **C**, An example PV⁺ cell. **D**, All pyramidal cells (n = 47) normalised by dividing each cell by its mean firing rate (over the whole 2 seconds) plotted as black lines with the population mean in red. **E**, All SOM⁺ interneurons (n = 13), same layout as D. **F**, All PV⁺ interneurons (n = 27), same layout as D. **G**, Mean normalised firing rates for all cell types with SEM error bars (Pyramidal cells - green, SOM⁺ cells - red, PV⁺ cells - blue). **H**, Layout is the same as G but with 95% confidence interval as the error envelope.

Here we see that the PV^+ cell peak in spiking occurs ~200 ms after stimulus onset. Pyr cells increase around the same time but peak later, at ~250 ms after stimulus onset (Figure 3.8 G,H). SOM^+ interneurons reach their peak latest and are still rising at 500 ms (Figure 3.8 G,H) after showing an initial reduction below mean firing between 100 and 200 ms following stimulus onset. It should be noted that throughout this timing analysis onset means the transition from one orientation of grating to another rather than the transition between a grey screen and a grating. Looking beyond the first 500 ms of activity the SOM^+ interneurons remain elevated in their activity relative level of activity compared to Pyr and PV^+ cells for the following 500 ms. After the 1 second mark until the end of the stimulus all cell types settle into a more steady state period when the firing frequency relative to the mean is distributed evenly over time.

3.3 Discussion

3.3.1 Summary of findings

Early experiments on the GAD65 animals allowed the establishment of the targeting technique (Figure 3.1) and showed that interneurons could be quite well tuned for orientation (Figure 3.2 C) an idea which was originally controversial (Sohya et al., 2007; Liu et al., 2009). However it soon became obvious that to understand interneuron diversity, clearly distinct interneuron groups needed to be targeted and compared rather than the mix of subtypes labeled in the GAD65 line. At the same time low firing rates under ketamine/xylazine and the publication of an excellent survey of visual cortex (Niell and Stryker, 2008) showed that chlorprothixene/urethane would be a better anaesthetic. It permitted the production of reliable large amplitude visual responses and their survey provided a reference to compare with data collected from the newly arrived GIN and PV-GFP animals. The other main parameter optimized during this time was the visual stimulus with the decision to omit gray blanks between stimuli. This concentrated

the responses on the transition between different grating orientations rather than the transition between grey screen and grating, which appeared to create a wide range of differential onset effects (Figure 3.3).

The data collected from Pyr, SOM^+, and PV^+ cells show that the largest and most frequent significant differences were between excitatory Pyr cells and the inhibitory interneurons. This was true for average firing rate, the untuned component of spiking, OSI, CV. Interestingly however, in all of those measures there appears to be a graded increase or decrease from Pyr cells to PV^+ cells with SOM^+ cells occupying the intermediate position. This is exemplified by the peak firing rate comparison, in which significant differences only occur between Pyr and PV^+ cells and not between SOM^+ cells and PV^+ cells. One reason that SOM^+ and PV^+ cells cannot be statistically separated in this data could be due to the lower number of SOM^+ recordings (n = 13) that may prevent the finer differences between SOM^+ and PV^+ cells from emerging. In the same way that SOM^+ cells have responses that appear intermediate between Pyr and PV^+ cells, their intrinsic electrophysiology is also intermediate between Pyr cells and PV^+ interneurons along many of the dimensions measured (Ma et al., 2006). It is interesting to note that the tuned component, direction selectivity index and HWHH measurements do not differ significantly between the groups. This suggests that many aspects of the orientation-tuned response component are similar across cell types but that these Gaussian responses ride on top of a large untuned component in SOM^+ and PV^+ cells.

3.3.2 Comparison with prior reports

During the course of this project many papers were published that examined aspects of interneuron tuning using a range of experimental configurations (different genotypes and stimuli). From this lively area of research eight papers are highly relevant to this study (Sohya et al., 2007; Niell and Stryker, 2008; Liu et al., 2009; Kerlin et al., 2010; Ma et al., 2010; Runyan et al., 2010; Hofer et al., 2011; Atallah et al., 2012). Not all of them look at all aspects of the data shown

here, but by comparing parameters one by one it is possible to assess how closely the data in this thesis match the field. Broadly, my data are in agreement with the findings of others which have PV+ interneurons as the highest firing and most broadly tuned, SOM^+ cells in an intermediate position though most similar to PV^+ cells and Pyr cells as more highly tuned with the lowest mean firing rates.

Looking first at average and peak firing rates produced by visual stimulation, the data presented in this thesis agree broadly with Niell and Strkyer (Niell and Stryker, 2008), although that study finds higher peak spiking values (Niell and Stryker, 2008 suppl fig 3) because stimuli were individually optimised for each neuron. However they do find an almost factor of 2 difference between Pyr cell and interneuron firing (likely to be predominantly PV^+ cells) as found in this study for peak spiking (Figure 3.5 B). Liu et al. Figure 4 D (Liu et al., 2009) find a similar trend from FS cells (fast spiking likely to be PV^+ (McCormick et al., 1985)) with the highest average firing rate, to Pyr cells with the lowest rate. GFP^+ regular spiking cells are likely to contain some SOM^+ cells and these are found to have an intermediate level of firing. Again, firing rates are generally higher than in this thesis because the stimuli were optimized for individual cells, but the relative pattern is the same. Ma et al. (Figure 1 G (Ma et al., 2010)) find SOM^+ cells fire at a significantly lower mean rate than PV^+ cells. This agrees with the trend in this thesis (Figure 3.5 A) though here the difference did not reach statistical significance. It is important to note that while the same GIN animal line (Oliva et al., 2000) was used to identify the SOM^+ cells, they used the G42 line (Chattopadhyaya et al., 2004) for the PV^+ cells while the PV-GFP line (Meyer et al., 2002) was used here. Runyan et al. (Runyan et al., 2010) recorded from PV^+ cells but do not show a mean firing rate or peak firing rate summary. The individual PV^+ cell-attached recordings they show are quite low frequency (~ 0.7 to ~ 3.5 peak firing frequency spikes/s). Atallah et al. (Atallah et al., 2012) used similar grating stimuli to this study, also not optimizing them to each individual cell. The PV^+ cell and Pyr cell average visually evoked spike rates found in this thesis closely match their results. Overall there is broad agreement that PV^+ cells have mean firing rates 2-3 times greater than Pyr cells and peak firing rates around 2 times greater. The absolute values of these firing rates depend one the

exact method of stimulus presentation. SOM^+ cell firing rates appear to be intermediate between the groups.

Many of these groups looked at the difference between OSI and CV across the different cell classes. Again there is variability in the mouse lines and the visual stimuli used. In addition there are many measures used for orientation selectivity. The main two measures used were either OSI, the way it is defined in this thesis (see methods) comparing the preferred peak to trough ratio or as a circular variance measurement which is a vector sum of all the orientations not just the peak and trough. One of the first mouse interneuron orientation tuning studies that used a genetic mouse line was carried out by Sohya et al. (Sohya et al., 2007) and found that interneurons are more broadly tuned than Pyr cells. While that is in general true and agrees with the data in this thesis, they did not find any cells that were well tuned (CV > 0.5) and only one cell that had a CV higher than 0.4 (Sohya et al. 2007 Figure 4 B). As they only sampled 28 interneurons it is possible that they did not identify cells with CV's approaching 0.7 that I found or that the animal that they used (supposed to express GFP in all interneurons) has some bias away from SOM^+ cells which tended to have higher CV scores. Niell and Stryker used the same measure as I did for OSI (Niell and Stryker, 2008), their Pyr cell data matches that data in this study (Figure 3.6 A) and they see interneurons with high levels of orientation tuning although they are not able to identify them with certainty. For the Liu et al. study, their Global OSI measure equates to the CV measure in this thesis. They use the same mouse line as is used in the Sohya et al. experiment (Tamamaki et al., 2003) and get similar results finding interneurons have a lower mean CV than Pyr cells but missing out on identifying any more highly tuned interneurons. The Ma paper also calls their CV measure Global OSI and use mouse lines to identify SOM^+ and PV^+ cells separately, their results are in very high concordance with mine with similar mean CVs and ranges of CV for all three cell types (apart from finding more weakly tuned Pyr cells than I do). This suggests that unlike when using the GAD67 animal used by Sohya et al. (Sohya et al., 2007) and Liu et al. (Liu et al., 2009), when you target SOM^+ cells specifically it is possible to find more highly tuned interneurons. Runyan et al. use a modified version of CV so comparison is more

difficult but it appears they find some highly tuned PV^+ cells which are as tuned as the most highly tuned Pyr cells, the data in this thesis does not agree with this and nor do the other papers quoted so far. They used a non-flexed viral construct injected into a Cre animal so it is possible they have some breakthrough expression non-PV^+ cells as shown by their immunostaining where not 100% of the labeled cells were positive for GABA. Kerlin uses the CV measure and the data broadly agree with this thesis, although the mean CV for excitatory cells is significantly lower (Figure 5, (Kerlin et al., 2010). It is not obvious why this is although the imaging experiments tend to find lower tuning scores for Pyr cells (Sohya et al., 2007; Hofer et al., 2011), possibly because they sample more cells, don't sample all of the spikes produced by cells or with cell-attached recordings there is some experimenter bias towards selecting tuned cells for recording. Atallah et al. also find a Pyr cell CV distribution that is shifted to be lower than that shown in this thesis (Figure 3.6 B). In summary there is agreement that Pyr cells differ clearly from interneurons, having a much higher mean orientation tuning though their distribution overlaps somewhat with the interneuron distributions. Experiments that have looked at separating SOM^+ cells (or non-FS cells) from PV^+ cells (or FS cells) show that there is some difference in the distributions with SOM^+ cell populations containing some highly orientation tuned cells (Ma et al., 2010). The data in this thesis agree best with Ma et al. who used the same mouse line for the SOM^+ cells as was used in this thesis.

The remaining two measures to compare with the literature are direction selectivity and tuning width. The direction selectivity data in this thesis agree with Niell and Stryker for both Pyr cells and interneurons. The PV^+ cell data disagrees with Runyan et al and Ma et al. The Runyan et al. data is slightly suspect as it disagrees with all of the other papers over PV^+ cell OSI. The Ma paper agrees with the rest of the data in this thesis so it is difficult to interpret this isolated discrepancy. Differing fitting algorithms may play a role, so without comparing raw data, it is difficult to draw any conclusions. Liu et al. and Atallah et al. show tuning width data that agree with what is shown here. Namely that Pyr cells have narrower tuning widths than interneurons, however they both find this difference to be significant while I do not ($P = 0.345$). There are fewer comparisons to make

for these parameters as fewer groups looked at direction selectivity and tuning width.

It is more difficult than might be expected to compare across different experiments that purport to study very similar phenomena. Differences in animal lines, visual stimulus protocols and a diversity of measures often make direct comparisons impossible. However the important distinctions between Pyr cells and interneurons in terms of firing rate and orientation are agreed with across these studies. The distinction between SOM^+ cells and PV^+ cells is less clear, this thesis finds a trend that doesn't reach significance while other studies find these groups to be significantly different.

In terms of the timing of the responses of different cell types the data in this thesis agree with the one other study that has looked at the difference in response timing between the SOM^+ and PV^+ cells (Ma et al., 2010). This study did not include Pyr cells but did find PV^+ cells to reach peak spiking before SOM^+ cells on a similar time scale to the results in Figure 3.7 and 3.8. Their results find both peaks to be slightly earlier but this could be due to their use of flash stimuli which may drive the circuit harder than the transition between two orientations of grating used in this thesis (this is also borne out by the larger relative amplitude of their PV^+ cell onset responses). Although SOM^+ cells were originally named low threshold cells and were thought to be early responders (Wang et al., 2004; Fanselow et al., 2008), a combination of the facilitating input they receive from Pyr cells (Thomson et al., 1993; Thomson, 1997; Thomson and Deuchars, 1997; Reyes et al., 1998; Wang et al., 1999; Kapfer et al., 2007; Silberberg, 2008) and the lack of excitatory projections directly onto them from layer 4 of cortex (Adesnik et al., 2012) probably contributes to their later response.

4 Optogenetic manipulation of small populations of somatostatin positive neurons

4.1 Introduction

The goal of this thesis is to learn how interneurons function within the cortical circuit, and what they contribute to the cortical processing of sensory input. Having examined how interneurons respond to visual stimuli the next step is to manipulate their activity and measure the effect of this on the other components of the network. Ideally this manipulation would be specific to a particular interneuron type and be as noninvasive as possible. There is also the question of how large the ideal manipulation would be; too large and the cortical network would be affected so profoundly that it would operate in a very different and potentially uninformative parameter space; too small and the effect could be undetectable. At the start of this project ChR2 had recently been implemented in mammalian neurons (Boyden et al., 2005). It provides the ideal tool for the stimulation of multiple cells with light and once expressed in the neurons can be activated without need to invade the tissue. This new protein could be combined with an exciting new technique that had been pioneered in our lab to permit the delivery of plasmids into a single cell or small number of cells (Kitamura et al., 2008; Judkewitz et al., 2009). At that time, the range of cell type-specific Cre lines now available did not exist. As a result, viral methods delivering a genetic construct of choice to large numbers of a single cell type were still problematic (Luo et al., 2008). Using transgenic animals expressing GFP in interneurons

(more specifically in SOM^+ interneurons in the case of the GIN mouse line that had arrived in the lab by this time (Oliva et al., 2000)) it was possible to visually target the electroporation of ChR2 to only one interneuron type. This chapter shows how small numbers of these interneurons can be electroporated to express ChR2 and spike under light control. The effects of this manipulation were small and could be detected in a population of putative PV^+ interneurons but not in Pyr cells, suggesting a differential effect of SOM^+ activity on the visual responses of PV^+ and Pyr neurons.

4.2 Results

Initially there was a period of testing the electroporation of ChR2 into SOM^+ interneurons, as the technique had only previously been used on Pyr cells (Kitamura et al., 2008; Judkewitz et al., 2009). Once the effects of ChR2 on SOM^+ cells were known and had been shown to be reproducible, other cells surrounding the electroporated cells were recorded to measure the effect of stimulation. The cortical circuit in which SOM^+ cells are embedded is shown in Figure 4.1. SOM^+ interneurons labeled yellow in the diagram are known to inhibit both Pyr cells (with a bias towards inhibiting the dendrites rather than soma) and PV^+ cells (Gibson et al., 1999; Wang et al., 2004). In turn PV^+ interneurons inhibit Pyr cells and SOM^+ interneurons and Pyr cells excite both types of interneuron. In a fully, and antagonistically, connected network like this it is not trivial to predict what will happen when you change the activity of one of the components to cells within the local area (Figure 4.1 B, C). By increasing SOM^+ cell activity, the other two cell types will be inhibited, but as PV^+ cells also inhibit Pyr cells, the resulting decrease in PV^+ activity would at the same time disinhibit Pyr cells. The ultimate effect depends upon the patterns of connectivity of SOM^+ cells and PV^+ cells and the strength of those connections. If SOM^+ inhibition was the most powerful force in the network one could hypothesise a situation in which all other cells are inhibited, despite some weak disinhibition created by inhibiting PV^+ cells (see Figure 4.1 C, Hypothesis 1). If there were a mixture of connectivity

in the local circuit where in some places direct inhibition of Pyr cells by SOM^+ cells dominated and in others disynaptic disinhibition via PV^+ cells dominated, the result could look more like a mixture of excitation and inhibition in the surrounding Pyr cells (Figure 4.1 C, Hypothesis 2). Finally, if disynaptic disinhibition is by far the most powerful route then all of the surrounding Pyr cells would be excited (Figure 4.1 C, Hypothesis 3). One would also expect the rarer PV^+ cells in the population to be inhibited in this situation (these cells are not shown in the diagram).

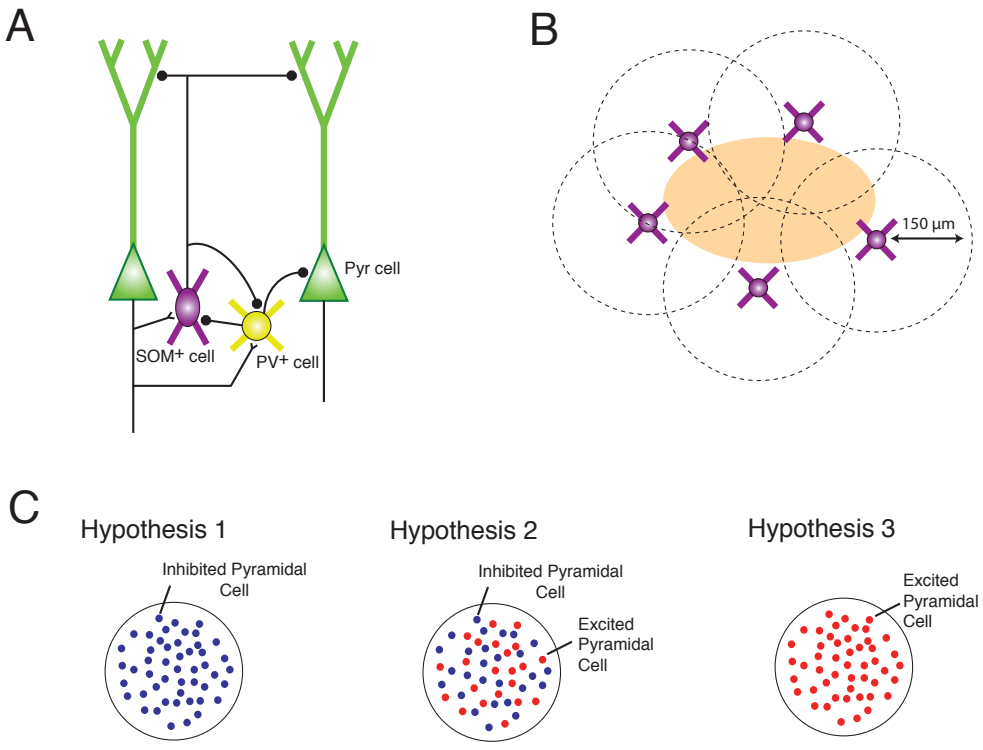

Figure 4.1 Single cell electroporation: network, location and hypotheses

A, Cell types and their connectivity within layer 2/3 of visual cortex, pyramidal cells in green, SOM^+ cells in purple and PV^+ cells in yellow. Excitatory synapses are shown by a black v-shape, inhibitory synapses are shown as filled black circles. **B**, A top down view of multiple electroporated SOM^+ interneurons with the most targeted recording are shown in beige. The 150 µm zone around each interneuron was the furthest recorded pyramidal cells were from an electroporated cell. **C**, Three hypotheses of the outcome of stimulating a small number of SOM^+ interneurons on the surrounding cells. In the first hypothesis all of the cells in the local region are inhibited, in the second hypothesis some are inhibited while others are excited, in the third hypothesis all pyramidal cells are excited.

4.2.1 Establishing single cell electroporation in interneurons and refining ChR2 stimulation parameters and experimental protocol

To deliver ChR2 to the GFP expressing SOM$^+$ interneurons in a GIN animal, a pipette containing intracellular solution and DNA plasmids was positioned juxtacellularly to individual interneurons, one by one. A voltage pulse protocol transiently permeabilised the cell membrane and pipette solution, including the DNA plasmids, entered the cells (Figure 4.2 A,B with further details in the methods section). The plasmids delivered in this experiment were a red fluorescent protein (TurboFP, a.k.a. Katushka, (Shcherbo et al., 2007)), to allow the identification of the transfected cells 48 hours later, and ChR2, to permit optogenetic manipulation.

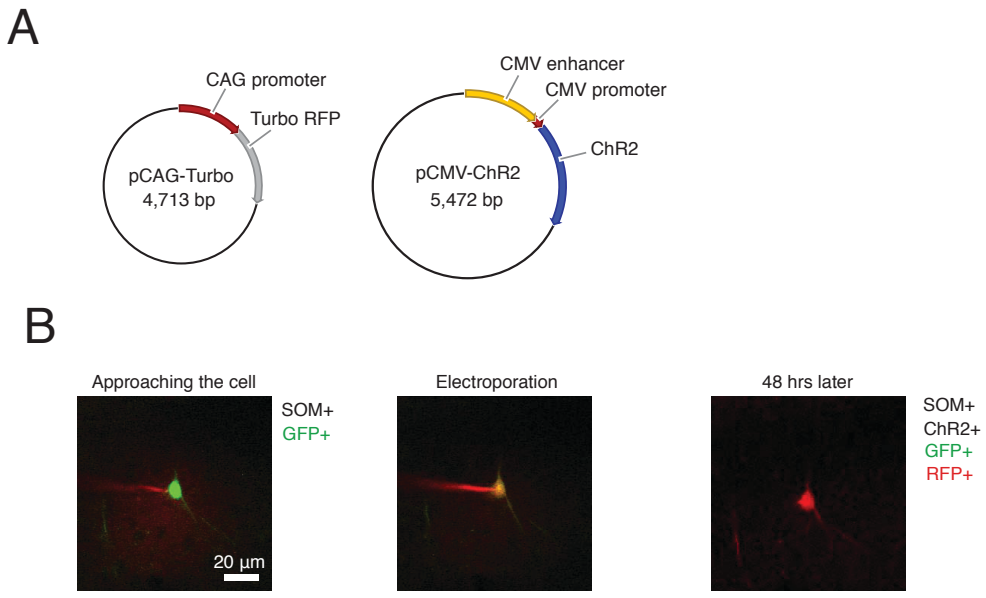

Figure 4.2 Single cell electroporation of SOM$^+$ interneurons with ChR2 and RFP

A, The two plasmids that were co-electroporated into SOM$^+$ interneurons one containing Turbo-RFP the other ChR2. **B**, Targeted single cell electroporation of a SOM$^+$ cell visualized by two-photon microscopy. First, an eYFP-expressing SOM$^+$ cell is visualized and approached by a micropipette containing a mixture of red dye and plasmid DNA for ChR2 and red fluorescent protein (RFP). A brief train of voltage pulses electroporates the plasmid-dye mixture into the cell, as shown by the red color visible in the soma. Two days later, expression is verified by visualization of RFP.

After the 48 hour wait giving time for the plasmids to be expressed, the cells that were expressing both GFP and RFP were targeted for cell-attached recordings. These cells were tested to establish whether ChR2 had been correctly expressed and find out the parameters of blue light necessary to produce spikes, ideally single spikes, at different frequencies. 1 ms pulses of blue light from an LED (more details in the Methods) were sufficient to produce spikes in the SOM$^+$ interneurons.

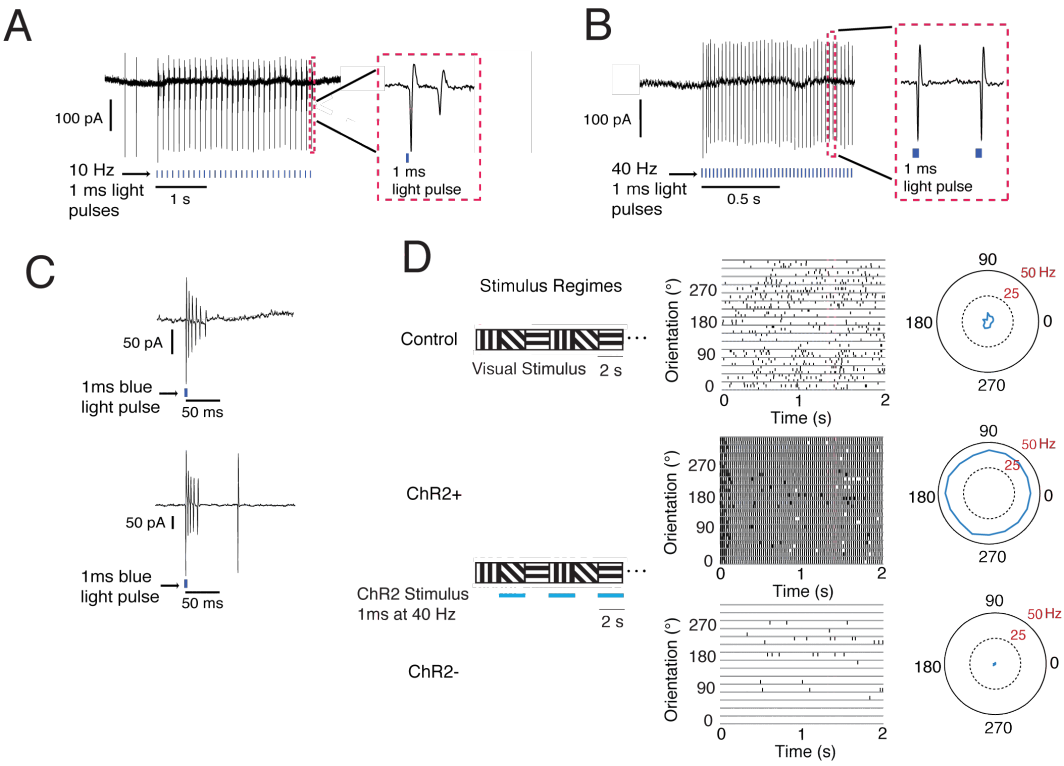

Figure 4.3 ChR2 driven spiking in SOM$^+$ interneurons

A, An example cell-attached recording from an electroporated SOM+ interneuron expressing ChR2 driven with 10 Hz, 1 ms blue light pulses. Red inset shows multiple spikes produced by a single blue light pulse. **B**, A second example, same layout as A, with blue light pulses at 40 Hz. The red inset shows a single spike being driven by each blue light pulse. **C**, Examples of single 1 ms blue light flashes in an electroporated SOM+ interneuron showing multiple spikes produced. **D**, A set of recordings from a ChR2 expressing SOM+ interneuron in the control condition showing the visual stimulus, a firing raster and radial plot. Below it, in the same format, are the responses for the same cell during interleaved 2 s of 40 Hz blue light pulses (ChR2+) separated by 2 s of no blue light pulses (ChR2-).

At 10 Hz stimulation frequency these light pulses produced spikes reliably and even multiple spikes per light pulse (Figure 4.3 A). 40 Hz stimulation frequency produced single spikes on each blue light pulse and did not produce any misses, meaning pulses of blue light producing no spikes (Figure 4.3 B). Single light pulses after a period without blue light produced many spikes, sometimes up to 6 (Figure 4.3 C) as all of the ChR2 molecules were in their deinactivated state. In contrast, during a train of pulses a proportion of molecules would be in an inactive state according to the ChR2 photocycle (Bamann et al., 2008), resulting in fewer spikes. Using an interleaved protocol, a SOM^+ cell would be stimulated for 2 seconds during the presentation of a particular grating, and then not for the following 2 seconds of visual stimulation. In this way there were 16 grating directions, each one with and without ChR2 stimulation for comparison (Figure 4.3 D). In the periods of non-stimulation the SOM^+ cell firing rate was depressed below normal, probably due to a cell-intrinsic mechanism following strong ChR2 stimulation. This was hard to avoid as it took tens of seconds for the SOM^+ cells to return to a normal firing pattern, so it was not practical to wait for this given the short recording time. This meant that the control period for these experiments (labeled ChR2- in Figure 4.3 D and Figure 4.5 B) is actually a period of lower spiking in these cells.

It is important to confirm that the spiking properties seen in the example cells in Figure 4.3 are consistent across electroporated cells. This is demonstrated by a summary of the number of spikes produced on average (n = 4) by a single light pulse within a train at different frequencies (Figure 4.4 A). At lower frequencies many spikes are often produced by a single blue light pulse and at the highest frequencies many blue light pulses do not produce any spikes at all. At 40 Hz, 1 ms blue light pulses produced a single spike over 90% of the time with almost no misses (Figure 4.4 A). This is also shown in a plot of the probability of a blue light pulse resulting in any spikes, this probability remains very high until 40 Hz after which it tails off as the SOM^+ cell is unable to keep up with the stimulation frequency (Figure 4.4 B). As a result of this analysis, 40 Hz was chosen as the stimulation frequency for all subsequent experiments. Not only did this allow us to reliably control the number of spikes elicited it also accounted for other

important factors: first, the stimulation frequency is significantly higher than the normal SOM$^+$ cell visual response rates, which increases the likelihood of evoking a visible effect in neighbouring cells when only a small number of SOM$^+$ cells were being stimulated. At the same time, the stimulation frequency is not so high that either the SOM$^+$ cell could not sustain those firing rates over long periods of time, or that it would affect the network unduly, driving it into an unrealistic regime of activity. Interleaved 40 Hz stimulation was followed by SOM$^+$ cells over many hours and is unlikely to change the large-scale network state in visual cortex during visual stimulation.

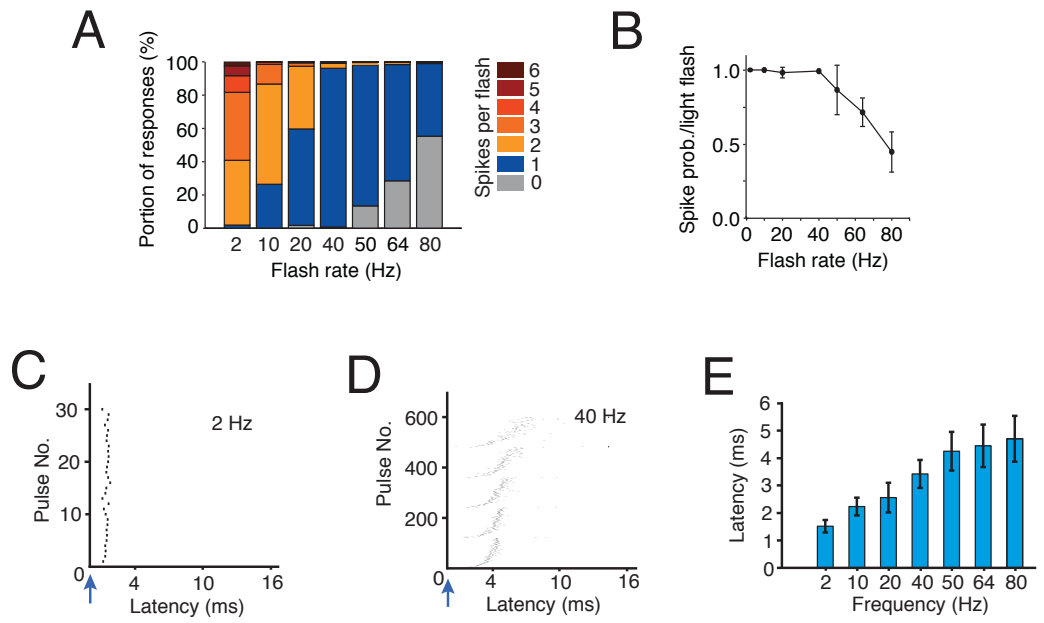

Figure 4.4 Summaries of ChR2 driven spiking in SOM$^+$ interneurons

A, A summary of the number of spikes produced by 1 ms blue light pulses at different frequencies (n = 4) shown as coloured stacked bars with each colour representing the proportion of spikes of that number according to the colour key. **B**, The probability of getting any spikes following a 1 ms light pulse at different frequencies (n = 4). **C**, An example raster plot of spike latency from blue light pulse (indicated by the blue arrow) during a 2 Hz spike train (only the first spike is shown for each trial). **D**, An example raster plot of spike latency from blue light pulse (indicated by the blue arrow) during five 3 s, 40 Hz spike trains. **E**, A summary of latency to first spike following the 1 ms blue light pulse at different frequencies (n = 4, error bars are SEM).

In addition, the spike latency from blue light pulse was examined to test how consistent it was and whether it was affected by stimulation frequency. At low stimulation frequencies spikes were consistently produced very soon after the blue pulse (Figure 4.4 C), while at higher frequencies the spikes occur at longer latencies which varied with the position of the pulse in the train, the later in the train the longer the latency (Figure 4.4 D). Mean latency at 40 Hz stimulation was 3.44 ms (Figure 4.4 E).

4.2.2 Activating small numbers of SOM+ cells and measuring their influence on surrounding cells

Having established that single cell electroporation of ChR2 into SOM^+ interneurons can be used to reliably stimulate them at 40 Hz, recordings could now be made from surrounding cells to measure the effect of this manipulation. Nearby cells were defined as those not further than 150 μm from an electroporated SOM^+ interneuron (Figure 4.1 B). Figure 4.5 A shows an image from one such experiment in which 4 SOM^+ cells are electroporated and express RFP, and a recording is being made from a putative Pyr cell. The Pyr cell cannot be seen directly as it is unlabelled, it could however be identified by negative staining during pipette approach. The structure of the experiment is shown as a schematic in Figure 4.5 B. Gratings of all 16 directions were shown in a random order once with ChR2 stimulation and once without. Recordings were made from surrounding cells and from SOM^+ interneurons to check that they were correctly expressing ChR2 (usually one or two SOM^+ neurons were tested per experiment). The recordings from the surrounding cells could then be analysed to compare their visual responses with and without ChR2 stimulation of SOM^+ interneurons. Before moving on to this comparison, a control was required to demonstrate that the blue light used to stimulate ChR2 did not change the activity of neurons in cortex on its own, whether influencing cells directly or stimulating the retina to change firing patterns. Electroporations were carried out on SOM^+ interneurons using only RFP plasmids and not ChR2. This meant that the surgery and

electroporation were the same as in the normal experiment, the only difference being that the SOM$^+$ cells did not express ChR2 and could therefore not be activated by blue light. These experiments found that neither the peak firing rate nor the average firing rate of Pyr cells in layer 2/3 were affected by the blue light stimulus alone (Figure 4.5 C,D). A colleague, Bassam Atallah, expressed concern that the blue ChR2-stimulating light may directly activate retinal photoreceptors (personal communication and SFN poster). I investigated this and found that when the visual stimulus monitor was showing either a full field grey screen or a grating at the same time there was no detectable effect of the blue light. Thus, if it was possible for that light to directly stimulate the retinal photoreceptors, the light from the screen was sufficient to mask any blue light escaping from the craniotomy area.

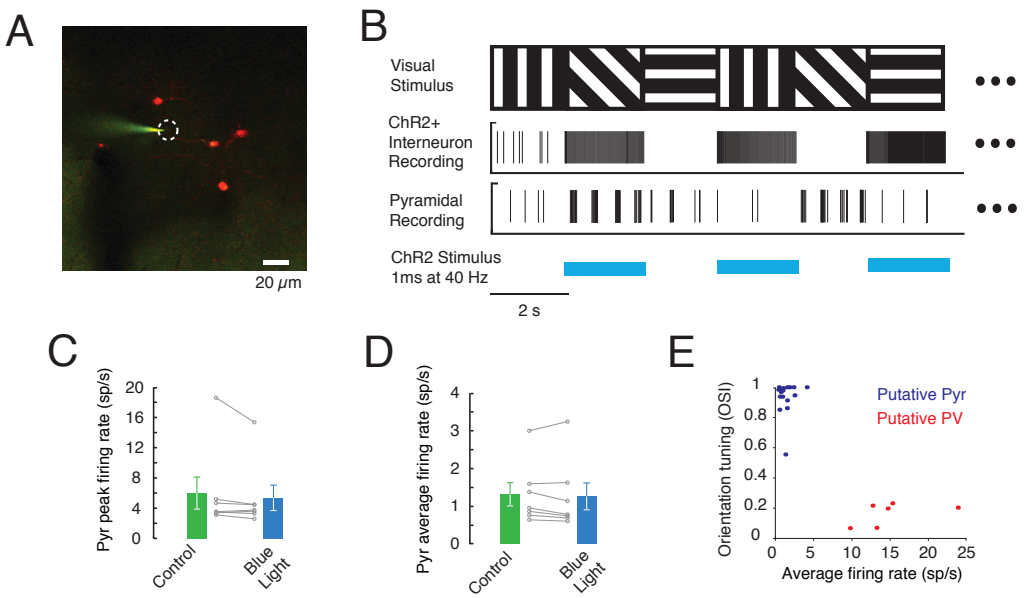

Figure 4.5 Experimental protocol, blue light controls and cell type identification

A, An image of a pyramidal cell-attached recording with four surrounding ChR2 expressing SOM+ interneurons, the pyramidal cell is indicated by a white dotted line. **B**, A schematic showing the structure of the experimental protocol with visual stimuli and interleaved periods of ChR2 stimulation. The interneuron and pyramidal cell rasters are real data taken from one of the experiments. **C**, Peak firing rate of Pyr cells is not affected by blue light in an animal with SOM+ cells electroporated with an RFP plasmid (n = 7, P = 0.219). **D**, Average firing of Pyr rates are also not affected by blue light stimulation alone, in the absence of ChR2

expression (n = 7, P = 0.375). Thus, direct stimulation of the visual pathway with blue light is not a significant factor in these experiments. **E**, Plotting average firing rate against orientation selectivity index shows the distinction between putative pyramidal cells and putative PV+ cells.

Figure 4.5 E shows a difference between putative Pyr cells and putative interneurons recorded. The putative Pyr cells tended to have low mean firing rates and higher levels of orientation tuning (OSI > 0.5). By contrast putative inhibitory cells had lower levels of orientation tuning (OSI < 0.5) and higher mean firing rates. Spike shapes were also used to distinguish between cells (more detail in methods) so it is expected that the putative interneurons represented here are fast-spiking PV^+ interneurons and that it is possible that some other cells are interneurons but were not identified as such.

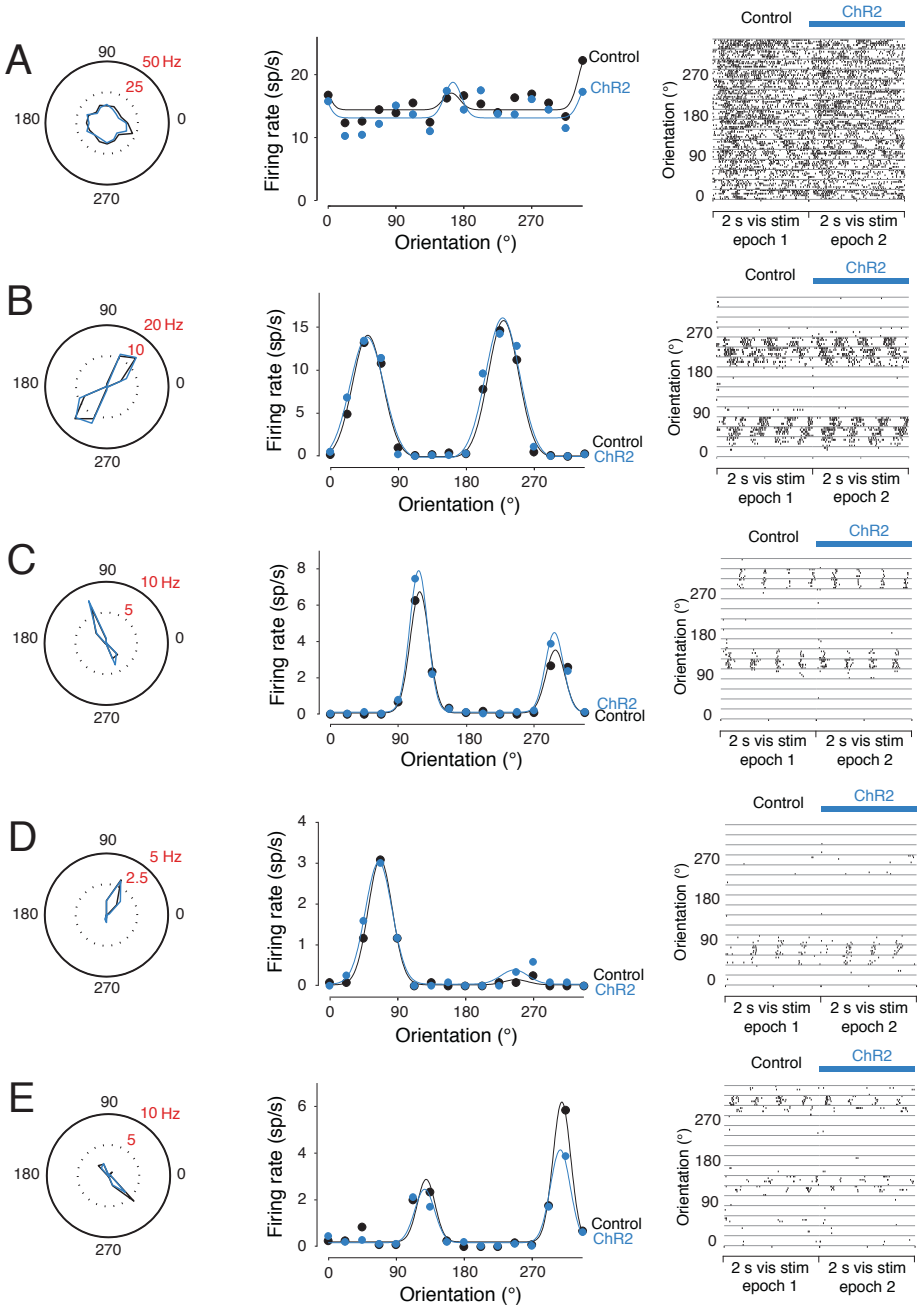

Figure 4.6 Example Pyr cells and a putative PV+ cell with and without SOM+ cell stimulation

A, A putative PV+ cell showing visual responses in the control and ChR2 stimulation condition as a radial plot, average firing rate with Gaussian fit and spike raster for all orientations. This putative interneuron shows an 8.25% reduction in firing in the ChR2 condition. **B-E**, Putative pyramidal recordings showing small changes in both directions or little change at all when exposed to the ChR2 condition.

Figure 4.6 shows example cells recorded while manipulating SOM^+ interneurons. The first cell (Figure 4.6 A) was classified as a putative interneuron due to its high mean firing rate and relative lack of tuning. This interneuron had a decreased mean firing rate in the presence of ChR2 stimulation (control mean firing rate = 15.28 Hz, ChR2 mean firing rate = 14.02 Hz, i.e. a decrease of 1.26 Hz or 8.25 % from control) and a decreased peak firing rate (control peak firing rate = 23.10 Hz, ChR2 peak firing rate = 18.60 Hz, i.e. a decrease of 4.5 Hz or 19.47 % from control). The rest of the cells in this figure are putative Pyr cells and they show a range of different results, though none show any significant change on their own (Figure 4.6 B-E). Two cells show almost no change at all (Figure 4.6 B,D) while for another cell the ChR2 condition shows some increase in mean firing (control mean firing rate = 0.95 Hz, ChR2 mean firing rate = 1.08 Hz, i.e. an increase of 0.13 Hz or 13.12 %) and peak firing (control peak firing rate = 6.74 Hz, ChR2 peak firing rate = 7.86 Hz, i.e. an increase of 1.12 Hz or 16.59 %) (Figure 4.6 C). Another shows some decrease in mean firing (control: 0.91 Hz, ChR2: 0.70 Hz, a decrease of 0.21 Hz or 23.07 %) and peak firing (control: 6.19 Hz, ChR2: 4.10 Hz, a decrease of 2.09 Hz or 33.69 %) (Figure 4.6 E). None of the changes seen in these cells is very large so the first point is that activating a small number of local SOM^+ cells does not appear to have a dramatic effect of the visual responses of cells nearby. The putative interneuron has the largest change in mean and peak spiking in Hz but the Pyr cells exceed it in terms of percentage change. Although the changes in their firing frequencies are low, their means are also low and most of the change occurs at the peaks.

Having looked at some example cells it is now time to examine the population data collected across multiple cells to see if any significant changes or clear trends can be identified. One of the variables that varies between experiments is the number of SOM^+ cells that have been electroporated. The design of the experiment was to have a range of values, so the dose of SOM^+ cell inhibition could be compared. This value varies between 2 and 7 cells electroporated. It was not possible to selectively target putative interneurons for recording so it was not possible to ensure recordings from interneurons in each animal. All putative

interneurons happened to be recorded from animals with 2-3 SOM$^+$ cells electroporated with ChR2.

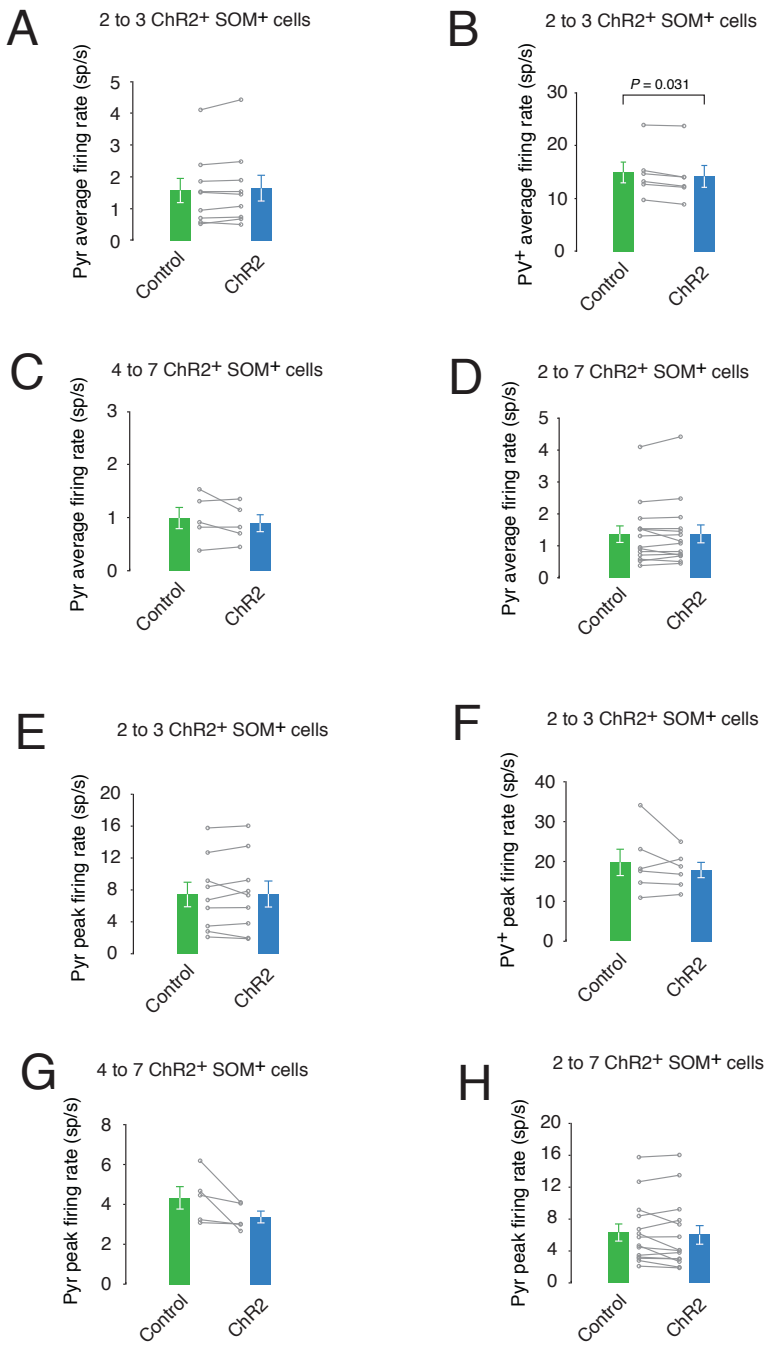

Figure 4.7 The outcome of SOM$^+$ cell stimulation on putative Pyr and PV$^+$ cells

A, Pyr cells did not change their mean firing rate (n = 9, P = 0.129) when 2-3 SOM$^+$ cells were activated during visual stimulation. **B**, The decrease in firing rate for PV$^+$ cells between control and ChR2 stimulation conditions during visual stimulation (n = 6, P = 0.031) shows that even activation of only 2-3 SOM$^+$ cells can significantly affect the activity of PV$^+$ cells.

C, Pyr cells did not change their mean firing rate (n = 5, P = 0.813) when 4-7 SOM+ cells were activated during visual stimulation. **D**, Pyr cells did not change their mean firing rate (n = 14, P = 0.463) when 2-7 SOM+ cells were activated during visual stimulation. **E**, Pyr cells did not change their peak firing rate (n = 9, P = 0.570) when 2-3 SOM+ cells were activated during visual stimulation. **F**, PV+ cells did not change their peak firing rate (n = 6, P = 0.438) when 2-3 SOM+ cells were activated during visual stimulation. **G**, Pyr cells see a reduction in peak firing rate when 4-7 SOM+ cells were activated during visual stimulation but it does not reach significance (n = 5 P = 0.063). **H**, Pyr cells did not change their peak firing rate (n = 14, P = 0.502) when 2-7 SOM+ cells were activated during visual stimulation.

The mean firing rate of Pyr cells was not significantly affected when 2-3 SOM^+ interneurons were activated (control mean firing rate = 1.57 +/- 0.38 Hz , ChR2 mean firing rate = 1.64 +/- 0.41 Hz, n = 9, P = 0.129, Figure 4.7 A). However mean firing rates of putative interneurons did decrease significantly when 2-3 SOM^+ interneurons were activated (control mean firing rate = 14.91 +/- 1.95 Hz , ChR2 mean firing rate = 14.18 +/- 2.04 Hz, n = 6, P = 0.031, Figure 4.7 B). Though the decrease in interneuron firing rate with SOM^+ cell activation is small in absolute terms (0.73 Hz) and in relative terms (4.90 %), the similarity in reduction across cells produces a significant result (paired t-test). Increasing the numbers of electroporated interneurons did not produce a significant reduction in mean firing rate in Pyr cells (control mean firing rate = 0.99 +/- 0.20 Hz , ChR2 mean firing rate = 0.89 +/- 0.16 Hz, n = 5, P = 0.813, Figure 4.7 C). Taking all of the Pyr cell data together also did not demonstrate a significant change in Pyr cell mean firing (Figure 4.7 D).

Similar analysis was carried out for peak firing rates. The peak spiking rate may be a more sensitive measure to detect changes in Pyr cell firing as they tend to be highly tuned and therefore small changes in average firing can result in much larger proportional changes in peak spiking. For interneurons, peak spiking is not expected to be particularly sensitive as a large proportion of the change in spiking occurs not at the peak but across all orientations, also interneuron responses are not represented as well by Gaussian curves as Pyr cell responses. The peak firing rate of Pyr cells was not significantly affected when 2-3 SOM^+ interneurons were

activated (control mean firing rate = 7.43 +/- 1.54 Hz , ChR2 mean firing rate = 7.49 +/- 1.63 Hz, n = 9, P = 0.570, Figure 4.7 E). The peak firing rate of putative interneurons was also not significantly affected when 2-3 SOM^+ interneurons were activated (control mean firing rate = 19.78 +/- 3.31 Hz , ChR2 mean firing rate = 17.86 +/- 1.92 Hz, n = 6, P = 0.438, Figure 4.7 F). When Pyr cells that had been exposed to the manipulation of 4-7 electroporated SOM^+ cells were examined, there was a trend towards decrease in peak firing rates (control mean firing rate = 4.33 +/- 0.56 Hz , ChR2 mean firing rate = 3.37 +/- 0.30 Hz, n = 5, P = 0.063, Figure 4.7 G). However, when all the Pyr cells are taken together, the effect of SOM^+ cell activation on peak firing is not significant. This is not surprising as the Pyr cells from the 2-3 interneuron electroporated class show no effect and so would dilute out any effect found in the Pyr cells exposed to the influence of larger numbers of SOM^+ interneurons.

The final figure in this chapter summarises the main points in a format that makes it easier to see the small differences detected when comparing responses with and without ChR2 activation of SOM^+ cells (Figure 4.8).

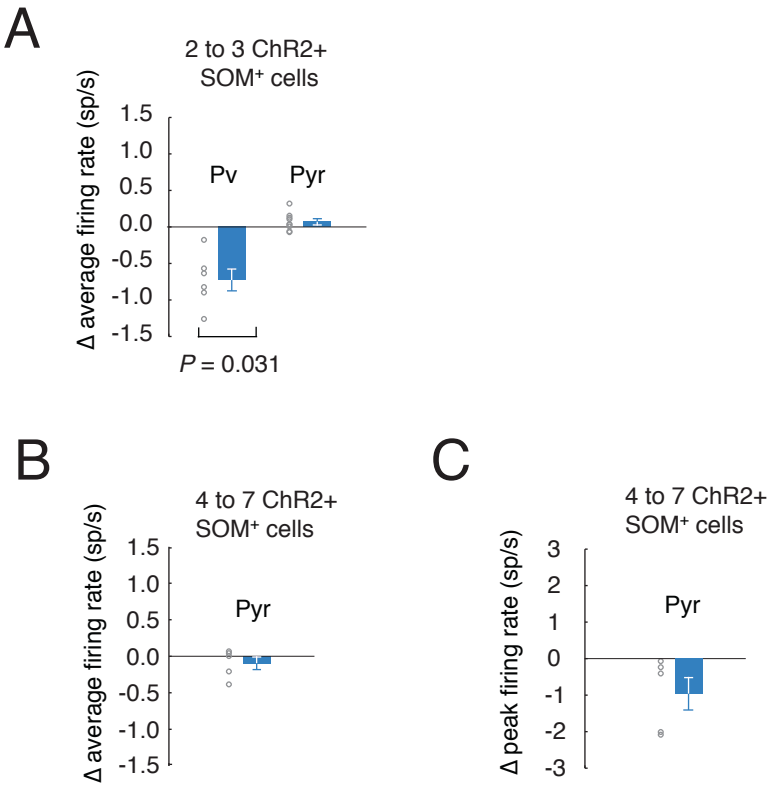

Figure 4.8 Normalised data showing the outcome of SOM$^+$ cell stimulation on populations of putative Pyr and PV$^+$ cells

A, The decrease in firing rate for PV+ cells between control and ChR2 stimulation conditions during visual stimulation (n = 6, P = 0.031) shows that even activation of only 2-3 SOM+ cells can significantly affect the activity of PV+ cells. In contrast, Pyr cells did not change their firing rate (n = 9, P = 0.129) when 2-3 SOM+ cells were activated during visual stimulation. **B**, Higher numbers (4 to 7) of SOM+ cells transfected via single cell electroporation do not produce a detectable change in Pyr cell mean firing rate when they are stimulated (n = 5, P = 0.813). **C**, Higher numbers (4 to 7) of SOM+ cells transfected via single cell electroporation do not produce a detectable change in Pyr cell peak firing rate when they are stimulated (n = 5, P = 0.063).

The change in average firing rate from control to ChR2 condition is detectable in putative interneurons but not in Pyr cells when 2-3 SOM$^+$ cells were activated (Figure 4.8 A). This type of plot rather than the raw data plot (Figure 4.7 A,B) allows the comparison of magnitudes of change side by side. Similarly, for average Pyr cell changes with 4-7 SOM$^+$ cells electroporated with ChR2 there is

no significant difference between the control and CHR2 conditions (Figure 4.8 B). Figure 4.8 C shows the changes in peak firing rate between the control and ChR2 condition for 4-7 electroporated SOM^+ cells. The magnitude of changes are greater than for peak firing frequency but though the changes approach significance ($P = 0.06$, $n = 5$), they do not reach it.

4.3 Discussion

In this chapter I have shown that single cell electroporation can be used to deliver ChR2 to SOM^+ interneurons, which can then be reliably controlled by blue light pulses. Recording from neighbouring neurons and comparing visual responses with and without ChR2 stimulation of SOM^+ interneurons did not show pronounced changes in either peak or average spiking. When the recorded cells were grouped separately as putative Pyr cell and putative fast spiking (PV^+) interneurons it was only possible to detect a significant reduction in firing during SOM^+ cell activation in the PV^+ interneurons. When stimulating larger numbers of SOM^+ interneurons there was a downward trend produced in Pyr cell firing which narrowly missed being significant, probably due to the small sample size ($n = 5$). With a higher number of recordings it might have been possible to show that by activating four or more adjacent SOM^+ cells it is possible to inhibit Pyr cells. Looking back to the hypotheses (Figure 4.1 C) it seems that for Pyr cells neither hypothesis 1 nor 2 is occurring with this level of stimulation. For putative interneurons, hypothesis 1 looks the most appropriate. If hypothesis 3 were the case for Pyr cells one would not expect a change in the mean firing rate as Pyr cells being excited and inhibited may cancel any change out. What would be expected would be a larger spread around the mean for cases in which more SOM^+ cells were activated as excited cells would be more strongly excited and inhibited cells would be more strongly inhibited. This did not appear to be the case in the data as the ranges covered by the change in mean firing values, and the standard deviations for these data for the 2-3 electroporated interneurons group

(range = -0.07 to 0.32, stdev = 0.12), and the 4-7 electroporated interneurons group (range = -0.39 to 0.07, stdev = 0.19), were very similar.

It is not known in detail how many cells of the different cell types are required to have a clear effect on cortical circuitry. Previous studies have shown that single Pyr cells can affect motor activity (Brecht et al., 2004), induce a behaviourally reportable effect (Houweling and Brecht, 2008), and change global brain state (Li et al., 2009). An experiment looking into the local network effect of Pyr cell stimulation found that single Pyr cell stimulation was able to increase activity in nearby Pyr cells and SOM^+ interneurons but not PV^+ interneurons (Kwan and Dan, 2012). Only one such experiment has been carried out manipulating interneurons which was part of a paper using viral manipulation of SOM^+ and PV^+ cells (Wilson et al., 2012). The authors claim to have stimulated single SOM^+ and PV^+ cells and seen suppression in cells in the nearby network. These results are questionable because neurons were stimulated in a virally transfected animal using one-photon blue light. Due to light spread, with this approach it is very unlikely that stimulation can be restricted to single cells among the hundreds of cells expressing ChR2, especially for SOM^+ interneurons, as these neurons have a thick mat of ChR2 containing axons in layer 1. Another problem is the use of Ca^{2+} imaging as a readout from the population of neurons. I have shown here that the effects are likely to be small even when cell-attached recordings are used, which yield reliable detection of single spikes. By contrast, Ca^{2+} imaging as used by Wilson et al. are unable to provide this fidelity, and thus will yield imprecise tuning curves. Nevertheless it is possible that the small proportion of suppressed neurons they saw (16.2 +/- 2.9 % of neurons) are PV^+ interneurons, which would match the data shown in this thesis.

As it is clear that these effects are at the threshold for detectability it would be interesting to be able to stimulate a larger population of SOM^+ interneurons and look at the larger effects produced. There appears to be a differential effect of SOM^+ interneuron stimulation on different cell types, PV^+ interneurons and Pyr cells, so it would be very useful to be able to definitively identify these two

different groups at the same time. These ideas and approaches are addressed in the following chapter.

5 Optogenetic manipulation of large populations of somatostatin positive neurons

5.1 Introduction

To establish the role of an interneuron subtype in the cortical processing of visual information it is important to know how that cell type responds to visual stimulation in comparison to the other cell types. Once this is established the next step is to manipulate the activity of one type of cell and measure its effects on the other components of the network. In the preceding chapter small-scale manipulations were made involving up to 7 SOM^+ interneurons. These manipulations produced modest effects; therefore in this chapter a higher number of SOM^+ cells will be stimulated to produce a larger effect on the other cell-types in the network and make the effect of additional SOM^+ cell inhibition clearer. Recently, the cortical network has often been simplified to a triadic network of three cell-types: Pyr cells and two of the most numerous and obviously separable interneuron classes - SOM^+ cells and PV^+ cells (Adesnik et al., 2012; Lee et al., 2012; Wilson et al., 2012). Ideally while stimulating the SOM^+ interneurons it would be desirable to record from and distinguish between the other two cell types in the same animal. In this chapter I will show how the specific stimulation of large populations of SOM^+ interneurons was achieved, and how the problem of distinguishing between the Pyr cells and PV^+ interneurons was overcome. An additional problem remained which was choosing the best level of stimulation of the SOM^+ cells as mentioned in the introduction to chapter 4. With large-scale

viral transfection it is possible to stimulate the SOM^+ cells strongly and in great numbers. The cortical network normally operates in a dynamic state of fluctuating excitation and inhibition (Haider and McCormick, 2009) these fluctuations are balanced to prevent extreme excitation or inhibition in normal circumstances. With extreme SOM^+ cell stimulation it may be possible to take the cortical network into a parameter space of excitation and inhibition that it would never normally enter. Recordings made in this state may not appropriately reflect the normal response of the network to SOM^+ cell firing and therefore would be uninformative as to SOM^+ cell function. The hypothetically ideal level of stimulation would be the minimum needed to produce an obviously detectable effect in one or both cell types.

5.2 Results

The first stage of this chapter is to describe the genetic technique used to allow the identification of the PV^+ cells while at the same time genetically targeting ChR2 to the SOM^+ cells. This was achieved by crossing transgenic lines together and provides a useful way of combining the specificity of Cre lines with a separate cell population labeled with a fluorescent protein. Having established the technique for specifically stimulating and recording particular cell types, the recorded data is analysed and differences between the responses of Pyr cells and PV^+ interneurons that were discovered in the previous chapter are examined in more detail.

5.2.1 A double transgenic to enable cell-type specific stimulation and recording

During the course of the single cell electroporation experiments shown in the previous chapter, a range of Cre mouse lines started to become available (Taniguchi et al., 2011). These transgenic mice express the Cre recombinase

enzyme derived from bacteriophage P1 (Austin et al., 1981), in specific cell populations depending on the promoter selected and the position of its insertion into the genetic code of the mouse (Luo et al., 2008). The Cre enzyme targets Lox sequences, producing recombination only in the cells expressing Cre (Sauer, 1998). This system allows the expression of ChR2 or other transgenes in large numbers of cells that share a genetic marker gene. This works even if the cell-type specific promoter is relatively weak as only a small amount of Cre is needed to recombine the loxed transgene of interest, which can be introduced via a virus or be inserted into the genome (Luo et al., 2008). This solves what had been a problem for interneuron specific expression in the past, as many of the interneuron specific promoters such as somatostatin and parvalbumin are weak and would not drive sufficient expression of ChR2 (Luo et al., 2008). The particular approach used to target ChR2 expression in this thesis was to inject an AAV virus carrying the ChR2 transgene into a SOM-Cre transgenic mouse (Figure 5.1 A, see methods for more details). The ChR2 transgene was double loxed within the AAV, meaning that it was originally in the reversed orientation preventing any leak expression in non Cre expressing cells (Atasoy et al., 2008). When Cre acts on it in SOM^+ cells, the orientation of the ChR2 transgene is reversed and three of the 4 lox sequences are excised so the gene cannot flip back.

Initial testing was carried out to establish how much time after virus injection was needed to express sufficient levels of ChR2 within the SOM^+ cells. Eight weeks of viral expression produced a very high level of ChR2-eYFP production (Figure 5.1 B). Images of individual cells taken at higher zoom confirmed this (Figure 5.1 C). Expressing cells looked misshapen, and it appeared the ChR2-eYFP conjugate protein had collected throughout the cytoplasm. Furthermore, when targeted cell-attached recordings were attempted from these cells it was difficult to form seals and no spontaneous spikes were recorded (n = 4). Following this evidence the expression times post injection were shortened to between two and three weeks. These shortened expression periods gave greatly improved results. Expression was much less intense in layer 2/3 of visual cortex (Figure 5.1 D) and the cells looked morphologically normal with expression limited to the cell membrane as shown by the dark cytoplasmic centres of the cells (Figure 5.1 E).

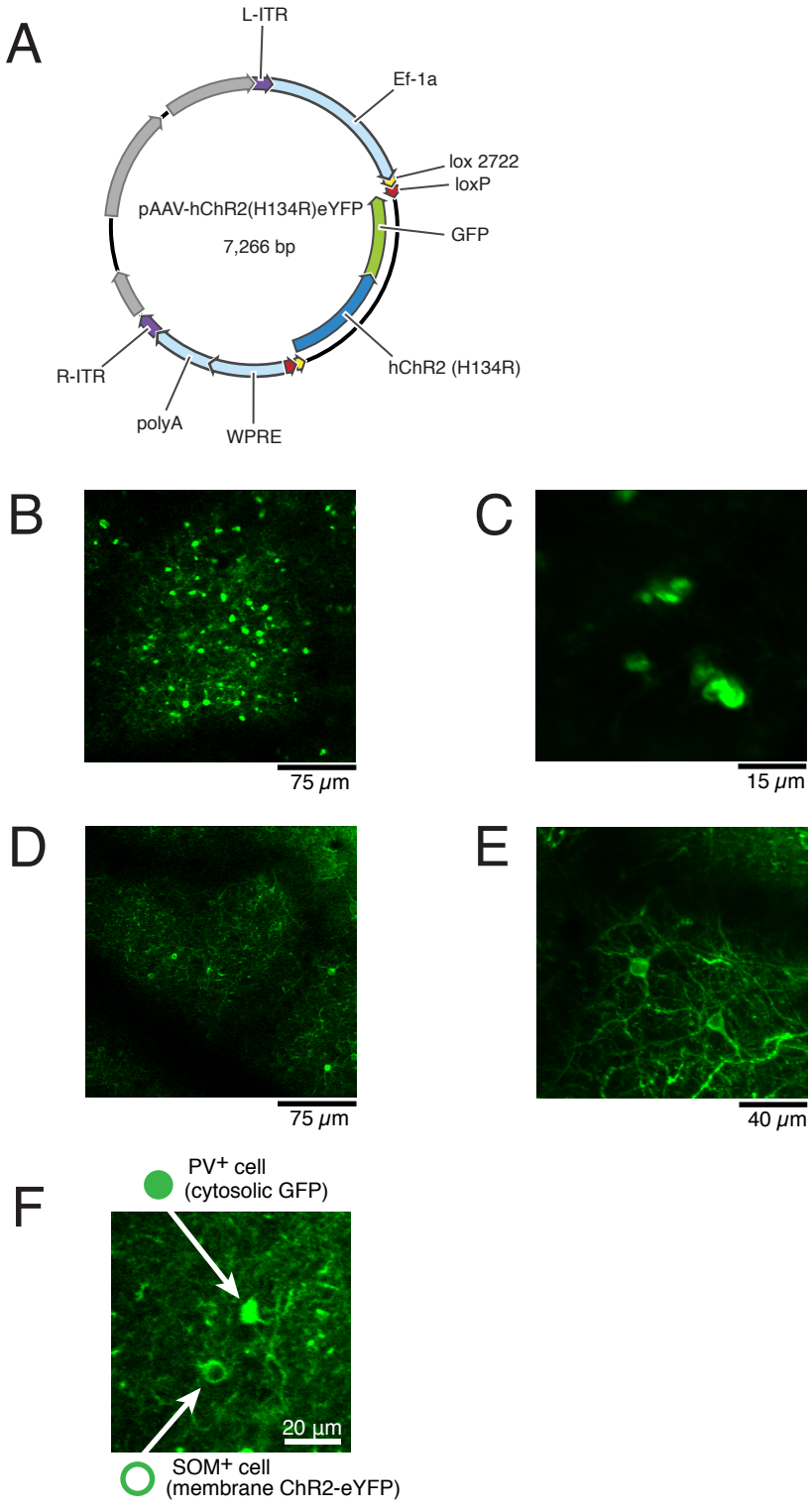

Figure 5.1 Viral transfection of SOM$^+$ cells

A, Design of viral plasmid with the ChR2-eYFP transgene reversed to be selectively flipped and expressed in the presence of Cre recombinase. **B**, An image of viral expression in a SOM-Cre animal 8 weeks after injection showing a high and dense level of expression. **C**, A higher zoom

image of cells from the same animal that are malformed and appear to have high levels of cytosolic ChR2-eYFP. **D**, An image of viral expression in a SOM-Cre animal 2 weeks after injection showing a lower levels of expression and lower expression density. **E**, A higher zoom image of the animals 2 weeks after injection showing healthy transfected cells in which ChR2-eYFP is restricted to the cell-membrane. **F**, An image showing that GFP-expressing PV^+ cells were easily distinguishable from ChR2-eYFP-expressing SOM^+ cells by the pattern of labeling, the former being cytosolic and the latter restricted to the membrane.

The next aim in creating the new transgenic mouse line was for PV^+ interneurons to be visible and distinguishable from the ChR2-transfected SOM^+ cells. This was achieved by crossing homozygous SOM-Cre animals with the heterozygotic PV-GFP animals used in Chapter 3 for the targeting of PV^+ cells. Of the resulting offspring, all expressed SOM-Cre and those also positive for PV-GFP could be selected using UV goggles, as the GFP was visible through the skin during the first 3-5 days after birth. When these double transgenic animals were injected with ChR2-AAV, the SOM^+ cells would selectively express ChR2-eYFP and the PV^+ cells would express GFP. These two fluorescent proteins are not easily spectrally separable but could be separated by the location of their fluorescence; the PV-GFP cells express GFP throughout their cytoplasm while in the SOM-ChR2-eYFP cells ChR2-eYFP is limited to the membrane, leaving a dark hollow in the centre of the cell (Figure 5.1 E).

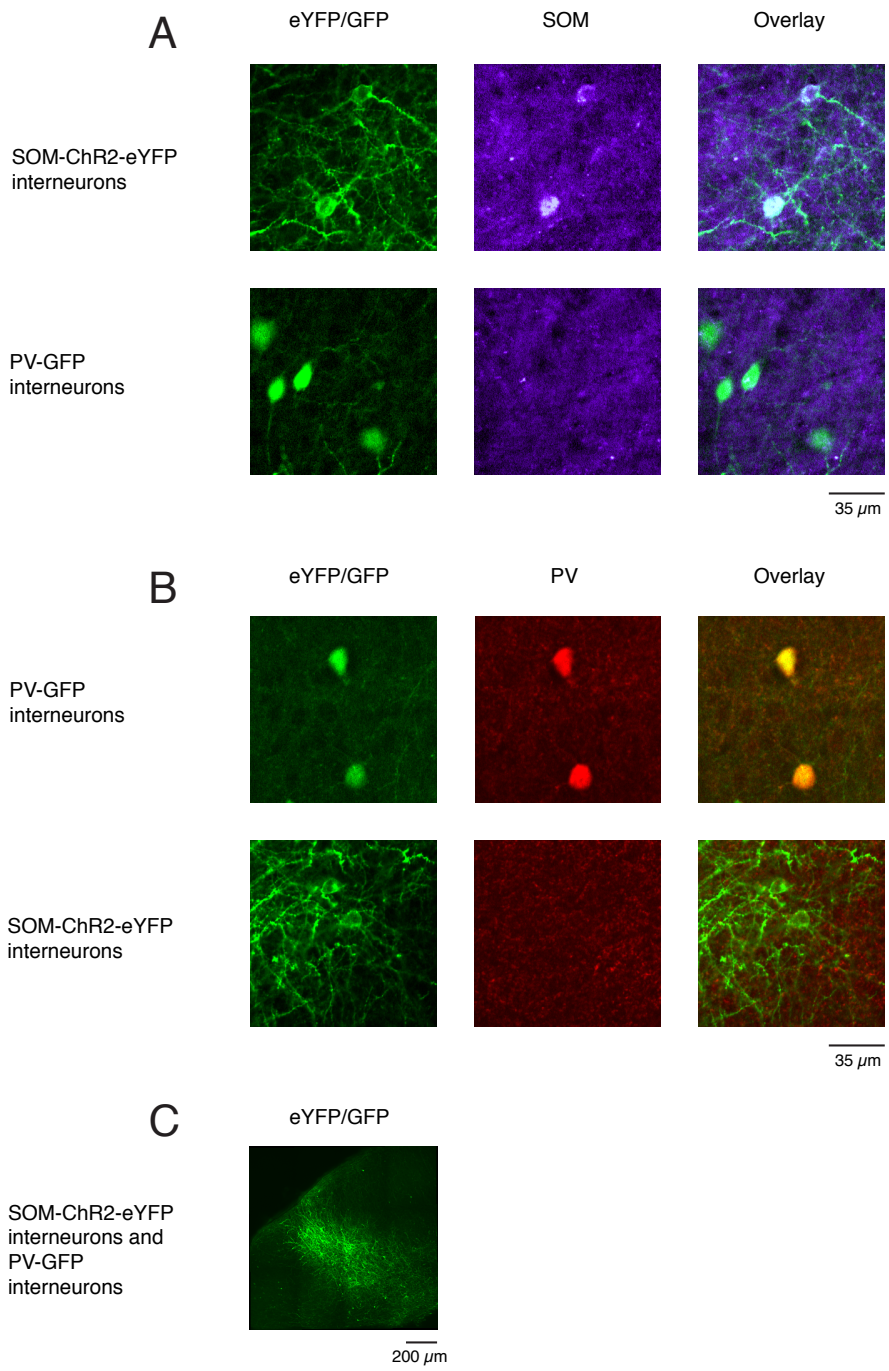

Figure 5.2 Immunohistochemical confirmation of differential SOM$^+$ cell and PV$^+$ cell labelling

A, Double-immunolabeling for eYFP/GFP and somatostatin. Cells expressing cell membrane-confined ChR2-eYFP were positive for SOM while no SOM labeling was detected in cells with cytosolic GFP labeling. **B**, Double-immunolabelling for eYFP/GFP and parvalbumin. Cells with cytosolic GFP labelling were positive for PV, while no PV labeling was detected in cells expressing cell membrane-confined ChR2-eYFP. **C**, Low magnification image of eYFP/GFP

labelling showing the extent of the cortical area transduced by viruses carrying SOM-ChR2-eYFP. SOM expressing cells within 50 μm of the injection site were labelled, with the proportion gradually declining to zero within 500 μm.

This visual distinction was confirmed using immunohistochemistry (Figure 5.2). A stain against somatostatin revealed that only cells with membrane labeling by the green fluorescent proteins were positive for somatostatin while those with labeling throughout the cytoplasm were negative for somatostatin (n = 12 in both cases, Figure 5.2 A). Likewise PV^+ cells were confirmed to be those with cytoplasmic labeling by a parvalbumin stain protocol in which only those cells were positive for parvalbumin, while cells with green membrane labeling were negative for parvalbumin (n = 12 in both cases, Figure 5.2 B). This confirms that the visual discrimination under the 2-photon microscope corresponds to a real protein expression difference between cells with different fluorescent protein labeling. The extent of the injection zone is also shown from an example animal (Figure 5.2 C).

This leaves mainly the Pyr cells as the unlabelled cells. While there are some interneurons that would also fall into the unlabelled group this is a small proportion. PV^+ cells make up 35-40% of the interneuron population in mouse visual cortex and SOM^+ cells make up 20-25% of the population (Gonchar et al., 2007). Taking these two groups together means that 55-75% of the interneuron population is labeled in this animal. This means that as interneurons are only 20% of the cortical cells (Markram et al., 2004), unlabeled interneurons would make up less than 10% of all unlabeled cells.

The final stage in preparing the animal for the large-scale SOM^+ cell manipulation experiment is to test that the ChR2 delivered by the virus into SOM^+ cells is functional and able to drive the cells to spike. Cell-attached recordings were made from SOM^+ cells expressing ChR2-eYFP and being stimulated at 40 Hz with 1 ms blue light pulses.

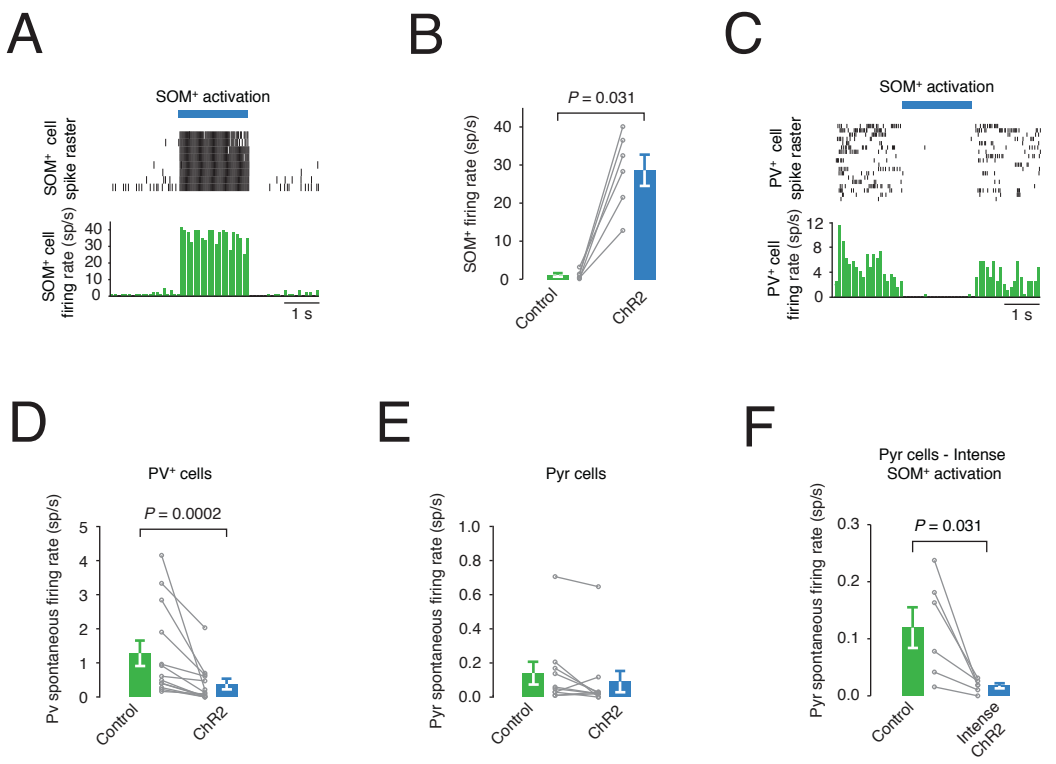

Figure 5.3 The effect of SOM$^+$ cell stimulation on Pyr and PV$^+$ cell spontaneous spike rates

A, Activation of ChR2 in a ChR2-expressing SOM+ cell drives it to fire spikes. **B**, SOM+ cells virally transfected with ChR2 increase their firing in response to activation by blue light (40 Hz trains of 1 ms flashes; n = 6, P = 0.031). **C**, Activation of ChR2-expressing SOM+ cells decreases the firing rate of a PV+ cell. **D,E** The effect of SOM+ cell stimulation on PV+ cell (n = 13, P = 0.0002) and Pyr cell (n = 10, P = 0.078) spontaneous activity. **F**, More intense SOM+ cell activation can significantly reduce Pyr cell spontaneous firing rates (n = 6, P = 0.031).

This produced spikes in the SOM$^+$ cells as shown in an example cell (Figures 5.3 A). When comparing the responses of stimulated cells it is clear that there is some variability in the accuracy of response across cells with different mean firing frequencies being achieved during blue light stimulation (Figure 5.3 B). The viral expression of ChR2 is somewhat less controlled than in the single cell electroporation case. Nevertheless an obvious increase in SOM$^+$ cell firing was achieved with a mean across all cells of 28.6 +/- 4.12 spikes/s (n = 6), which aligns closely with the firing rates seen in awake mouse cortex when running

(Adesnik et al. 2012). As predicted, driving SOM^+ cells to spike in this way inhibited other cells within the microcircuit (Figure 5.3 C).

5.2.2 The effects of population SOM^+ cell stimulation on PV^+ and Pyr cells in visual cortex

With the challenges of specific manipulation and identification of recorded cells resolved, data was collected from PV^+ cells and Pyr cells during SOM^+ cell stimulation. Firstly the effect of SOM^+ cell activation on spontaneous firing in the two cell types was measured. The spontaneous firing rate of PV^+ cells was strongly inhibited (70.4 ± 12.2% decrease from control levels, $P = 0.0002$, n = 13; Figure 5.3 D), while Pyr cell firing was only modestly affected (35.6 ± 44.7% decrease from control levels, $P = 0.078$, n = 10; Figure 5.3 E). Pyr cells had low spontaneous firing rates, and while no significant changes in spontaneous rate were evoked with the usual 40 Hz SOM^+ cell activation, more intense SOM^+ cell activation (see methods for details) was able to produce a reduction in spontaneous firing rate (85.4 ± 3.9% decrease from control levels, $P = 0.031$, n = 6; Figure 5.3 F). This more intense level of stimulation was also able to strongly inhibit the firing of Pyr cells during visual stimulation (Figure 5.4). Six cells showed that intense SOM^+ cell activation was able to strongly inhibit Pyr cell firing (Figure 5.4 A), in some to the point of almost complete silencing of cell firing despite the input they received from visual stimulation (Figure 5.4 A cell 4,5). This reduction in firing can be seen clearly in the raster plots of spiking for the preferred orientation of all cells (Figure 5.4 B, summarized as a histogram in the lower panel). In addition to the spontaneous rate reduction this strong stimulation specifically reduced the untuned component of visual responses, which is the firing rate amplitude at the lowest point of the Gaussian fit (81.7 ± 9.5% decrease from control levels, $P = 0.031$, n = 6; Figure 5.4 C), as well as the peak firing rate (66.5 ± 11.4% decrease from control levels, $P = 0.031$, n = 6; Figure 5.4 D).

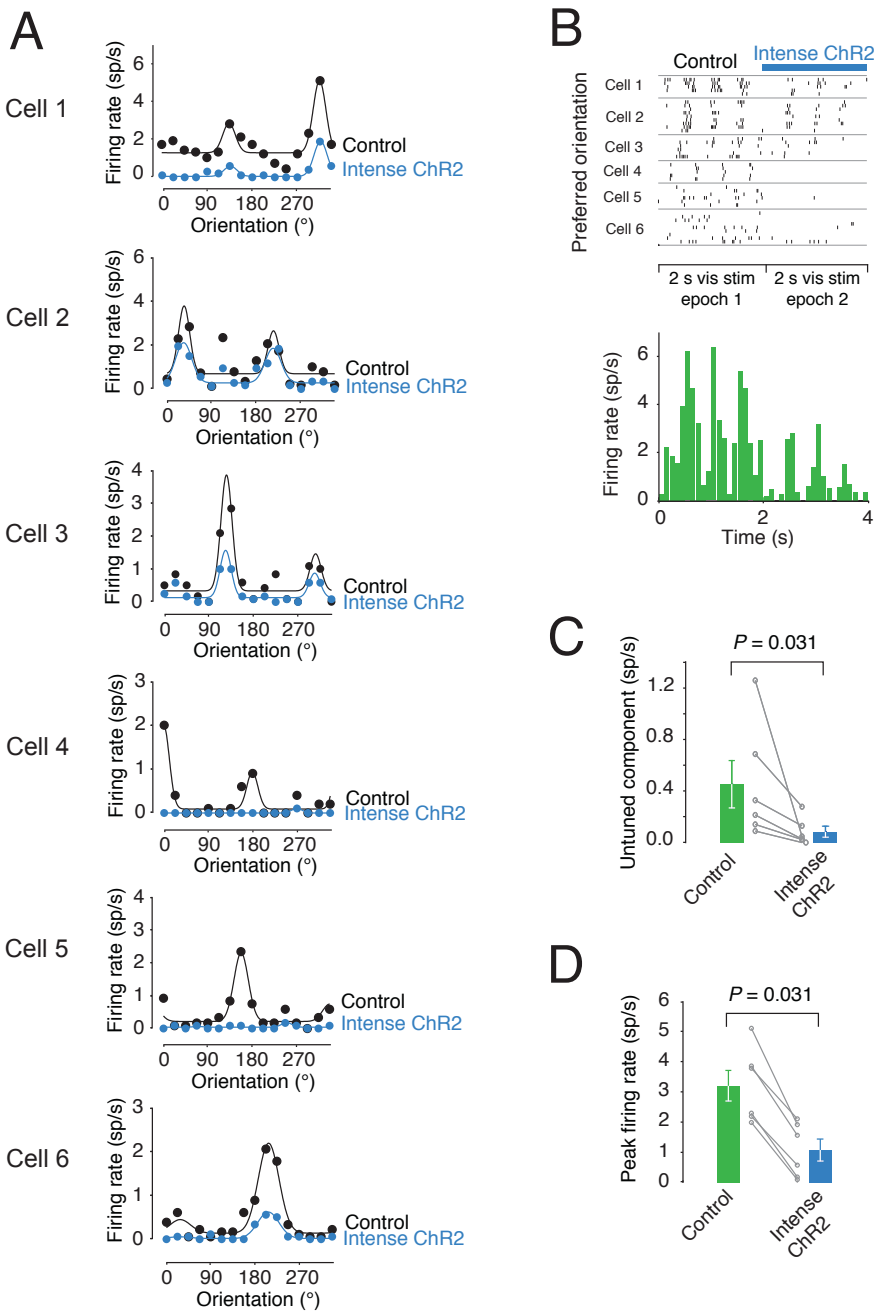

Figure 5.4 The effect of strong SOM$^+$ cell stimulation of Pyr cell firing

A, Intense SOM⁺ activation was achieved by increasing blue light intensity and ensuring the recorded cells were closer to the viral injection center. The Pyr cell visual tuning curves are shown with and without SOM⁺ activation. **B**, The preferred orientation of each cell is plotted as a raster with and without SOM⁺ activation, the results across all cells are summarized in the histogram below. **C**, The untuned component is significantly decreased with SOM⁺ activation (n = 6, P = 0.031). **D**, The peak firing rate is significantly decreased with SOM⁺ activation (n = 6, P = 0.031).

The original level of SOM$^+$ cell activation (i.e. 40 Hz stimulation) was used throughout the rest of this chapter and corresponds with the level used in the first tests of PV$^+$ cell and Pyr cell spontaneous activity (Figure 5.3 D,E). Excessive levels of stimulation can push the cortex into a state of activity that is so far removed from normal functioning as to be uninformative to physiological circuit behaviour.

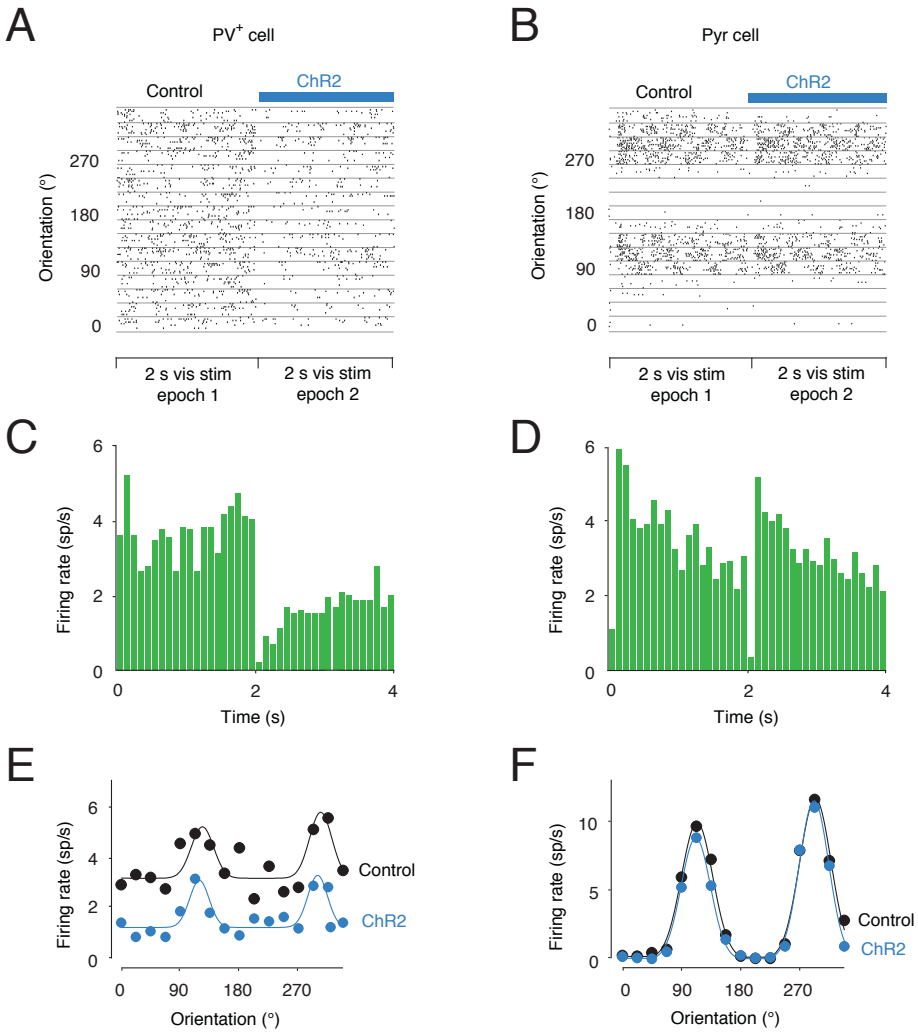

Figure 5.5 Example PV$^+$ and Pyr cells receiving visual stimulus alongside SOM$^+$ activation

A,B Example PV+ and Pyr cell spike rasters and **C,D** peristimulus time histograms showing visual responses with and without SOM+ cell ChR2 stimulation. **E,F** Mean responses for the same example cells fitted with Gaussian tuning curves.

Using the original lower level of stimulation, a dataset was collected comparing the effects of SOM^+ cell activation during visual stimuli on PV^+ interneurons and Pyr cells. Figure 5.5 shows an example PV^+ cell and an example Pyr cell with and without SOM^+ cell activation. First the raster plots for the responses at all orientations are shown with the 2 s periods with and without ChR2 stimulation shown next to each other (Figure 5.5 A,B). It is clear by eye that there is a reduction in PV^+ cell firing during the ChR2 condition relative to the control condition with the original pattern of responses in time staying roughly constant (Figure 5.5 A). For the Pyr cell it is much less clear by eye that there is any difference between the control and ChR2 conditions (Figure 5.5 B). Below the rasters, are histograms of the spiking data, which again show the reduction of firing rate in the PV^+ cell while the reduction of firing rate in the Pyr cell is much less obvious, although there does appear to be some small reduction at the peak (Figure 5.5 C,D). Interestingly there appears to be a disproportionate reduction in firing towards the early stages of the PV^+ cell response suggesting, in this cell at least, that SOM^+ cell activation may not affect the firing rate equally over time (Figure 5.5 C). Finally the mean firing rates for each orientation are plotted and fit with Gaussians for both conditions in each cell (Figure 5.5 E,F). The example PV^+ cell shows a clear reduction in firing rate across all orientations without a large change in the Gaussian fit, for this cell it looks like the Gaussian has simply been shifted downwards (Figure 5.5 E). For the example Pyr cell, the ChR2 condition looks like it is very slightly lower than the control but the change is so small that it is unlikely to be resolvable statistically (Figure 5.5 F).

Moving now to the population data, 21 PV^+ cells and 12 Pyr cells were recorded from during visual stimulation in the control and ChR2 conditions, as seen in the example cells of Figure 5.5. The effects of this protocol were analysed and the main results are shown in Figure 5.6.

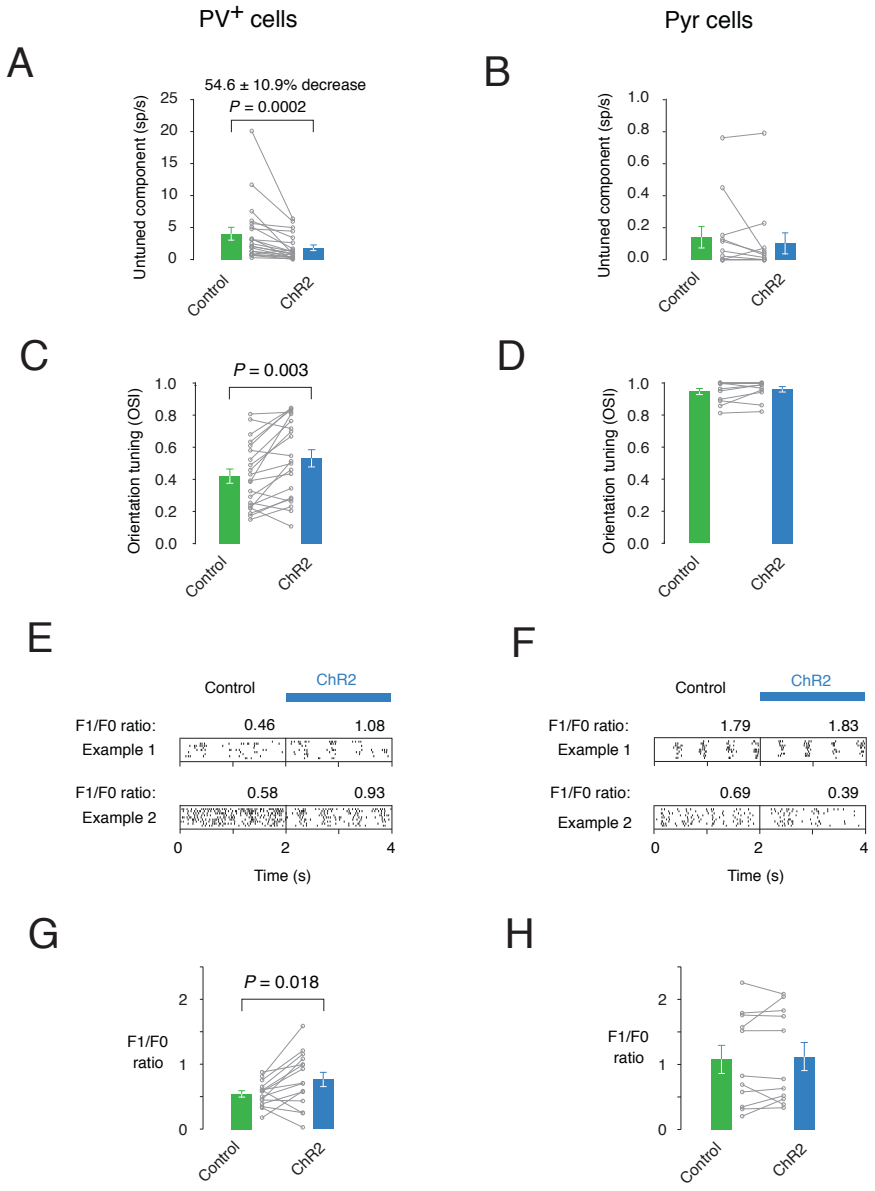

Figure 5.6 The effects of SOM+ activation on the untuned component, OSI and F1F0 ratio of PV+ cells and Pyr cells

A,B The untuned component of the tuning curve decreases for PV+ cells between control and ChR2 stimulation conditions (n = 21, P = 0.0002) but not for Pyr cells (n = 12, P = 0.492). **C,D** The effect of SOM+ cell stimulation on the orientation selectivity index in PV+ (n = 21, P = 0.003) and Pyr cells (n = 12, P = 0.232). **E,F** Example rasters showing the preferred orientation responses and F1/F0 ratios (a measure of stimulus phase selectivity which is over 1 for simple cells) of 2 PV+ cells (left) and 2 Pyr cells (right). **G,H** The F1/F0 ratios under control and SOM+ cell stimulation conditions for PV+ cells (n = 15, P = 0.018) and Pyr cells (n = 11, P = 0.520) show that PV+ cells become more like simple cells.

The untuned component was significantly reduced in PV^+ cells (54.6 ± 10.9% decrease from control levels, $P = 0.0002$, n = 21; Figure 5.6 A) but not in Pyr cells (27.1 ± 46.5% decrease from control levels, $P = 0.492$, n = 12; Figure 5.6 B). The untuned component is the DC offset of the lowest point of the Gaussian curve above zero (see methods for further details). In terms of the orientation selectivity index PV^+ interneurons become more orientation selective with SOM^+ cell stimulation (26.3 ± 12.8% increase from control levels, $P = 0.003$, n = 21; Figure 5.6 C), while Pyr cells show no change (1.4 ± 1.8% increase from control levels, $P = 0.23$, n = 12; Figure 5.6 D).

As well as changing their firing rate and orientation selectivity PV^+ cells also become more simple with SOM^+ cell activation (Figure 5.6 E,G). Simple cells fire in phase with the grating when the lines of contrast move over their receptive fields (Hubel and Wiesel, 1959, 1962) in this case when the grating is drifting at 2 Hz this leads to bursts of firing twice a second. Complex cells have a differently structured receptive field and fire throughout the passage of the drifting grating not only when it is in certain positions (Hubel and Wiesel, 1959, 1962). A clearly simple cell is shown in Figure 5.6 F (example 1). Example 2 in Figure 5.6 F shows a complex cell in which the spiking is not grouped into short periods but distributed. Simple and complex response preferences are measured using the F1/F0 ratio which divides the temporally modulated component of the response (F1) by the mean firing rate (F0) (Skottun et al., 1991; Mechler and Ringach, 2002). This produces a range of values with those below one being thought of as complex and those above one being considered simple. Pyr cells can be complex or simple and display a bimodal distribution with peaks centred around 0.5 and 1.75 with few to no cells with values around 1 (Skottun et al., 1991; Mechler and Ringach, 2002). PV^+ interneurons have been thought of as mostly complex cells (Liu 2009, Ma 2010) with all data in the control condition shown here having an F1/F0 ratio below 1. Pyr cell F1/F0 ratios did not change significantly between control and ChR2 conditions (4.0 ± 20.0% increase from control levels, $P = 0.52$, n = 12; Figure 5.6 H). In contrast, PV^+ cells became significantly simpler (41.2 ± 20.2% increase from control levels, $P = 0.018$, n = 21; Figure 5.6 G) as shown by the example cells (Figure 5.6 E) and the population data (Figure 5.6 G).

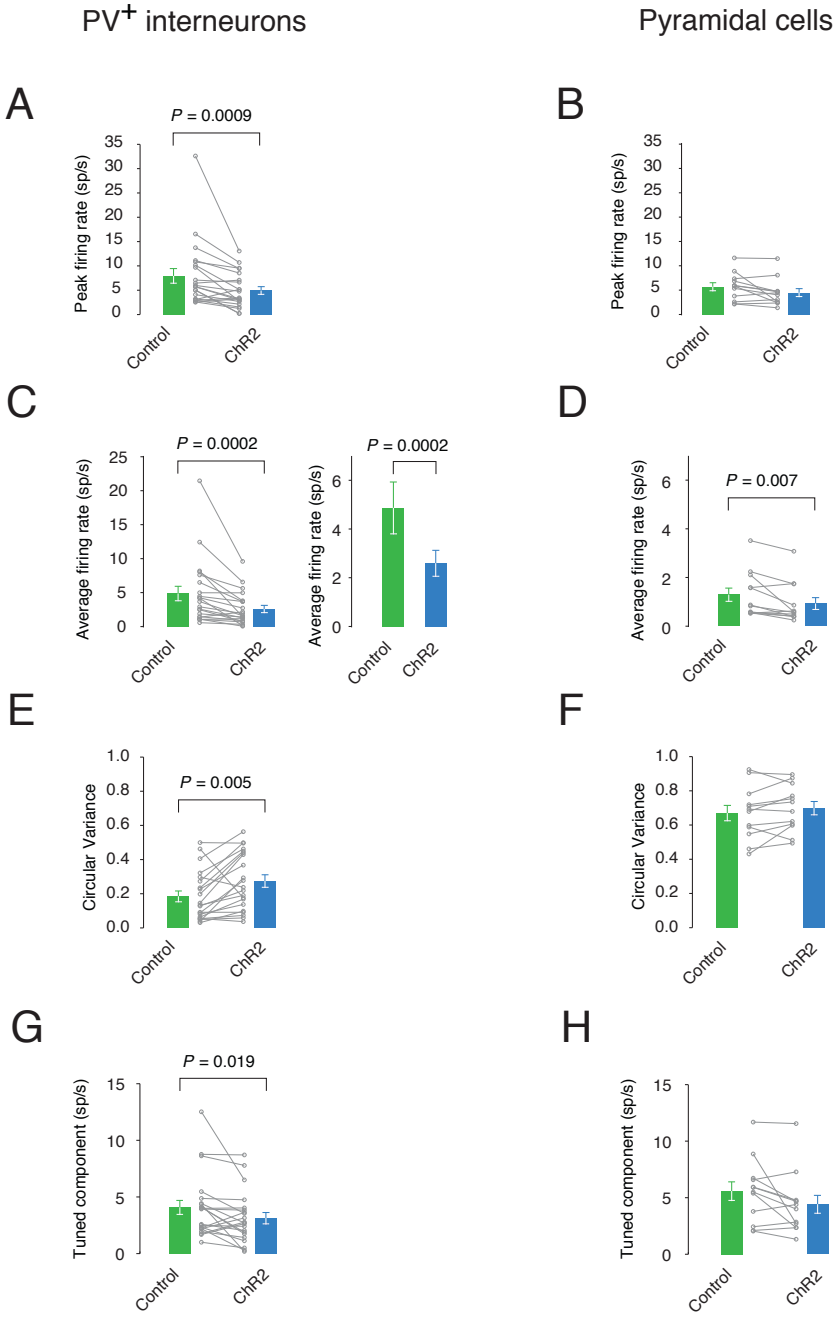

Figure 5.7 Effects of SOM+ activation on other firing rate and tuning measures of PV+ cells and Pyr cells

A,B The effect of SOM+ cell stimulation on peak firing in PV+ (n = 21, P = 0.0009) and Pyr cells (n = 12, P = 0.052). **C,D** Average firing rate is significantly reduced in PV+ cells (n = 21, P = 0.0002) and Pyr cells (n = 12, P = 0.007) upon SOM+ cell stimulation. **E,F** Circular variance increases in PV+ cells (n = 21, P = 0.005) with ChR2 stimulation but not in Pyr cells (n = 12, P = 0.151). **G,H** The tuned component is significantly reduced in PV+ cells (n = 21, P = 0.019) but only approaches significance in Pyr cells (n = 12, P = 0.052).

In addition to these analyses, there are some alternative measures of the firing rate and tuning of the visual response that should also be considered (Figure 5.7 and 5.8). The peak firing rate decreases significantly with SOM^+ cell activation in PV^+ cells (37.8 ± 9.9% decrease from control levels, $P = 0.0009$, n = 21; Figure 5.7 A) but not in Pyr cells (21.1 ± 14.2% decrease from control levels, $P = 0.052$, n = 12; Figure 5.7 B) although they closely approach significance. Another firing rate measure is mean firing rate; this is reduced significantly in both PV^+ (46.7 ± 10.9% decrease from control levels, $P = 0.0002$, n = 21; Figure 5.7 C) and Pyr cells (28.1 ± 18.8% decrease from control levels, $P = 0.007$, n = 12; Figure 5.7 D) with SOM^+ cell activation. It was shown in Figure 5.6 that PV^+ cells become more orientation selective. Circular variance is an alternate orientation tuning measure that takes all orientation values into account (see methods for more details). This agrees with the OSI measure used earlier that PV^+ cells become significantly more orientation selective (48.6 ± 19.9% increase from control levels, $P = 0.005$, n = 21; Figure 5.7 E) while Pyr cells do not (4.3 ± 5.9% increase from control levels, $P = 0.15$, n = 12; Figure 5.7 F). A second alternative measure of tuning is the tuned component which rides on top of the untuned component and is measured as the peak to trough amplitude of the Gaussian fit of the visual responses. This is significantly reduced with ChR2 stimulation in PV^+ cells (23.3 ± 12.3% decrease from control levels, $P = 0.019$, n = 21; Figure 5.7 G), but not quite in Pyr cells (20.0 ± 14.2% decrease from control levels, $P = 0.052$, n = 12; Figure 5.7 H). Despite the range of changes measured in PV^+ cells that occur with SOM^+ cell activation the preferred orientation does not change between control and ChR2 conditions in PV^+(average Δorientation = 9.6^o, n = 21, Figure 5.8 A) or Pyr cells (average Δorientation = 3.6^o, n = 12, Figure 5.8 B). PV^+ cells tended to have less clearly Gaussian visual tuning curves and were therefore worse fit than Pyr cells, this could account for the higher change in preferred orientation than for Pyr cells though both changes are small. Half width at half height measures the width of the Gaussian fits to the tuning curves. This doesn't change significantly in either PV^+ (11.7 ± 10.4% decrease from control levels, $P = 0.375$, n = 21; Figure 5.8 C) or Pyr cells (4.6 ± 12.9% decrease from control levels, $P = 0.380$, n = 12; Figure 5.8 D). Finally, direction selectivity measures the degree to which a cell responds

more strongly to one of the two directions of motion for a preferred orientation. This does not change significantly with SOM^+ cell activation in PV^+ cells (5.0 ± 20.9% decrease from control levels, P = 0.679, n = 21; Figure 5.8 E). It approaches significance in Pyr cells (16.1 ± 22.7% increase from control levels, P = 0.052, n = 12; Figure 5.8 F) but does not reach it.

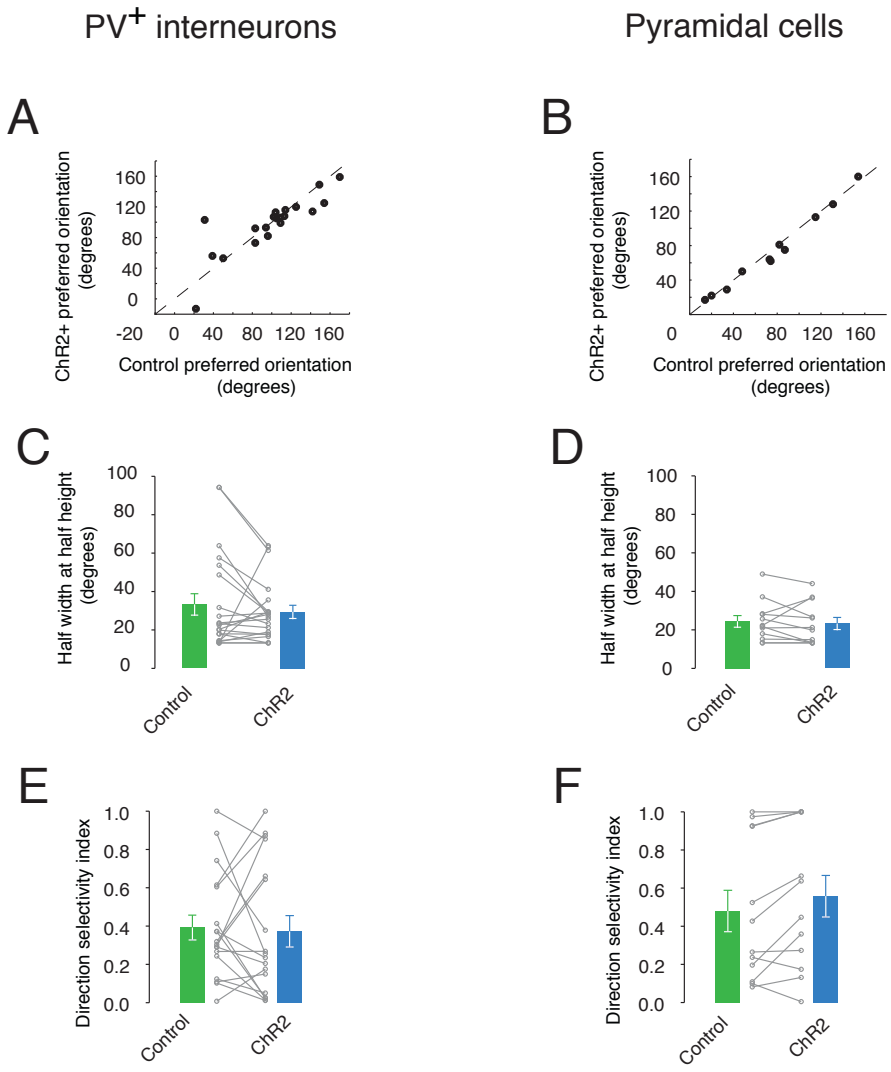

Figure 5.8 The effects of SOM^+ activation on further tuning measures of PV^+ cells and pyramidal neurons

A,B Preferred orientation does not change much for PV+ cells (n = 21, mean Δorientation = 9.56°) or Pyr cells (n = 12, mean Δ orientation = 3.59°). **C,D** The half width at half height did not change in PV+ cells (n = 21, P = 0.375) or Pyr cells (n = 12, P = 0.380). **E,F** Direction

selectivity is unchanged for PV+ cells (n = 18, P = 0.679) with ChR2 stimulation but approaches significance in Pyr cells (n = 12, P = 0.052).

Previous studies have looked at whether the effect of inhibition produced by a particular interneuron type is divisive or subtractive (Lee et al., 2012; Wilson et al., 2012). Subtractive inhibition removes the same number of spikes at all orientations effectively shifting the response curve downwards while divisive inhibition applies a division to the curve shifting the curve downwards but also reducing the size of the tuned component.

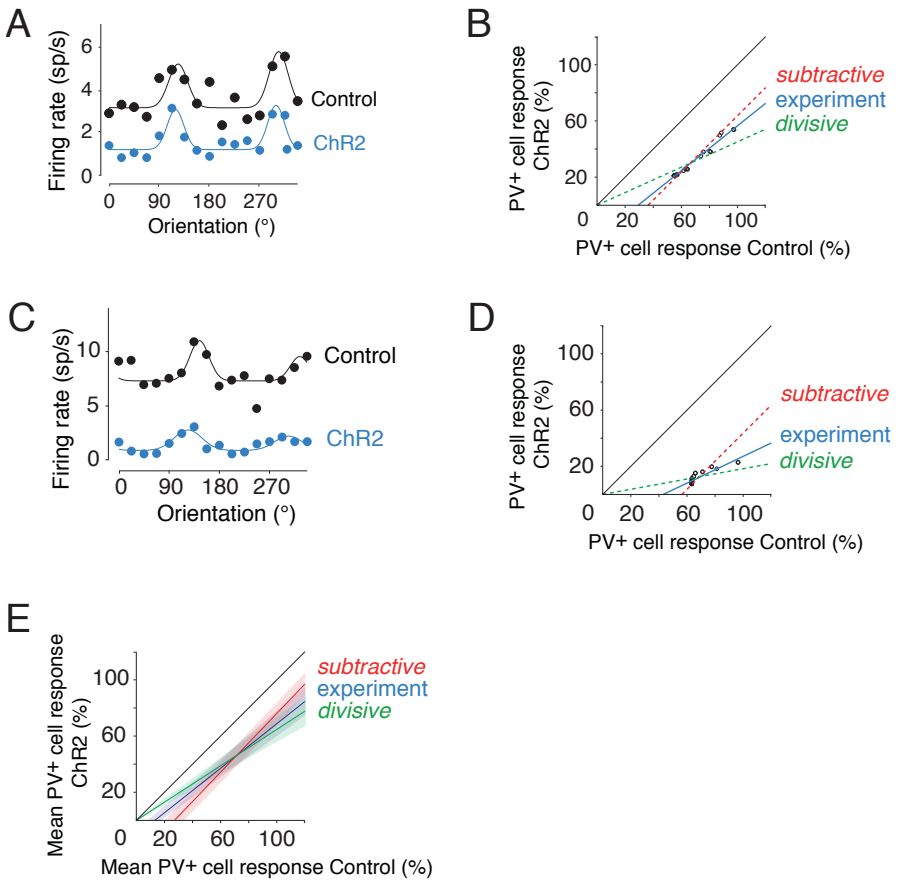

Figure 5.9 Neither pure subtraction nor pure division account for the changes in PV+ tuning

A, The visual responses of a representative PV+ cell, showing responses with and without ChR2 stimulation. **B**, Control and ChR2 stimulated PV+ responses from the cell in A as a percentage of the maximal response plotted against each other. The black (unity) line represents no difference between the two conditions. The blue line is a linear fit (y = 0.799x - 23.36) of 30 points sampled from the control and ChR2 Gaussian curves in A. The red dashed

line represents hypothetical pure subtraction while the green dashed line represents hypothetical pure division. **C,D** A second representative PV+ cell with the same layout; the linear fit for the experimental data is (y = 0.525x - 29.28). **E**, Pooled data for the entire PV+ cell population (n = 21). Using the same layout as in B,D, the blue line (y = 0.7790x - 9.83) shows the control versus ChR2 responses averaged across all cells; the envelope around this line shows the standard error. The black (unity) line represents no difference between the two conditions, the red dashed line represents hypothetical pure subtraction while the green dashed line represents hypothetical pure division and their envelopes show standard error.

We found that SOM^+ cell inhibition reduces both the untuned and the tuned components of the PV^+ cell response (Figure 5.6 A, Figure 5.7 G). The untuned component is reduced more than would be expected by division alone. This suggests that the inhibition can be described as neither purely subtractive nor purely divisive. To quantify this, we carried out least-mean-square-fit analyses, which compared the control condition with the ChR2 condition while modifying the control curve in either a purely subtractive or a purely divisive manner. At the end of the fitting process, a similar average mean squared error was obtained for subtraction (0.40 ± 0.23, n = 21) and division (0.38 ± 0.16, n = 21), with no significant difference between the hypothesized inhibition types (P = 0.61). We therefore conclude that although subtraction may dominate (through a larger decrease in the untuned component), SOM^+-mediated inhibition of PV^+ cells cannot be described as purely subtractive or divisive. This has been further demonstrated graphically for representative PV^+ cells (Figure 5.9 A-D) and for an average of all PV^+ cells (Figure 5.9 E).

In Chapter 3 of this thesis the temporal responses of the different cell classes were investigated (Figure 3.7, Figure 3.8). Different cell classes responded differently to the onset of a new orientation of drifting grating but after around a second they had all settled into a similar constant pattern. Following on from these findings it would be useful to know whether the ChR2 driven activation of SOM^+ interneurons affects a given cell-type equally over the 2 seconds of 40 Hz blue light stimulation and whether this differs between the two different cell types recorded.

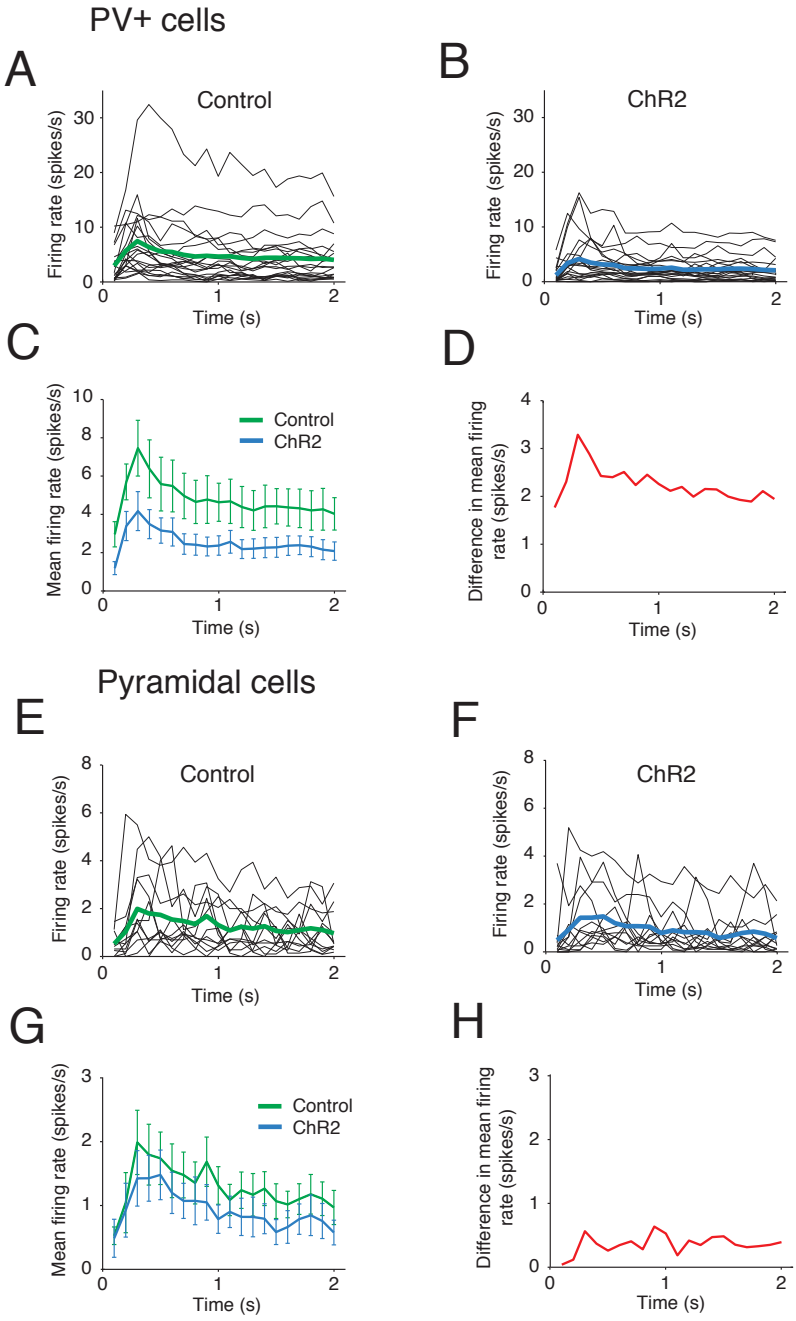

Figure 5.10 Timing of the ChR2 driven reduction in firing

A, All PV+ cells (n = 21) with their control mean firing rates plotted as black lines and the control population mean in green. **B**, All PV+ cells (n = 21) with their ChR2 mean firing rates plotted as black lines and the ChR2 population mean in green. **C**, The PV+ control population mean firing rate is plotted in green and the PV+ ChR2 population mean firing rate is plotted in blue. Error bars are SEM. **D**, The difference in mean firing rates between the control and ChR2 population means. **E-H**, Pyramidal cell data (n = 12) in the same format as above.

Figure 5.10 examines the temporal distribution of spike reduction in both cell types beginning with the PV^+ interneurons (Figure 5.10 A-D). First the range of mean firing rates for each cell in the control condition are shown together with the overall mean (Figure 5.10 A). These values have not been normalized this time unlike in chapter 3 (Figure 3.7, Figure 3.8), because the comparison in this case is within a single cell-type and so the raw mean firing rates can be used as was done to calculate other non-temporal measures (Figure 5.6, Figure 5.7, Figure 5.8). The individual responses of PV^+ neurons during ChR2 stimulation are shown in Figure 5.10 B, and these have lower individual and mean firing rates as would be expected from the strong inhibition of PV^+ cells shown previously (Figure 5.6, Figure 5.7, Figure 5.8). When the population means are compared from the control and ChR2 conditions it is clear that inhibition is occurring throughout the whole 2 second stimulation period as the blue ChR2 curve is shifted below the control curve at all time points (Figure 5.10 C). Whether the amount that PV^+ cells are inhibited is the same throughout the 2 second period is easier to visualize when the difference is taken between the control population mean and the ChR2 population mean (Figure 5.10 D). This shows that although a reduction of at least 2 spikes/s is occurring on average throughout the stimulation, there is a period between 200 and 400 ms from onset when there is an additional spike reduction of ~1 spike/s. This is the same as saying that SOM^+ cell activation removes 33% extra spikes during this period compared with the rest of the stimulation. The data for Pyr cells is laid out in a similar fashion (Figure 5.10 E-H). Looking at the initial raw means for each cell and the population averages, it is less clear that there is a reduction in firing than for the PV^+ interneurons (Figure 5.10 E,F). This matches with the result that PV^+ cells are more strongly affected by SOM^+ cell activation than Pyr cells (Figure 5.6, Figure 5.7, Figure 5.8). When the population means from the control and ChR2 conditions for Pyr cells are compared, it is clear that there is some reduction but the overlapping SEM error bars show that this reduction is likely to be less significant than the one occurring in the PV^+ cell case (Figure 5.10 G). When the difference between the control and ChR2 population means is examined it does not appear the same as was seen with the PV^+ cells (Figure 5.10 H). For the Pyr cells there appears to be little or no change between

the control and ChR2 conditions for the first 200 ms and after that a reasonably constant level of spike reduction, albeit somewhat jagged (Figure 5.10 H). It appears that not only are there differences in how strongly these two cell-types are affected by ChR2 driven SOM^+ cell activation but also differences in the way this inhibition is distributed in time.

5.3 Discussion

The use of a novel combination of transgenic animals has allowed the collection of a unique dataset in which the effect of population SOM^+ cell activation using ChR2 can be compared between two different cell types, Pyr cells and PV^+ cells. The first clear result is that PV^+ cells are approximately two times more strongly inhibited by SOM^+ cells than Pyr cells. This is found across all measures of firing rate in response to visual stimuli as well as for spontaneous rates (Figure 5.3, Figure 5.6, Figure 5.7). Though Pyr cells are less strongly inhibited, there does appear to be a consistent spiking reduction across measures (Figure 5.6, Figure 5.7). While this is not significant for every measure, it is for average firing rate (Figure 5.7 D), and peak firing rate closely approaches significance (Figure 5.7 B). The mechanism underlying this difference at the level of spiking is presently unclear. SOM^+ cells are thought to connect promiscuously in the network (Fino and Yuste, 2011) and previous studies that have looked at connection strength in cortical layer 2/3 have found larger inhibitory currents in Pyr cells as opposed to PV^+ cells (Xu et al., 2013). In terms of the hypotheses originally put forward in chapter 4 (Figure 4.1 C) it appears that in the viral case hypothesis 1 is correct, so that despite the potential for disinhibition via the disynaptic pathway through PV^+ cells the overall results is a reduction in firing in surrounding Pyr cells and PV^+ interneurons. Two recent studies investigated the effect of SOM^+ cell stimulation on Pyr cells (Lee et al., 2012; Wilson et al., 2012). They both used strong enough ChR2 activation of SOM^+ cells to obtain significant suppression of Pyr cell firing. They were not able to target PV^+ cells at the same time to compare with the Pyr

cells and from the data in this thesis, I would hypothesise that the PV^+ cells were even more inhibited than the Pyr cells.

In addition to the differences in the level of inhibition of spiking between the two recorded cell types, the second main effect is that SOM^+ cell inhibition of PV^+ cells appears to increase PV^+ cell orientation tuning while leaving Pyr cells unaffected (Figure 5.6, Figure 5.7). This increase in PV^+ orientation tuning according to the measures of OSI and CV used in this study is primarily due to a large reduction in the untuned component of the visual response. This means that the tuned component of the response becomes a higher proportion of the total response and therefore the cells become more similar to Pyr cells, which have very small untuned components (Figure 5.6B). This tuning composition in Pyr cells can also explain why their orientation tuning is unaffected by SOM^+ cell activation: they are already highly tuned so there is not much more improvement that can be made (Figure 5.6 D). As an explanation for why PV^+ cells would become more tuned with SOM^+ cell inhibition it may be instructive to look at the excitatory inputs that SOM^+ cells receive. PV^+ cells receive strong feedforward input from layer 4 and feedback inputs from surrounding Pyr cells in layer 2/3 and PV^+ interneurons exhibit significant orientation tuning in mice at early stages of development (P17-19, (Kuhlman et al., 2011)). It may be that PV^+ cells receive layer 4 inputs but are not yet fully integrated laterally into layer 2/3. This hypothesis would mean that layer 2/3 excitatory connectivity is effectively *untuning* PV^+ interneurons. It is possible to observe in control conditions that PV^+ cells still have some level of tuning riding on a large DC offset, by inhibiting activity in both layer 2/3 cell-types SOM^+ cells may be reducing the layer 2/3 influence on PV^+ interneurons allowing them to express more the patterns of input they receive from layer 4. A similar explanation can also be used to explain the increase in F1/F0 ratio seen in PV^+ cells during SOM^+ cell stimulation (Figure 5.6 G). If the inputs arriving at PV^+ cells from layer 4 are more tuned and simple than the lateral layer 2/3 inputs, then reducing lateral 2/3 input to PV^+ cells will give the layer 4 cells more influence over the final spike output of the PV^+ cells.

As there was a clear reduction in PV^+ cell spiking, I examined whether this reduction was driven by subtractive or divisive processes. This question has been addressed in computational (Carandini and Heeger, 1994) and more recently in experimental studies (Lee et al., 2012; Wilson et al., 2012) and is thought to shed light on the computations that different interneuron types are a part of. Both the untuned and tuned components of PV^+ cell responses were significantly reduced (Figure 5.6 A, Figure 5.7 G) and fitting tests were unable to distinguish between subtraction and division. In other studies, changes were rounded up to either full subtraction or full division but here the data is simply shown as it is and the suggestion is that it can be a false distinction in this and potentially other cases to attempt to distinguish in a binary way between the two options.

Finally, another interesting aspect of this set of experiments is the response timing. Here it was shown that PV^+ cells are affected more by SOM^+ cell activation 200-400 ms after stimulus onset than the rest of the time (Figure 5.10 D). Pyr cells were unaffected by SOM^+ cell activation initially (first 200 ms) and then had a similar level of spike reduction throughout the rest of the stimulation period (Figure 5.10 H). From the original control responses recorded in Chapter 3 (Figure 3.7, Figure 3.8) it is clear that PV^+ cells have a stronger onset response than Pyr cells and SOM^+ cells. Despite this strong onset spiking SOM^+ cell activation was able to remove the most spikes during the early stages of the stimulus periods. It is unclear why there is greater inhibition earlier. This could be due to fatigue of SOM^+ cell inhibition over time or short term plasticity at the pre or postsynaptic level. Alternatively, there are many more spikes at this early stage in PV^+ cells that can potentially be blocked. It might have been expected knowing the network connectivity (Figure 4.1 A) that the time of highest inhibition for PV^+ cells would lead to less inhibition in Pyr cells due to disynaptic disinhibition. This does not appear to be the case, as there is no obvious reduction in the difference between control and ChR2 conditions between 200-400 ms in the Pyr cells (Figure 5.10 H). If the inhibition fatigues over time and is stronger at the beginning then it is not clear why the smallest inhibitory effect on Pyr cells is at the start. This could be a time when PV^+ cells are still firing at reasonably high rates and are able to control Pyr cell firing. In summary SOM^+ cell stimulation

suppresses PV^+ cell firing twice as much as Pyr cell firing and results in the PV^+ cell becoming more orientation tuned and phase modulated. This manipulation does not affect the preferred orientation of any of the cells involved.

6 General discussion and outlook

6.1 Introduction

In this thesis I used cell-type-specific labeling and optogenetic manipulations to study interneuron responses in mouse V1 and the effects of SOM^+ cell manipulation. PV^+, SOM^+ and Pyr cells exhibited a graded set of visual responses from PV^+ cells, the highest firing and least tuned, to Pyr cells, the lowest firing and most tuned. SOM^+ cell responses were closer to PV^+ cells than Pyr cells. Manipulation of SOM^+ interneurons suppressed the firing of PV^+ cells more than Pyr cells. This effect occurred both at the small scale when manipulating small numbers of cells, and at the large scale with the viral manipulation. The large scale manipulation affected PV^+ cell tuning indices and the modulation index. In addition the spikes removed were not distributed equally over time.

In this section I will discuss the context, causes and meaning of these results in more detail and look forward to future experiments, both in this area and in the field of functional cortical microcircuits more widely.

6.2 Different cell types and their visual responses

6.2.1 Cell type classification

Before recordings are made to compare the responses of different interneuron types it is important that we have a robust concept of what a cell type is and how much variability within a cell type is possible. In the introduction (1.2) I detailed the problems with developing a clear interneuron taxonomy. These centered around the overlap between different characteristics across putative cell types whether morphological, molecular or electrophysiological and the amount of intragroup variability. Function is the best arbiter of interneuron classification as it concentrates on only the similarities and differences between interneurons that are necessary to allow the brain to operate normally. However as we know relatively little about how specific interneuron types contribute to brain function it is not yet possible to use this functional discriminator clearly. As each interneuron is wired into the network in a particular way it is likely that its function may not be completely different in every context. Although a given interneuron type may not operate in every context (such as a particular stimulus), it is likely that when it does, it will apply a similar mathematical function to the cell it innervates. In this way, finding cells for particular functions like a particular type of gain control or size tuning may be impossible as many interneurons operate at the same time and it is the summed outcome of these relatively stereotyped operations that produces the overall outcome (although see (Adesnik et al., 2012)).

Very recently a group of scientists have proposed a new interneuron classification scheme (Defelipe et al., 2013). As any functional classification is hampered by our lack of full understanding of circuit function, they take a more pragmatic stance. A working grouping of interneurons will allow us to design experiments that should further illuminate function and therefore help with classification even if some of the original grouping is flawed. They identify the axon morphology as the most informative feature separating interneurons and suggest it is very likely

that it is closely associated with cell function. They then identify 6 axonal features many of which are binary or have a limited selection of choices. Having established their classification scheme they test it against the performance of 42 experts. As would be expected some of the 6 features are more consistently agreed upon amongst the experts than others. It helps to know which are more reliable as ultimately they could be weighted to take this uncertainty into account. Finally they provide this classification scheme to the community in the form of a useful online tool. Hopefully this will become widely used although there have been a number of previous attempts at this type of tool that now linger on as zombie sites on the web due to lack of community take-up (Bota and Swanson, 2007). In the case of this project I compared two of the most distinct cell types that differ from each other on almost every dimension (1.2.2) and are therefore likely candidates for differing functions. I was limited to comparing SOM^+ and PV^+ cells in layer 2/3 as 2 photon imaging does not work effectively much lower. The ideal layer to study the separation of function of these two cell types is layer 5, since PV^+ basket cells have axons that remain within layer 5 while SOM^+ cells have axons that project all the way up to layer 1. In layer 2/3 these differences are somewhat compacted as they are displayed over a much smaller distance so there is more overlap between the regions of axonal innervation onto Pyr cells.

6.2.2 Interpreting the visual responses of Pyr, SOM^+, PV^+ cells

The three main visual response properties that vary across the cell types are firing rate, orientation tuning and timing. Looking at mean firing rates, Pyr cells have the lowest, then SOM^+ cells, then PV^+ cells. What is the functional role of having higher firing rates in interneurons? One answer to this deals with inhibitory capacity. Interneurons make up only 20% of the cells in neocortex but must be able to balance excitation while participating in the local fluctuations of activity that allow the variety of functional connectivity in cortex, and therefore its heterogeneity and high information processing capacity (Haider and McCormick, 2009). For fewer inhibitory cells to balance the activity of a larger group of excitatory cells they must fire more than the excitatory cells. In fact, a back of the

envelope calculation shows that inhibitory cells produce roughly the same amount of spikes in cortex as excitatory cells, despite being outnumbered 4 to 1. If a network of 100 cells is considered, firing for 1 second under visual stimulation using the mean firing data from this study: 80% of cells are pyramidal and fire at a mean rate of 1.28 Hz across all orientations therefore producing around 102 spikes (80*1.28) during 1 second of visual stimulation. Interneurons make up 20% of the neuronal population and of that 20% are SOM^+, 40% and PV^+, leaving 40%. SOM^+ cells fire at 3.59 Hz from my data and so contribute 14 spikes (4*3.59), PV^+ cells have a mean firing rate of 6.67 Hz and so contribute 53 spikes (8*6.67). For the remaining 40% of interneurons I have no data but will assume the lower firing rate of the SOM^+ cell (although there will be variability within this group), therefore they contribute 29 spikes (3.59*8). In total therefore the interneurons produce 96 spikes, which closely matches the 102 produced by the Pyr cells. However, not all spikes are equal, as some inhibitory spikes may be much more powerful at shutting down excitatory activity than others. For example chandelier cell inhibition targeted to the axonal initial segment of Pyr cells may be highly potent at preventing Pyr cell spiking, more so than a more peripheral dendritic inhibitory input. Having Pyr cells as the most numerous neuron which fires less, while having a lower proportion of interneurons which fire more may be a near optimum arrangement. It allows for balance between inhibition and excitation to be maintained while having a great excess of projecting Pyr cells. This allows for more complex wiring and higher potential capacity for processing information by specifically projecting Pyr cells while interneurons appear to connect promiscuously to all target cells in the local area (Fino and Yuste, 2011; Packer and Yuste, 2011).

Orientation tuning is also graded across cell types with Pyr cells being the most tuned, SOM^+ interneurons spanning the whole range and PV^+ interneurons being the least orientation tuned. Differences in cell intrinsic properties such as spiking threshold and input resistance may account for some of the differences between SOM^+ cells and PV^+ cells (Ma et al., 2010). However there are other differences to consider such as the sources of input of excitatory input which vary between groups (Ma et al., 2010; Adesnik et al., 2012). Whatever the cause of the

differences in tuning, what might the function be of having differently tuned interneurons? It is fairly clear that PV^+ interneurons with their broad tuning act to set a dynamic threshold in the cells they innervate that exists across orientations (Priebe and Ferster, 2008). While Pyr cells connect to each other in a pattern biased in favour of shared orientation preferences within layer 2/3, PV^+ cells contact and are contacted by cells of all orientations (Bock et al., 2011; Ko et al., 2011; Packer and Yuste, 2011). We know less about the orientation tuning of inputs to SOM^+ interneurons but know that they connect promiscuously to Pyr cells within the local area (Fino and Yuste, 2011). What might having tuned SOM^+ interneurons contribute to visual processing? It is likely that due to their promiscuous connectivity and the fact that multiple different SOM+ interneurons connect to the same Pyr cell that effects of a rare tuned interneuron would be washed out. To hypothesize a function for this tuning would require subcellular specificity where the SOM^+ tuned cell contacts and inhibits a particular dendritic branch of a Pyr cell. While not impossible, this sets a high bar, so it is safer to assume no particular role for these inputs until more positive evidence for such a role is found.

The timing results with PV^+ cells responding more quickly than SOM^+ cells can be explained as the differences between the roles of feedforward and feedback inhibition (Silberberg, 2008). PV^+ cells receive much more feedforward input from L4 than SOM^+ interneurons and so are able to reach spike threshold much more quickly (Adesnik et al., 2012). PV^+ cells also receive depressing excitatory inputs so that during a train of spikes they initially receive a lot of input driving spiking but less over time. SOM^+ cells on the other hand receive facilitating inputs and so require many spikes arriving from Pyr cells before they are driven sufficiently hard to spike. In addition to these two effects that are likely to make SOM^+ cells spike later there is also the fact that the two interneuron subtypes inhibit each other (Gibson et al., 1999). Therefore the early high levels of activity in PV^+ cells inhibit SOM^+ cells and make it even harder for them to reach threshold. Later in the visual stimulus once the PV^+ cell inputs have depressed SOM^+ cells are able to take over and in turn inhibit PV^+ cells. This switch reveals some clues as to the function of these cells in time. PV^+ cells inhibit Pyr cells

during the first surge of visual information and then over time if the stimulus stays relatively constant inhibition shifts along the somatodendritic axis to be controlled at the dendrites by SOM^+ cells. This will be dealt with in more detail when discussing the results from Chapter 5 (Discussion 6.4).

The responses of neurons in visual cortex vary in different brain states (Haider and McCormick, 2009). Likewise under conditions of anaesthesia versus wakefulness there are likely to be large differences. The urethane/chlorprothixene protocol used in this thesis has the benefit of matching with previous surveys of visual cortex and allowing long stable recordings in mice but may not represent the true brain state during wakefulness. Isoflurane recordings approach this more closely by having a reduction in up and down states and a more wakeful-like tonic level of depolarization (Poulet and Petersen, 2008). Awake recordings must be the goal as it has been shown the scale of inhibitory activity is even larger than in the anaesthetized condition (Haider et al., 2013). This increased level of inhibition has a pronounced effect on the temporal dynamics of cortical activity, greatly curtailing the Pyr cell response and presumably altering the dynamics of the interneurons as well (Haider et al., 2013). The activity of SOM^+ cells may be particularly affected by the change between anaesthetized and the awake moving state (Adesnik et al., 2012).

Although it is sometimes difficult to compare across data sets, as discussed in Chapter 3, due to many minor differences in methodology I believe my data broadly agrees with published data and helps clarify the roles of, and the relationships between, these three cell types.

6.3 Manipulating small populations of SOM^+ cells

The single cell electroporation data showed that the manipulation of small numbers SOM^+ interneurons could produce a detectable suppression in putative PV^+ cells but not in Pyr cells. This was surprising as although it is known that interneurons inhibit each other as well as Pyr cells it was originally thought that their main role was to inhibit Pyr cells.

6.3.1 A discussion of the data

A higher n number throughout these experiments would help to bolster the reliability of the findings. These experiments are technically demanding and have low success rates which made collecting large amounts of data difficult. Nevertheless there appears to be a consistent reduction in firing in the putative PV^+ cells we recorded from while stimulating SOM^+ cells. The consistency is more important than the size of the effect, as a large effect would not be expected from the stimulation of only 2-3 SOM^+ cells. A higher n may also have uncovered an effect in the suppressive trend seen in Pyr cell peak firing rate when 4-7 SOM^+ cells were simulated. If this trend were shown to be real it would be very interesting as it would show that small numbers of SOM^+ cells can suppress Pyr cell firing, but only if 4 or more are stimulated setting a lower bound for detectability. Multiple cells were sampled in each animal but these were often low numbers not nearly covering the hundred or so neurons in each field of view. It is possible that there are some inhibited Pyr cells, but that they are distributed sparsely around the population and so I missed them with my cell-attached recordings. Despite this, the fact that I saw consistent suppression in putative PV^+ cells is still interesting as it shows that SOM^+ cells inhibit them densely. The result here also matched up with what I found when carrying out a large scale manipulation of SOM^+ cells, lending further weight to my argument.

There is only one other study that purports to have stimulated single SOM^+ cells and measured their effects on the local network (Wilson et al., 2012). They report

that they saw sparse suppression of cells too numerous to just be PV^+ cells. This means that they claim to see the sparse Pyr cell suppression that I may not have detected with my sparse sampling. However there are serious problems with this study. First, to stimulate single cells they used a beam of one-photon blue light, and this cannot reliably stimulate single SOM^+ cells because there is a very dense mat of transfected SOM^+ cell axons in layer 1 and upper layer 2/3. The intensity of blue light required to evoke spikes in the cell bodies of SOM^+ interneurons 100 μm and more below the surface, would also stimulate many tens or hundreds of axons lying above, which receive even stronger blue light. A second factor that is strange is that the effect sizes in the Pyr cells are of a similar amplitude to those they see when doing the non-focal stimulation suggesting that they are indeed stimulating more than one cell in the focal stimulation case. They use Ca^{2+} imaging to record from the large number of cells in the local area at once. This is problematic when looking for small effects as it does not provide anything like single spike resolution, making it less likely that they would be able to detect and distinguish small effects. Finally in their analysis of these differences they carry out a paired t-test for every cell in the field of view. Carrying out so many tests means that it is likely they would detect a number of effects in either direction purely by chance. Having said all of that, it is not impossible that some sparse suppression of Pyr cells may be the case whether or not I think that the Wilson experiment is able to create the correct conditions or detect the result. A new form a genetically expressed Ca^{2+} sensor has recently been produced that allows much better signal to noise ratios in the imaging data (GCamP6). This could be used in concert with single cell electroporation of ChR2 to ensure single cells are being stimulated and small effects are able to be distinguished in Pyr cells.

6.3.2 Possible mechanisms to explain the results of the manipulation

The differential effect I have observed between Pyr cells and putative PV^+ cells could be explained by a number of mechanisms. Firstly PV^+ cells could receive more inhibitory input than Pyr cells thereby reducing their spiking more. Secondly they could both receive the same amount of inhibitory input but this has the effect of reducing firing more in PV^+ cells due to differences in cell properties between the two cell types. Thirdly the secondary effect of disinhibition of Pyr cells by reduced firing in PV^+ cells may play a large role in masking the effect of SOM^+ inibition in Pyr cells. This secondary effect could operate as a bolt on option to either the first or second explanation.

In order to distinguish between these different effects more work would be needed. Intracellular recordings from Pyr cells would be able to measure if the total amount of inhibitory input increased, decreased or stayed constant which would help to distinguish how prominent the secondary effects are. Comparison in the size of SOM^+ cell inputs could be made to distinguish between option one and two above by recording intracellularly from Pyr and PV^+ cells and comparing the size of the inhibitory currents while stimulating SOM^+ cells with light. The set frequency of blue light ChR2 stimulation would be useful in identifying which events were caused by SOM+ cell inhibitory inputs.

6.4 Manipulating large populations of SOM$^+$ cells

6.4.1 Conclusions from the viral data

The results from the large scale SOM$^+$ cell stimulation experiment confirm the findings of the single cell electroporation experiment. They show that the spiking of PV$^+$ interneurons was reduced twice as much as that of Pyr cells. Much of the concentration in the inhibitory literature has been on the effect of inhibitory cells on Pyr cells. I show that the largest effect is actually on another interneuron type responsible for inhibiting a different part of the Pyr cell somatodendritic axis. This data appears to contradict recent evidence from the barrel cortex in which it was shown that SOM$^+$ cells deliver larger inhibitory currents to layer 2/3 Pyr cells rather than PV$^+$ cells (Xu et al., 2013). This may still be compatible with my data if the outcome in terms of spiking is a greater reduction in PV$^+$ cell spiking than Pyr cell spiking. The results of their SOM$^+$ cell silencing experiment are more problematic as they see an increase in Pyr spiking even though according to my data the PV$^+$ cells might be expected increase their spiking more under SOM$^+$ cell silencing and therefore inhibit Pyr cells more. There is in vivo data to suggest that the barrel cortex microcircuitry may be organized and operate differently to the visual cortex (Gentet et al., 2012). This data shows that while fast spiking and non-fast spiking interneurons increase their firing in response to a whisker stimulus in the awake animal SOM$^+$ cells decrease their firing (Gentet et al., 2012). This is not true in visual cortex and suggests each modality of sensory cortex may have its own connectivity weight matrix. This may stem from the fact that different modalities deal with different stimulus temporal and spatial frequency patterns and may be optimized accordingly. However as the whisker stimulation in this experiment is only 2 ms long it could be that the connectivity matrix is the same as visual cortex but SOM$^+$ cells do not receive strong enough input during such a short burst of stimulus, whereas PV$^+$ cells designed to respond to such an input do have the opportunity to fire and therefore suppress SOM$^+$ cells. In addition the awake whisker deflection was not created by active touch but

by a stimulus unexpected by the mouse which could further create different effects from normal whisking. With arguments both for and against, it will be essential to measure the connectivity strength between SOM^+, PV^+ and Pyr cells to have a certain answer to this question.

One area in which the reduction in PV^+ cell firing could help explain a recent controversy in the literature is the recent pair of Nature papers both looking at viral PV^+ cell and SOM^+ cell stimulation (Lee et al., 2012; Wilson et al., 2012). These papers found the opposite inhibitory transformations caused by the cell classes. Wilson et al. found that SOM^+ cell stimulation caused subtractive inhibition and a reduction in the tuning width of Pyr cells, while PV^+ cell stimulation caused divisive inhibition in Pyr cells. Lee et al. found PV^+ cell stimulation caused subtractive inhibition and a reduction in the tuning width of Pyr cells with SOM^+ cell stimulation causing divisive inhibition. There are many differences between these studies in terms of layers recorded from, stimulus regimes and recording methods. Lee et al. collected data from all layers with only around a quarter of their cells being in layer 2/3, while Wilson et al. collected data exclusively from layer 2/3. Wilson et al. used 10 ms pulses of blue light at 10 Hz, while Lee et al. used a long period of solid blue light stimulation. Recordings were made by Lee et al. using multichannel electrophysiological probes, while data was collected in the Wilson et al. experiment using Ca^{2+} imaging. All of these differences may contribute to the differences in results between these groups and should be examined in more detail. As well as the relationship between the stimulated interneuron type and the Pyr cells it is important to know what effects this stimulation has on other cells in the cortical network. My data shows that in the case of SOM^+ cell stimulation, the largest effect is on PV^+ interneurons rather than Pyr cells. As the inhibitory connections between SOM^+ and PV^+ cells are reciprocal (Gibson et al., 1999), it means that both of these groups were unable to change the activity of the two interneuron types independently. In fact the largest changes they were making in the SOM^+ cell stimulation case was on the PV^+ cells. This means that even if a particular interneuron cell type were purely subtractive or divisive, stimulation of that cell type would lead to an additive or multiplicative change being applied by the disinhibition of the other cell type. As I will discuss

in the final part of this section when dealing with function, this mutually inhibitory relationship between the SOM^+ and PV^+ interneuron groups is likely to play a key role of their processing of sensory information.

Similar to the thoughts about how interneurons operate across different cortical areas, there is also the question about how they function across different species. Firstly there is not exact concordance in interneuron diversity even in relatively closely related species (Xu et al., 2010). Secondly although rodents display the salt and pepper organization pattern of orientation selectivity in visual cortex (Ohki et al., 2005) cats and monkeys have a pinwheel organization (Hubel and Wiesel, 1974b; Blasdel and Salama, 1986) in which cells close to each other have the same orientation tuning including interneurons. Having tuned inhibition will not provide an equal level of inhibition across orientations and therefore will require some change in the level of excitation if the response curves are to be kept similar to those in the rodents.

Interneuron manipulation appears to have no effect on orientation preference. This suggests that Priebe and Ferster are correct that orientation tuning is defined by feedforward excitation and matches Hubel and Wiesel's original model (Hubel and Wiesel, 1962). My data show that no matter how hard you drive SOM^+ interneurons they do not change the preferred orientation in Pyr cells. Lee et al. and Wilson et al. stimulated both SOM^+ and PV^+ interneurons and also saw no change in preferred orientation (Lee et al., 2012; Wilson et al., 2012).

SOM^+ interneuron stimulation was able to increase the orientation selectivity index and circular variance of PV^+ cells. Inhibition of PV^+ cells reduced both the tuned and the untuned components but reduced the untuned component more, making the tuned component a higher proportion of the total remaining PV^+ cell response. In some cells the untuned DC offset was completely removed leaving only a Gaussian curve with a trough at zero that strongly resembled a reasonably tuned Pyr cell. A similar change took place with the F1/F0 ratio which became more modulated and simple-cell-like by the removal of a large proportion of the unmodulated spiking. Do both of these changes occur in vivo and what is their function? In vivo it is possible for SOM^+ cells to fire at high rates in the awake

moving animal (Adesnik et al., 2012) similar to those induced using ChR2 in these experiments. Less obvious is the function of having PV^+ cells with higher orientation selectivity indices. It would be expected that this tuning would be washed out by the many different PV^+ cells connecting to any single Pyr cell and so should not affect Pyr cell output in a specific way.

The timing results show SOM^+ cell inhibition removing most spikes from PV^+ cells when they are receiving the most excitatory drive and should be responding the most vigorously. As mentioned in Chapter 5 this could be because SOM^+ cell inhibition fatigues over time. However it is the surprising that the level of spike suppression is so stable for the rest of the stimulus rather than steadily decreasing with increasing fatigue. It may be that the arrangement of SOM^+ cell inhibition onto PV^+ interneurons means that it is most effective when PV^+ cells receive more excitation. It is known that SOM^+ cell inhibitory inputs are mainly located on the dendrites of PV^+ cells (Hioki et al., 2013) colocalised with the majority of the excitatory inputs (Kameda et al., 2012) unlike other inhibitory inputs to PV^+ cells. This means that high levels of SOM^+ cell inhibitory input could shunt excitation in the dendrites, in this way high excitatory input would lead to more shunting and an even higher level of spike suppression.

6.4.2 Drawbacks and possible pitfalls

The experimental tools used in this thesis are cutting-edge with many only recently becoming available and several I had access to before they were widely published. Despite this, some of these tools are still a long way from the ideal that a neuroscientist would desire if there were no technical restrictions.

A potential problem that needs to be discussed is the use of double transgenics. In this project I crossed SOM-Cre animals with PV-GFP animals to produce a line in which both cell types could be separately identified. To my knowledge this combination has not been carried out before and the combination appeared stable, with specific expression confirmed by immunohistochemistry. However as mice are derived from a number of different exotic background lines (Jackson, 2013a)

and their transgenes vary in genetic location it is likely that some lines may not be compatible for this sort of cross. It is important to get the genetic backgrounds as similar as possible through backcrossing, but this is often not done for enough generations. Mice should be continually monitored for any obvious physical defects and tested by genotyping and immunohistochemistry to ensure a particular double transgenic is viable.

ChR2 is an excellent tool for cell-type-specific non-invasive stimulation on single spike timescales. However it has certain drawbacks especially when used across a large population. Firstly all the cells transfected will be stimulated at the same time. The 40 Hz pulses used in this study entrained all of the transfected SOM^+ cells to the same frequency and phase within that frequency. This does not reflect the normal pattern of activity but does have the benefit of offering some precision to how many spikes are added to the network and when. This can be circumvented by using long periods of blue light with the aim of increasing the level of the endogenous activity to maintain its patterns. This may work to some extent but gives less control over the level activity has been increased and is more likely to lead to ChR2 entering the inactive state within its photocycle due to high levels of blue light exposure (Bamann et al., 2008).

With large scale viral delivery of ChR2 into interneurons the level of stimulation used is important. I showed in the viral data that different light levels can produce everything from small effects to complete cortical shutdown. Realistic stimulation is the ideal but if you wish to see beyond the natural stimulus responses the manipulation will by definition need to be to some extent artificial. In future it would be sensible for experiments such as my own and the Lee et al. and Wilson et al. studies to use at least 3 and ideally more levels of stimulation. This might reveal a dose dependent curve of the effects and help separate out primary and secondary effects.

6.4.3 What this means for interneuron function

Mutual inhibition between SOM^+ and PV^+ cell inhibition ensures that a balance between the two is maintained. When somatic inhibition increases, it decreases dendritic SOM^+ cell inhibition and when PV^+ cells no longer have an initial strong excitatory drive, SOM^+ inhibition of the dendrites play a larger role. As PV^+ cells are activated most strongly by feedforward input they act to balance the feedforward input into Pyr cells. By contrast SOM^+ cells are mainly activated by feedback excitation and so are the system for regulating the level of feedback input. If both inhibitory systems were too active at once they would prevent the cell from firing. Both are increased and decreased in relation to the level of their respective inputs and inhibit each other to make sure the overall level of inhibition is not too high. Each one receives their excitatory inputs and fires accordingly, then soon after receives the inhibitory inputs from the other group as a balancing factor. In the case of ongoing visual stimulation, both the feedforward and feedback circuits are being continually stimulated. Therefore both inhibitory cell types fire throughout, but their effects controlling each other may be greater than the inhibition they are delivering to the Pyr cell (I only present evidence in the SOM^+ cell to PV^+ cell direction). This emphasizes the importance of the accurate balance between these two cell types, it is not an afterthought in the circuit but a function that is likely to be equally important as their inhibition of the Pyr cells.

An important goal of the field is to study the roles of the interneuron circuits I have just described in the awake behaving animal. Two recent studies have suggested specific roles for particular types of interneurons and I would like to examine both briefly.

The first is a study suggesting that SOM^+ interneurons are responsible for surround suppression, a classical visual receptive field property (Adesnik et al., 2012). This study shows that the responses of SOM^+ cells increase with the size of the circular grating visual stimuli. Pyr cells and PV^+ cells show an initial increase and then suppression over a certain size. This increasing activity of SOM^+ cells occurs because they receive plentiful excitatory input from within layer 2/3 that spans a wide area (as they demonstrate in slice). As the size of the visual stimulus

increases, SOM^+ cells are recruited more and more strongly until they suppress the activity of the Pyr cells and the PV^+ cells. This therefore suggests that one interneuron type may play a dominant part in a specific function within visual cortex. There are a few problems with the story. They did not compare the extent of PV^+ excitation over distance in slice with ChR2 to confirm that increasing excitation over a large distance is an exclusively SOM^+ cell property. Additionally the blocking of SOM^+ cell activity by 90%, decreases the surround suppression effect by only about 30% (Adesnik Figure 4d inset) suggesting SOM^+ cells are not exclusively responsible for surround suppression. This study raises the question of what we mean by interneuron function. In this case it is the long range Pyr cell connectivity within layer 2/3 onto SOM^+ cells that allows them to have a response rate that increases with stimulus size. It could equally have been the PV^+ interneurons that received this special Pyr cell input so it is not a property of the SOM^+ cells themselves that defined this function but rather one of specific Pyr cell connectivity.

The second study to show a function of interneurons is a study into the mechanism behind auditory fear conditioning (Letzkus et al., 2011). Here disinhibition of L2/3 PV^+ cells is required for fear learning. Specific interneurons in layer 1 likely to be the single bouquet cells (Jiang et al., 2013) respond to footshock and inhibit layer 2/3 PV^+ cells. This allows more firing in Pyr cells in the local network that is then thought to aid with the forming of associations between the sweep tones and the shock. This study is very exciting and is exactly the sort of awake behavioural experiment that needs to be done. However it does not clearly demonstrate that other cells types apart from PV^+ cells are not also involved. If indeed the single bouquet cells are the same in rat as in mouse, then it is known that they connect to a range of interneuron types in layer 2/3 not just PV^+ cells (Jiang et al., 2013). SOM^+ cells are hard to distinguish from PV^+ cells on the basis of spiking alone especially when taken from cell attached recordings. They are also rarer than PV^+ cells and so may been underrepresented in their sample as they were not labeled with GFP. SOM^+ cells may also contribute to this effect which doesn't by any means invalidate this excellent study but would mean that it was not interneuron cell type specific in layer 2/3. They have concentrated

on layer 2/3 as it is accessible to microscopy but they have not confirmed that the disinhibition in layer 2/3 is necessary (Letzkus et al., 2011). The same mechanism will disinhibit layer 5 Pyr cells along their entire somatodendritic axis (Jiang et al., 2013) so it is possible these cells may be more important than those in layer 2/3.

Cortical interneurons are often described as being merely a buffer of excitation to prevent epileptic activity. As I learnt more about their incredible diversity, on almost every dimension you could think of, I began to think they could be responsible for a myriad of functions. Perhaps they could be the key components of cortical computation with Pyr cells merely relaying the outcome of these computations to the next cortical stage. At the end of this project I have returned back towards the simpler idea that interneurons act in a suppressive manner. Clearly excitation is complex and varies on many timescales so a variety of interneurons must exist to balance particular forms of excitation. In this way we can see PV^+ cells as surge protectors against feedforward over-excitation but also definers of the time window of possible Pyr cell activity. SOM^+ cells are slower to respond and balance feedback activity while also regulating the excitability of the dendrites. These dendrites are the location of the arrival of excitation and important processes like plasticity that take place there. As we saw with the Adesnik et al. study, Pyr cell wiring is as crucial in defining the roles of interneurons as the cell intrinsic properties of the interneuron cell-type. In the debate between the contributions made by Pyr cells versus interneurons to the computations of the brain, it is clear that specificity of Pyr cell wiring is probably the most important feature. However to function as a network, processing information in time, the filter and timing properties provided by the interneurons are crucial and necessary for basic function. Most importantly they are needed for flexibility of function in different stimulus contexts and for learning over time.

6.5 Outlook

As an extension of the work in this thesis it is key to know the underlying connectivity strengths between the different cell types, and to work out by which mechanism Pyr cells are suppressed less than PV^+ cells by SOM^+ cell stimulation. This connectivity weight matrix could be discovered by recording pairs of different cell types in slice and measuring connection strengths. This has been carried out for layer 2/3 cells in the barrel cortex (Xu et al., 2013) but not yet in visual cortex where the weights may be different. In addition intracellular recordings could be made from Pyr cells *in vivo* during combined visual and interneuron ChR2 stimulation. This would allow the changes in inhibitory inputs to be measured directly. It would also be interesting to activate the circuit the other way around, stimulating the PV^+ cells and recording from Pyr and SOM^+ cells.

In the future these type of experiments will be done more frequently in awake animals to prevent the artificial anaesthetized state from giving results that don't represent true brain activity. Inhibition dominates sensory responses in the awake cortex which may lead to very different set of Pyr cell responses in the awake animal, especially in the temporal domain (Haider et al., 2013). In the same way it will be very interesting to compare results in sensory cortices between conditions when the mouse is stationary and running. Studies have shown large changes in activity rates between the two due to feedback from motor areas to sensory areas (Niell and Stryker, 2010; Adesnik et al., 2012; Keller et al., 2012). Finally rather than just recording from areas when the mouse may not be concentrating on sensation, behavioural tasks will provide a handle to ensure the sensory representations being recorded are actively being used and therefore contain the necessary information for task completion (Wahlsten et al., 2003). These tasks should also help minimize inter-trial variability due to changing brain-state which are less of a problem in the more controlled conditions of anaesthesia.

New tools will give us unprecedented access to the cortical circuit to carry out these experiments. Deeper imaging will allow access to all layers of the cortical

network for a fuller idea of the flow of information between the layers (Scientifica, 2013). New recording techniques may give us access to the spiking activity of every cell in the brain. Genetic electrophysiology, although not currently available, offers a hugely promising approach to get cells to record their own electrophysiology on a nucleotide sequence that can be recovered later (Alivisatos et al., 2012). Alongside these new recording techniques, the improvement of methods to stimulate and suppress cell activity will continue giving us new levels of access to manipulate the cortical circuit.

There remain many questions about what to do with all of the data that will be produced by these novel techniques. Without a strong conceptual and theoretical backbone permeating the design of new experiments, it is easy to collect lots of data that do not further a deeper understanding of the cortical network. Hubel and Wiesel's seminal work on visual receptive fields laid much of the conceptual groundwork for work done in this thesis and in the field of visual neuroscience as a whole. Using these novel techniques to discover new patterns of neuronal activity that clearly correlate with sensory input, and deconstructing their mechanism in relation to behaviour, should help to keep data collection focused on explaining cortical network function.

References

Abbott A, Schiermeier Q (2013) Research prize boost for Europe. Nature 493:585-586.

Adesnik H, Bruns W, Taniguchi H, Huang ZJ, Scanziani M (2012) A neural circuit for spatial summation in visual cortex. Nature 490:226-231.

Airan RD, Thompson KR, Fenno LE, Bernstein H, Deisseroth K (2009) Temporally precise in vivo control of intracellular signalling. Nature 458:1025-1029.

Alivisatos AP, Chun M, Church GM, Greenspan RJ, Roukes ML, Yuste R (2012) The brain activity map project and the challenge of functional connectomics. Neuron 74:970-974.

Alivisatos AP, Chun M, Church GM, Deisseroth K, Donoghue JP, Greenspan RJ, McEuen PL, Roukes ML, Sejnowski TJ, Weiss PS, Yuste R (2013) Neuroscience. The brain activity map. Science 339:1284-1285.

Alonso JM, Martinez LM (1998) Functional connectivity between simple cells and complex cells in cat striate cortex. Nat Neurosci 1:395-403.

Anderson CT, Sheets PL, Kiritani T, Shepherd GM (2010) Sublayer-specific microcircuits of corticospinal and corticostriatal neurons in motor cortex. Nat Neurosci 13:739-744.

Anderson JC, Martin KA, Picanco-Diniz CW (1992) The neurons in layer 1 of cat visual cortex. Proc Biol Sci 248:27-33.

Anderson JS, Carandini M, Ferster D (2000a) Orientation tuning of input conductance, excitation, and inhibition in cat primary visual cortex. J Neurophysiol 84:909-926.

Anderson JS, Lampl I, Gillespie DC, Ferster D (2000b) The contribution of noise to contrast invariance of orientation tuning in cat visual cortex. Science 290:1968-1972.

Arenz A, Bracey EF, Margrie TW (2009) Sensory representations in cerebellar granule cells. Curr Opin Neurobiol 19:445-451.

Ascoli GA et al. (2008) Petilla terminology: nomenclature of features of GABAergic interneurons of the cerebral cortex. Nat Rev Neurosci 9:557-568.

Atallah BV, Bruns W, Carandini M, Scanziani M (2012) Parvalbumin-expressing interneurons linearly transform cortical responses to visual stimuli. Neuron 73:159-170.

Atasoy D, Aponte Y, Su HH, Sternson SM (2008) A FLEX switch targets Channelrhodopsin-2 to multiple cell types for imaging and long-range circuit mapping. J Neurosci 28:7025-7030.

Austin S, Ziese M, Sternberg N (1981) A novel role for site-specific recombination in maintenance of bacterial replicons. Cell 25:729-736.

Bair W (2005) Visual receptive field organization. Curr Opin Neurobiol 15:459-464.

Bamann C, Kirsch T, Nagel G, Bamberg E (2008) Spectral characteristics of the photocycle of channelrhodopsin-2 and its implication for channel function. J Mol Biol 375:686-694.

Battaglia D, Karagiannis A, Gallopin T, Gutch HW, Cauli B (2013) Beyond the frontiers of neuronal types. Front Neural Circuits 7:13.

Beed P, Bendels MH, Wiegand HF, Leibold C, Johenning FW, Schmitz D (2010) Analysis of excitatory microcircuitry in the medial entorhinal cortex reveals cell-type-specific differences. Neuron 68:1059-1066.

Beierlein M, Gibson JR, Connors BW (2003) Two dynamically distinct inhibitory networks in layer 4 of the neocortex. J Neurophysiol 90:2987-3000.

Berger TK, Silberberg G, Perin R, Markram H (2010) Brief bursts self-inhibit and correlate the pyramidal network. PLoS Biol 8.

Berndt A, Yizhar O, Gunaydin LA, Hegemann P, Deisseroth K (2009) Bi-stable neural state switches. Nat Neurosci 12:229-234.

Blasdel GG, Salama G (1986) Voltage-sensitive dyes reveal a modular organization in monkey striate cortex. Nature 321:579-585.

Blatow M, Caputi A, Monyer H (2005) Molecular diversity of neocortical GABAergic interneurones. J Physiol 562:99-105.

Bock DD, Lee WC, Kerlin AM, Andermann ML, Hood G, Wetzel AW, Yurgenson S, Soucy ER, Kim HS, Reid RC (2011) Network anatomy and in vivo physiology of visual cortical neurons. Nature 471:177-182.

Borg-Graham LJ, Monier C, Fregnac Y (1998) Visual input evokes transient and strong shunting inhibition in visual cortical neurons. Nature 393:369-373.

Bota M, Swanson LW (2007) The neuron classification problem. Brain Res Rev 56:79-88.

Bourassa J, Pinault D, Deschenes M (1995) Corticothalamic projections from the cortical barrel field to the somatosensory thalamus in rats: a single-fibre study using biocytin as an anterograde tracer. Eur J Neurosci 7:19-30.

Boyden ES, Zhang F, Bamberg E, Nagel G, Deisseroth K (2005) Millisecond-timescale, genetically targeted optical control of neural activity. Nat Neurosci 8:1263-1268.

Brainard DH (1997) The Psychophysics Toolbox. Spat Vis 10:433-436.

Brecht M, Schneider M, Sakmann B, Margrie TW (2004) Whisker movements evoked by stimulation of single pyramidal cells in rat motor cortex. Nature 427:704-710.

Brodmann KLG (1994) Brodmann's 'Localisation in the cerebral cortex'. Smith-Gordon, London.

Brown SP, Hestrin S (2009) Intracortical circuits of pyramidal neurons reflect their long-range axonal targets. Nature 457:1133-1136.

Butt SJ, Fuccillo M, Nery S, Noctor S, Kriegstein A, Corbin JG, Fishell G (2005) The temporal and spatial origins of cortical interneurons predict their physiological subtype. Neuron 48:591-604.

Cajal SR (1909) Histology Due Systeme Nerveux de Homme et des Vertebrates. Maloine.

Campbell FW, Cleland BG, Cooper GF, Enroth-Cugell C (1968) The angular selectivity of visual cortical cells to moving gratings. J Physiol 198:237-250.

Carandini M, Heeger DJ (1994) Summation and division by neurons in primate visual cortex. Science 264:1333-1336.

Carandini M, Ferster D (2000) Membrane potential and firing rate in cat primary visual cortex. J Neurosci 20:470-484.

Cardin JA, Carlen M, Meletis K, Knoblich U, Zhang F, Deisseroth K, Tsai LH, Moore CI (2009) Driving fast-spiking cells induces gamma rhythm and controls sensory responses. Nature 459:663-667.

Cardin JA, Carlen M, Meletis K, Knoblich U, Zhang F, Deisseroth K, Tsai LH, Moore CI (2010) Targeted optogenetic stimulation and recording of neurons in vivo using cell-type-specific expression of Channelrhodopsin-2. Nat Protoc 5:247-254.

Cauli B, Porter JT, Tsuzuki K, Lambolez B, Rossier J, Quenet B, Audinat E (2000) Classification of fusiform neocortical interneurons based on unsupervised clustering. Proc Natl Acad Sci U S A 97:6144-6149.

Cauli B, Audinat E, Lambolez B, Angulo MC, Ropert N, Tsuzuki K, Hestrin S, Rossier J (1997) Molecular and physiological diversity of cortical nonpyramidal cells. J Neurosci 17:3894-3906.

Cauller LJ, Clancy B, Connors BW (1998) Backward cortical projections to primary somatosensory cortex in rats extend long horizontal axons in layer I. J Comp Neurol 390:297-310.

Cavazzini M, Bliss T, Emptage N (2005) Ca2+ and synaptic plasticity. Cell Calcium 38:355-367.

Chalupa LM, Werner JS (2004) The visual neurosciences. MIT Press.

Chalupa LM, Williams RW (2008) Eye, retina, and visual system of the mouse. MIT Press.

Chattopadhyaya B, Di Cristo G, Higashiyama H, Knott GW, Kuhlman SJ, Welker E, Huang ZJ (2004) Experience and activity-dependent maturation of perisomatic GABAergic innervation in primary visual cortex during a postnatal critical period. J Neurosci 24:9598-9611.

Chen X, Leischner U, Rochefort NL, Nelken I, Konnerth A (2011) Functional mapping of single spines in cortical neurons in vivo. Nature 475:501-505.

Chow A, Erisir A, Farb C, Nadal MS, Ozaita A, Lau D, Welker E, Rudy B (1999) K(+) channel expression distinguishes subpopulations of parvalbumin- and somatostatin-containing neocortical interneurons. J Neurosci 19:9332-9345.

Chow BY, Han X, Dobry AS, Qian X, Chuong AS, Li M, Henninger MA, Belfort GM, Lin Y, Monahan PE, Boyden ES (2010) High-performance genetically targetable optical neural silencing by light-driven proton pumps. Nature 463:98-102.

Chu Z, Galarreta M, Hestrin S (2003) Synaptic interactions of late-spiking neocortical neurons in layer 1. J Neurosci 23:96-102.

Connors BW, Gutnick MJ (1990) Intrinsic firing patterns of diverse neocortical neurons. Trends Neurosci 13:99-104.

Coogan TA, Burkhalter A (1990) Conserved patterns of cortico-cortical connections define areal hierarchy in rat visual cortex. Exp Brain Res 80:49-53.

Corbetta M, Shulman GL (2002) Control of goal-directed and stimulus-driven attention in the brain. Nat Rev Neurosci 3:201-215.

DeFelipe J (1999) Chandelier cells and epilepsy. Brain 122 (Pt 10):1807-1822.

DeFelipe J (2002) Cortical interneurons: from Cajal to 2001. Prog Brain Res 136:215-238.

DeFelipe J, Hendry SH, Jones EG (1989) Visualization of chandelier cell axons by parvalbumin immunoreactivity in monkey cerebral cortex. Proc Natl Acad Sci U S A 86:2093-2097.

DeFelipe J, Hendry SH, Hashikawa T, Molinari M, Jones EG (1990) A microcolumnar structure of monkey cerebral cortex revealed by immunocytochemical studies of double bouquet cell axons. Neuroscience 37:655-673.

Defelipe J et al. (2013) New insights into the classification and nomenclature of cortical GABAergic interneurons. Nat Rev Neurosci 14:202-216.

Demeulemeester H, Vandesande F, Orban GA, Heizmann CW, Pochet R (1989) Calbindin D-28K and parvalbumin immunoreactivity is confined to two separate neuronal subpopulations in the cat visual cortex, whereas partial coexistence is shown in the dorsal lateral geniculate nucleus. Neurosci Lett 99:6-11.

Denk W, Strickler JH, Webb WW (1990) Two-photon laser scanning fluorescence microscopy. Science 248:73-76.

Douglas RJ, Martin KA (2004) Neuronal circuits of the neocortex. Annu Rev Neurosci 27:419-451.

Douglas RJ, Martin KA, Whitteridge D (1988) Selective responses of visual cortical cells do not depend on shunting inhibition. Nature 332:642-644.

Doyle DA, Morais Cabral J, Pfuetzner RA, Kuo A, Gulbis JM, Cohen SL, Chait BT, MacKinnon R (1998) The structure of the potassium channel: molecular basis of K+ conduction and selectivity. Science 280:69-77.

Drager UC (1975) Receptive fields of single cells and topography in mouse visual cortex. J Comp Neurol 160:269-290.

Drager UC (1978) Observations on monocular deprivation in mice. J Neurophysiol 41:28-42.

Dreifuss JJ, Kelly JS, Krnjevic K (1969) Cortical inhibition and gamma-aminobutyric acid. Exp Brain Res 9:137-154.

Erisir A, Lau D, Rudy B, Leonard CS (1999) Function of specific K(+) channels in sustained high-frequency firing of fast-spiking neocortical interneurons. J Neurophysiol 82:2476-2489.

Fairen A (2007) Cajal and Lorente de No on cortical interneurons: coincidences and progress. Brain Res Rev 55:430-444.

Fanselow EE, Richardson KA, Connors BW (2008) Selective, state-dependent activation of somatostatin-expressing inhibitory interneurons in mouse neocortex. J Neurophysiol 100:2640-2652.

Felleman DJ, Van Essen DC (1991) Distributed hierarchical processing in the primate cerebral cortex. Cereb Cortex 1:1-47.

Ferster D (1988) Spatially opponent excitation and inhibition in simple cells of the cat visual cortex. J Neurosci 8:1172-1180.

Finn IM, Priebe NJ, Ferster D (2007) The emergence of contrast-invariant orientation tuning in simple cells of cat visual cortex. Neuron 54:137-152.

Fino E, Yuste R (2011) Dense inhibitory connectivity in neocortex. Neuron 69:1188-1203.

Foldy C, Dyhrfjeld-Johnsen J, Soltesz I (2005) Structure of cortical microcircuit theory. J Physiol 562:47-54.

Franks NP, Lieb WR (1994) Molecular and cellular mechanisms of general anaesthesia. Nature 367:607-614.

Freund TF, Katona I (2007) Perisomatic inhibition. Neuron 56:33-42.

Gentet LJ, Avermann M, Matyas F, Staiger JF, Petersen CC (2010) Membrane potential dynamics of GABAergic neurons in the barrel cortex of behaving mice. Neuron 65:422-435.

Gentet LJ, Kremer Y, Taniguchi H, Huang ZJ, Staiger JF, Petersen CC (2012) Unique functional properties of somatostatin-expressing GABAergic neurons in mouse barrel cortex. Nat Neurosci 15:607-612.

Gibson JR, Beierlein M, Connors BW (1999) Two networks of electrically coupled inhibitory neurons in neocortex. Nature 402:75-79.

Gidon A, Segev I (2012) Principles governing the operation of synaptic inhibition in dendrites. Neuron 75:330-341.

Gonchar Y, Wang Q, Burkhalter A (2007) Multiple distinct subtypes of GABAergic neurons in mouse visual cortex identified by triple immunostaining. Front Neuroanat 1:3.

Gordon JA, Stryker MP (1996) Experience-dependent plasticity of binocular responses in the primary visual cortex of the mouse. J Neurosci 16:3274-3286.

Gradinaru V, Thompson KR, Deisseroth K (2008) eNpHR: a Natronomonas halorhodopsin enhanced for optogenetic applications. Brain Cell Biol 36:129-139.

Guerra L, McGarry LM, Robles V, Bielza C, Larranaga P, Yuste R (2011) Comparison between supervised and unsupervised classifications of neuronal cell types: a case study. Dev Neurobiol 71:71-82.

Gunaydin LA, Yizhar O, Berndt A, Sohal VS, Deisseroth K, Hegemann P (2010) Ultrafast optogenetic control. Nat Neurosci 13:387-392.

Haider B, McCormick DA (2009) Rapid neocortical dynamics: cellular and network mechanisms. Neuron 62:171-189.

Haider B, Hausser M, Carandini M (2013) Inhibition dominates sensory responses in the awake cortex. Nature 493:97-100.

Hao J, Wang XD, Dan Y, Poo MM, Zhang XH (2009) An arithmetic rule for spatial summation of excitatory and inhibitory inputs in pyramidal neurons. Proc Natl Acad Sci U S A 106:21906-21911.

Hausser M, Smith SL (2007) Neuroscience: controlling neural circuits with light. Nature 446:617-619.

Hausser M, Spruston N, Stuart GJ (2000) Diversity and dynamics of dendritic signaling. Science 290:739-744.

Helmchen F, Svoboda K, Denk W, Tank DW (1999) In vivo dendritic calcium dynamics in deep-layer cortical pyramidal neurons. Nat Neurosci 2:989-996.

Hendry SH, Jones EG, Emson PC (1984a) Morphology, distribution, and synaptic relations of somatostatin- and neuropeptide Y-immunoreactive neurons in rat and monkey neocortex. J Neurosci 4:2497-2517.

Hendry SH, Jones EG, DeFelipe J, Schmechel D, Brandon C, Emson PC (1984b) Neuropeptide-containing neurons of the cerebral cortex are also GABAergic. Proc Natl Acad Sci U S A 81:6526-6530.

Hestrin S, Armstrong WE (1996) Morphology and physiology of cortical neurons in layer I. J Neurosci 16:5290-5300.

Hioki H, Okamoto S, Konno M, Kameda H, Sohn J, Kuramoto E, Fujiyama F, Kaneko T (2013) Cell type-specific inhibitory inputs to dendritic and somatic compartments of parvalbumin-expressing neocortical interneuron. J Neurosci 33:544-555.

Hirsch JA, Alonso JM, Reid RC (1995) Visually evoked calcium action potentials in cat striate cortex. Nature 378:612-616.

Hirsch JA, Martinez LM, Pillai C, Alonso JM, Wang Q, Sommer FT (2003) Functionally distinct inhibitory neurons at the first stage of visual cortical processing. Nat Neurosci 6:1300-1308.

Hofer SB, Ko H, Pichler B, Vogelstein J, Ros H, Zeng H, Lein E, Lesica NA, Mrsic-Flogel TD (2011) Differential connectivity and response dynamics of excitatory and inhibitory neurons in visual cortex. Nat Neurosci 14:1045-1052.

Houser CR, Vaughn JE, Hendry SH, Jones EG, Peters A (1984) Cerebral Cortex: Functional Properties of Cortical Cells. Plenum:63-90.

Houweling AR, Brecht M (2008) Behavioural report of single neuron stimulation in somatosensory cortex. Nature 451:65-68.

Hubel DH (1982) Cortical neurobiology: a slanted historical perspective. Annu Rev Neurosci 5:363-370.

Hubel DH, Wiesel TN (1959) Receptive fields of single neurones in the cat's striate cortex. J Physiol 148:574-591.

Hubel DH, Wiesel TN (1962) Receptive fields, binocular interaction and functional architecture in the cat's visual cortex. J Physiol 160:106-154.

Hubel DH, Wiesel TN (1974a) Uniformity of monkey striate cortex: a parallel relationship between field size, scatter, and magnification factor. J Comp Neurol 158:295-305.

Hubel DH, Wiesel TN (1974b) Sequence regularity and geometry of orientation columns in the monkey striate cortex. J Comp Neurol 158:267-293.

Hubener M (2003) Mouse visual cortex. Curr Opin Neurobiol 13:413-420.

Ivanova E, Pan ZH (2009) Evaluation of the adeno-associated virus mediated long-term expression of channelrhodopsin-2 in the mouse retina. Mol Vis 15:1680-1689.

Jackson L (2013a) http://jaxmice.jax.org/findmice/popular.html. Background Lines.

Jackson L (2013b) http://jaxmice.jax.org/list/rax13.html.

Jiang X, Wang G, Lee AJ, Stornetta RL, Zhu JJ (2013) The organization of two new cortical interneuronal circuits. Nat Neurosci 16:210-218.

Jones EG (1984) Cerebral Cortex. Plenum.

Judkewitz B, Rizzi M, Kitamura K, Hausser M (2009) Targeted single-cell electroporation of mammalian neurons in vivo. Nat Protoc 4:862-869.

Kaas JH (2011) Neocortex in early mammals and its subsequent variations. Ann N Y Acad Sci 1225:28-36.

Kameda H, Hioki H, Tanaka YH, Tanaka T, Sohn J, Sonomura T, Furuta T, Fujiyama F, Kaneko T (2012) Parvalbumin-producing cortical interneurons receive inhibitory inputs on proximal portions and cortical excitatory inputs on distal dendrites. Eur J Neurosci 35:838-854.

Kampa BM, Letzkus JJ, Stuart GJ (2006) Cortical feed-forward networks for binding different streams of sensory information. Nat Neurosci 9:1472-1473.

Kanemoto Y, Matsuzaki M, Morita S, Hayama T, Noguchi J, Senda N, Momotake A, Arai T, Kasai H (2011) Spatial distributions of GABA receptors and local inhibition of Ca^{2+} transients studied with GABA uncaging in the dendrites of CA1 pyramidal neurons. PLoS One 6:e22652.

Kapfer C, Glickfeld LL, Atallah BV, Scanziani M (2007) Supralinear increase of recurrent inhibition during sparse activity in the somatosensory cortex. Nat Neurosci 10:743-753.

Kawaguchi Y (1993) Groupings of nonpyramidal and pyramidal cells with specific physiological and morphological characteristics in rat frontal cortex. J Neurophysiol 69:416-431.

Kawaguchi Y, Kubota Y (1993) Correlation of physiological subgroupings of nonpyramidal cells with parvalbumin- and calbindinD28k-immunoreactive neurons in layer V of rat frontal cortex. J Neurophysiol 70:387-396.

Kawaguchi Y, Kubota Y (1996) Physiological and morphological identification of somatostatin- or vasoactive intestinal polypeptide-containing cells among GABAergic cell subtypes in rat frontal cortex. J Neurosci 16:2701-2715.

Kawaguchi Y, Kubota Y (1997) GABAergic cell subtypes and their synaptic connections in rat frontal cortex. Cereb Cortex 7:476-486.

Kawaguchi Y, Kubota Y (1998) Neurochemical features and synaptic connections of large physiologically-identified GABAergic cells in the rat frontal cortex. Neuroscience 85:677-701.

Keller GB, Bonhoeffer T, Hubener M (2012) Sensorimotor mismatch signals in primary visual cortex of the behaving mouse. Neuron 74:809-815.

Kerlin AM, Andermann ML, Berezovskii VK, Reid RC (2010) Broadly tuned response properties of diverse inhibitory neuron subtypes in mouse visual cortex. Neuron 67:858-871.

Khawaled R, Bruening-Wright A, Adelman JP, Maylie J (1999) Bicuculline block of small-conductance calcium-activated potassium channels. Pflugers Arch 438:314-321.

Kim HG, Beierlein M, Connors BW (1995) Inhibitory control of excitable dendrites in neocortex. J Neurophysiol 74:1810-1814.

Kisvarday ZF, Martin KA, Whitteridge D, Somogyi P (1985) Synaptic connections of intracellularly filled clutch cells: a type of small basket cell in the visual cortex of the cat. J Comp Neurol 241:111-137.

Kitamura K, Judkewitz B, Kano M, Denk W, Hausser M (2008) Targeted patch-clamp recordings and single-cell electroporation of unlabeled neurons in vivo. Nat Methods 5:61-67.

Klausberger T (2009) GABAergic interneurons targeting dendrites of pyramidal cells in the CA1 area of the hippocampus. Eur J Neurosci 30:947-957.

Klausberger T, Magill PJ, Marton LF, Roberts JD, Cobden PM, Buzsaki G, Somogyi P (2003) Brain-state- and cell-type-specific firing of hippocampal interneurons in vivo. Nature 421:844-848.

Ko H, Hofer SB, Pichler B, Buchanan KA, Sjostrom PJ, Mrsic-Flogel TD (2011) Functional specificity of local synaptic connections in neocortical networks. Nature 473:87-91.

Koch C, Poggio T, Torre V (1983) Nonlinear interactions in a dendritic tree: localization, timing, and role in information processing. Proc Natl Acad Sci U S A 80:2799-2802.

Krook-Magnuson E, Varga C, Lee SH, Soltesz I (2011) New dimensions of interneuronal specialization unmasked by principal cell heterogeneity. Trends Neurosci 35:175-184.

Kubota Y, Hattori R, Yui Y (1994) Three distinct subpopulations of GABAergic neurons in rat frontal agranular cortex. Brain Res 649:159-173.

Kuhlman SJ, Huang ZJ (2008) High-resolution labeling and functional manipulation of specific neuron types in mouse brain by Cre-activated viral gene expression. PLoS One 3:e2005.

Kuhlman SJ, Tring E, Trachtenberg JT (2011) Fast-spiking interneurons have an initial orientation bias that is lost with vision. Nat Neurosci 14:1121-1123.

Kwan AC, Dan Y (2012) Dissection of cortical microcircuits by single-neuron stimulation in vivo. Curr Biol 22:1459-1467.

Larkum ME, Zhu JJ (2002) Signaling of layer 1 and whisker-evoked Ca^{2+} and Na^{+} action potentials in distal and terminal dendrites of rat neocortical pyramidal neurons in vitro and in vivo. J Neurosci 22:6991-7005.

Larkum ME, Zhu JJ, Sakmann B (1999) A new cellular mechanism for coupling inputs arriving at different cortical layers. Nature 398:338-341.

Larkum ME, Nevian T, Sandler M, Polsky A, Schiller J (2009) Synaptic integration in tuft dendrites of layer 5 pyramidal neurons: a new unifying principle. Science 325:756-760.

Le Be JV, Silberberg G, Wang Y, Markram H (2007) Morphological, electrophysiological, and synaptic properties of corticocallosal pyramidal cells in the neonatal rat neocortex. Cereb Cortex 17:2204-2213.

Ledergerber D, Larkum ME (2010) Properties of layer 6 pyramidal neuron apical dendrites. J Neurosci 30:13031-13044.

Lee SH, Kwan AC, Zhang S, Phoumthipphavong V, Flannery JG, Masmanidis SC, Taniguchi H, Huang ZJ, Zhang F, Boyden ES, Deisseroth K, Dan Y (2012) Activation of specific interneurons improves V1 feature selectivity and visual perception. Nature 488:379-383.

Letzkus JJ, Wolff SB, Meyer EM, Tovote P, Courtin J, Herry C, Luthi A (2011) A disinhibitory microcircuit for associative fear learning in the auditory cortex. Nature 480:331-335.

Li CY, Poo MM, Dan Y (2009) Burst spiking of a single cortical neuron modifies global brain state. Science 324:643-646.

Li Y, Lu H, Cheng PL, Ge S, Xu H, Shi SH, Dan Y (2012) Clonally related visual cortical neurons show similar stimulus feature selectivity. Nature 486:118-121.

Lin JY, Lin MZ, Steinbach P, Tsien RY (2009) Characterization of engineered channelrhodopsin variants with improved properties and kinetics. Biophys J 96:1803-1814.

Liu BH, Li P, Li YT, Sun YJ, Yanagawa Y, Obata K, Zhang LI, Tao HW (2009) Visual receptive field structure of cortical inhibitory neurons revealed by two-photon imaging guided recording. J Neurosci 29:10520-10532.

Liu G (2004) Local structural balance and functional interaction of excitatory and inhibitory synapses in hippocampal dendrites. Nat Neurosci 7:373-379.

Llinas RR (1988) The intrinsic electrophysiological properties of mammalian neurons: insights into central nervous system function. Science 242:1654-1664.

London M, Schreibman A, Hausser M, Larkum ME, Segev I (2002) The information efficacy of a synapse. Nat Neurosci 5:332-340.

Lopez-Bendito G, Sturgess K, Erdelyi F, Szabo G, Molnar Z, Paulsen O (2004) Preferential origin and layer destination of GAD65-GFP cortical interneurons. Cereb Cortex 14:1122-1133.

Lovett-Barron M, Turi GF, Kaifosh P, Lee PH, Bolze F, Sun XH, Nicoud JF, Zemelman BV, Sternson SM, Losonczy A (2012) Regulation of neuronal input transformations by tunable dendritic inhibition. Nat Neurosci 15:423-430, S421-423.

Luo L, Callaway EM, Svoboda K (2008) Genetic dissection of neural circuits. Neuron 57:634-660.

Ma WP, Liu BH, Li YT, Huang ZJ, Zhang LI, Tao HW (2010) Visual representations by cortical somatostatin inhibitory neurons--selective but with weak and delayed responses. J Neurosci 30:14371-14379.

Ma Y, Hu H, Berrebi AS, Mathers PH, Agmon A (2006) Distinct subtypes of somatostatin-containing neocortical interneurons revealed in transgenic mice. J Neurosci 26:5069-5082.

Maccaferri G, Lacaille JC (2003) Interneuron Diversity series: Hippocampal interneuron classifications--making things as simple as possible, not simpler. Trends Neurosci 26:564-571.

Macdonald RL, Olsen RW (1994) GABAA receptor channels. Annu Rev Neurosci 17:569-602.

Madisen L et al. (2012) A toolbox of Cre-dependent optogenetic transgenic mice for light-induced activation and silencing. Nat Neurosci 15:793-802.

Maess B, Koelsch S, Gunter TC, Friederici AD (2001) Musical syntax is processed in Broca's area: an MEG study. Nat Neurosci 4:540-545.

Magee JC (1998) Dendritic hyperpolarization-activated currents modify the integrative properties of hippocampal CA1 pyramidal neurons. J Neurosci 18:7613-7624.

Mangini NJ, Pearlman AL (1980) Laminar distribution of receptive field properties in the primary visual cortex of the mouse. J Comp Neurol 193:203-222.

Marin-Padilla M (1969) Origin of the pericellular baskets of the pyramidal cells of the human motor cortex: a Golgi study. Brain Res 14:633-646.

Markof J (2013) Obama seeking to boost study of human brain. The New York Times.

Markram H (2006) The blue brain project. Nat Rev Neurosci 7:153-160.

Markram H, Wang Y, Tsodyks M (1998) Differential signaling via the same axon of neocortical pyramidal neurons. Proc Natl Acad Sci U S A 95:5323-5328.

Markram H, Toledo-Rodriguez M, Wang Y, Gupta A, Silberberg G, Wu C (2004) Interneurons of the neocortical inhibitory system. Nat Rev Neurosci 5:793-807.

Martina M, Schultz JH, Ehmke H, Monyer H, Jonas P (1998) Functional and molecular differences between voltage-gated K+ channels of fast-spiking interneurons and pyramidal neurons of rat hippocampus. J Neurosci 18:8111-8125.

McBain CJ, Fisahn A (2001) Interneurons unbound. Nat Rev Neurosci 2:11-23.

McCormick DA, Connors BW, Lighthall JW, Prince DA (1985) Comparative electrophysiology of pyramidal and sparsely spiny stellate neurons of the neocortex. J Neurophysiol 54:782-806.

McGarry LM, Packer AM, Fino E, Nikolenko V, Sippy T, Yuste R (2010) Quantitative classification of somatostatin-positive neocortical interneurons identifies three interneuron subtypes. Front Neural Circuits 4:12.

Mechler F, Ringach DL (2002) On the classification of simple and complex cells. Vision Res 42:1017-1033.

Mehaffey WH, Doiron B, Maler L, Turner RW (2005) Deterministic multiplicative gain control with active dendrites. J Neurosci 25:9968-9977.

Meinecke DL, Peters A (1986) Somatostatin immunoreactive neurons in rat visual cortex: a light and electron microscopic study. J Neurocytol 15:121-136.

Meliza CD, Dan Y (2006) Receptive-field modification in rat visual cortex induced by paired visual stimulation and single-cell spiking. Neuron 49:183-189.

Menendez de la Prida L, Trevelyan AJ (2011) Cellular mechanisms of high frequency oscillations in epilepsy: on the diverse sources of pathological activities. Epilepsy Res 97:308-317.

Metin C, Godement P, Imbert M (1988) The primary visual cortex in the mouse: receptive field properties and functional organization. Exp Brain Res 69:594-612.

Meyer AH, Katona I, Blatow M, Rozov A, Monyer H (2002) In vivo labeling of parvalbumin-positive interneurons and analysis of electrical coupling in identified neurons. J Neurosci 22:7055-7064.

Molnar Z, Cheung AF (2006) Towards the classification of subpopulations of layer V pyramidal projection neurons. Neurosci Res 55:105-115.

Monyer H, Markram H (2004) Interneuron Diversity series: Molecular and genetic tools to study GABAergic interneuron diversity and function. Trends Neurosci 27:90-97.

Monyer H, Sprengel R, Schoepfer R, Herb A, Higuchi M, Lomeli H, Burnashev N, Sakmann B, Seeburg PH (1992) Heteromeric NMDA receptors: molecular and functional distinction of subtypes. Science 256:1217-1221.

Morishima M, Kawaguchi Y (2006) Recurrent connection patterns of corticostriatal pyramidal cells in frontal cortex. J Neurosci 26:4394-4405.

Morishima M, Morita K, Kubota Y, Kawaguchi Y (2011) Highly differentiated projection-specific cortical subnetworks. J Neurosci 31:10380-10391.

Morrison JH, Magistretti PJ, Benoit R, Bloom FE (1984) The distribution and morphological characteristics of the intracortical VIP-positive cell: an immunohistochemical analysis. Brain Res 292:269-282.

Mrsic-Flogel TD, Hofer SB, Ohki K, Reid RC, Bonhoeffer T, Hubener M (2007) Homeostatic regulation of eye-specific responses in visual cortex during ocular dominance plasticity. Neuron 54:961-972.

Murayama M, Perez-Garci E, Nevian T, Bock T, Senn W, Larkum ME (2009) Dendritic encoding of sensory stimuli controlled by deep cortical interneurons. Nature 457:1137-1141.

Nagel G, Szellas T, Huhn W, Kateriya S, Adeishvili N, Berthold P, Ollig D, Hegemann P, Bamberg E (2003) Channelrhodopsin-2, a directly light-gated cation-selective membrane channel. Proc Natl Acad Sci U S A 100:13940-13945.

Naik SR, Guidotti A, Costa E (1976) Central GABA receptor agonists: comparison of muscimol and baclofen. Neuropharmacology 15:479-484.

Nelson S, Toth L, Sheth B, Sur M (1994) Orientation selectivity of cortical neurons during intracellular blockade of inhibition. Science 265:774-777.

Nelson SB, Sugino K, Hempel CM (2006) The problem of neuronal cell types: a physiological genomics approach. Trends Neurosci 29:339-345.

Niell CM, Stryker MP (2008) Highly selective receptive fields in mouse visual cortex. J Neurosci 28:7520-7536.

Niell CM, Stryker MP (2010) Modulation of visual responses by behavioral state in mouse visual cortex. Neuron 65:472-479.

No LD (1938) Cerebral cortex: architecture, intracortical connections, motor projections. In: Fulton, JF (Ed), Physiology of Nervous System, 2nd edition Oxford University Press, :291–339.

Northcutt RG, Kaas JH (1995) The emergence and evolution of mammalian neocortex. Trends Neurosci 18:373-379.

Nowak LG, Sanchez-Vives MV, McCormick DA (2008) Lack of orientation and direction selectivity in a subgroup of fast-spiking inhibitory interneurons: cellular and synaptic mechanisms and comparison with other electrophysiological cell types. Cereb Cortex 18:1058-1078.

O'Keefe J, Recce ML (1993) Phase relationship between hippocampal place units and the EEG theta rhythm. Hippocampus 3:317-330.

Ohki K, Chung S, Ch'ng YH, Kara P, Reid RC (2005) Functional imaging with cellular resolution reveals precise micro-architecture in visual cortex. Nature 433:597-603.

Ohtsuki G, Nishiyama M, Yoshida T, Murakami T, Histed M, Lois C, Ohki K (2012) Similarity of visual selectivity among clonally related neurons in visual cortex. Neuron 75:65-72.

Olah S, Komlosi G, Szabadics J, Varga C, Toth E, Barzo P, Tamas G (2007) Output of neurogliaform cells to various neuron types in the human and rat cerebral cortex. Front Neural Circuits 1:4.

Oliva AA, Jr., Jiang M, Lam T, Smith KL, Swann JW (2000) Novel hippocampal interneuronal subtypes identified using transgenic mice that express green fluorescent protein in GABAergic interneurons. J Neurosci 20:3354-3368.

Otsuka T, Kawaguchi Y (2008) Firing-pattern-dependent specificity of cortical excitatory feed-forward subnetworks. J Neurosci 28:11186-11195.

Otsuka T, Kawaguchi Y (2011) Cell diversity and connection specificity between callosal projection neurons in the frontal cortex. J Neurosci 31:3862-3870.

Packer AM, Yuste R (2011) Dense, unspecific connectivity of neocortical parvalbumin-positive interneurons: a canonical microcircuit for inhibition? J Neurosci 31:13260-13271.

Palmer L, Murayama M, Larkum M (2012a) Inhibitory Regulation of Dendritic Activity in vivo. Front Neural Circuits 6:26.

Palmer LM, Schulz JM, Murphy SC, Ledergerber D, Murayama M, Larkum ME (2012b) The cellular basis of GABA(B)-mediated interhemispheric inhibition. Science 335:989-993.

Parra P, Gulyas AI, Miles R (1998) How many subtypes of inhibitory cells in the hippocampus? Neuron 20:983-993.

Penfield WBE (1937) Somatic motor and sensory representation in the cerebral cortex of man as studied by electrical stimulation. Brain 60:389-443.

Perez-Garci E, Gassmann M, Bettler B, Larkum ME (2006) The GABAB1b isoform mediates long-lasting inhibition of dendritic Ca^{2+} spikes in layer 5 somatosensory pyramidal neurons. Neuron 50:603-616.

Peters A (1984) Cellular Components of the Cerebral Cortex (eds Peters, A. & Jones, E. G.). Plenum:381–408.

Petreanu L, Mao T, Sternson SM, Svoboda K (2009) The subcellular organization of neocortical excitatory connections. Nature 457:1142-1145.

Pettit DL, Wang SS, Gee KR, Augustine GJ (1997) Chemical two-photon uncaging: a novel approach to mapping glutamate receptors. Neuron 19:465-471.

Porter JT, Cauli B, Staiger JF, Lambolez B, Rossier J, Audinat E (1998) Properties of bipolar VIPergic interneurons and their excitation by pyramidal neurons in the rat neocortex. Eur J Neurosci 10:3617-3628.

Potez S, Larkum ME (2008) Effect of common anesthetics on dendritic properties in layer 5 neocortical pyramidal neurons. J Neurophysiol 99:1461-1477.

Poulet JF, Petersen CC (2008) Internal brain state regulates membrane potential synchrony in barrel cortex of behaving mice. Nature 454:881-885.

Priebe NJ, Ferster D (2008) Inhibition, spike threshold, and stimulus selectivity in primary visual cortex. Neuron 57:482-497.

Priebe NJ, Ferster D (2012) Mechanisms of neuronal computation in mammalian visual cortex. Neuron 75:194-208.

Reyes A, Lujan R, Rozov A, Burnashev N, Somogyi P, Sakmann B (1998) Target-cell-specific facilitation and depression in neocortical circuits. Nat Neurosci 1:279-285.

Rochefort NL, Narushima M, Grienberger C, Marandi N, Hill DN, Konnerth A (2011) Development of direction selectivity in mouse cortical neurons. Neuron 71:425-432.

Rockland KS, Pandya DN (1979) Laminar origins and terminations of cortical connections of the occipital lobe in the rhesus monkey. Brain Res 179:3-20.

Rogers JH, Resibois A (1992) Calretinin and calbindin-D28k in rat brain: patterns of partial co-localization. Neuroscience 51:843-865.

Rudy B, McBain CJ (2001) Kv3 channels: voltage-gated K+ channels designed for high-frequency repetitive firing. Trends Neurosci 24:517-526.

Rudy B, Fishell G, Lee S, Hjerling-Leffler J (2011) Three groups of interneurons account for nearly 100% of neocortical GABAergic neurons. Dev Neurobiol 71:45-61.

Runyan CA, Schummers J, Van Wart A, Kuhlman SJ, Wilson NR, Huang ZJ, Sur M (2010) Response features of parvalbumin-expressing interneurons suggest precise roles for subtypes of inhibition in visual cortex. Neuron 67:847-857.

Sato TR, Svoboda K (2010) The functional properties of barrel cortex neurons projecting to the primary motor cortex. J Neurosci 30:4256-4260.

Sauer B (1998) Inducible gene targeting in mice using the Cre/lox system. Methods 14:381-392.

Schultheis C, Liewald JF, Bamberg E, Nagel G, Gottschalk A (2011) Optogenetic long-term manipulation of behavior and animal development. PLoS One 6:e18766.

Scientifica (2013) http://www.scientifica.uk.com/products/multiphoton-technology?dm_i=7B7,1B14B,Q723W,4FB8Y,1. Deep imaging technology down to 900 um.

Shcherbo D, Merzlyak EM, Chepurnykh TV, Fradkov AF, Ermakova GV, Solovieva EA, Lukyanov KA, Bogdanova EA, Zaraisky AG, Lukyanov S, Chudakov DM (2007) Bright far-red fluorescent protein for whole-body imaging. Nat Methods 4:741-746.

Shipp S (2007) Structure and function of the cerebral cortex. Curr Biol 17:R443-449.

Silberberg G (2008) Polysynaptic subcircuits in the neocortex: spatial and temporal diversity. Curr Opin Neurobiol 18:332-337.

Silberberg G, Markram H (2007) Disynaptic inhibition between neocortical pyramidal cells mediated by Martinotti cells. Neuron 53:735-746.

Silberberg G, Gupta A, Markram H (2002) Stereotypy in neocortical microcircuits. Trends Neurosci 25:227-230.

Sillito AM (1975) The contribution of inhibitory mechanisms to the receptive field properties of neurones in the striate cortex of the cat. J Physiol 250:305-329.

Skottun BC, De Valois RL, Grosof DH, Movshon JA, Albrecht DG, Bonds AB (1991) Classifying simple and complex cells on the basis of response modulation. Vision Res 31:1079-1086.

Smith SL, Hausser M (2010) Parallel processing of visual space by neighboring neurons in mouse visual cortex. Nat Neurosci 13:1144-1149.

Snider RS, Stowell A (1944) Receiving areas of the tactile, auditory, and visual systems in the cerebellum. Journal of Neurophysiology 7:331-357.

Sohal VS, Zhang F, Yizhar O, Deisseroth K (2009) Parvalbumin neurons and gamma rhythms enhance cortical circuit performance. Nature 459:698-702.

Sohya K, Kameyama K, Yanagawa Y, Obata K, Tsumoto T (2007) GABAergic neurons are less selective to stimulus orientation than excitatory neurons in layer II/III of visual cortex, as revealed by in vivo functional Ca2+ imaging in transgenic mice. J Neurosci 27:2145-2149.

Somogyi P (1977) A specific 'axo-axonal' interneuron in the visual cortex of the rat. Brain Res 136:345-350.

Somogyi P, Cowey A (1981) Combined Golgi and electron microscopic study on the synapses formed by double bouquet cells in the visual cortex of the cat and monkey. J Comp Neurol 195:547-566.

Somogyi P, Cowey A (1984) Cellular Components of the Cerebral Cortex (eds Peters, A. & Jones, E. G.). Plenum:337–360.

Somogyi P, Tamas G, Lujan R, Buhl EH (1998) Salient features of synaptic organisation in the cerebral cortex. Brain Res Brain Res Rev 26:113-135.

Stosiek C, Garaschuk O, Holthoff K, Konnerth A (2003) In vivo two-photon calcium imaging of neuronal networks. Proc Natl Acad Sci U S A 100:7319-7324.

Stuart G, Spruston N (1998) Determinants of voltage attenuation in neocortical pyramidal neuron dendrites. J Neurosci 18:3501-3510.

Svoboda K, Helmchen F, Denk W, Tank DW (1999) Spread of dendritic excitation in layer 2/3 pyramidal neurons in rat barrel cortex in vivo. Nat Neurosci 2:65-73.

Swadlow HA (1988) Efferent neurons and suspected interneurons in binocular visual cortex of the awake rabbit: receptive fields and binocular properties. J Neurophysiol 59:1162-1187.

Tabata H, Nakajima K (2001) Efficient in utero gene transfer system to the developing mouse brain using electroporation: visualization of neuronal migration in the developing cortex. Neuroscience 103:865-872.

Tamamaki N, Yanagawa Y, Tomioka R, Miyazaki J, Obata K, Kaneko T (2003) Green fluorescent protein expression and colocalization with calretinin, parvalbumin, and somatostatin in the GAD67-GFP knock-in mouse. J Comp Neurol 467:60-79.

Tamas G, Lorincz A, Simon A, Szabadics J (2003) Identified sources and targets of slow inhibition in the neocortex. Science 299:1902-1905.

Taniguchi H, He M, Wu P, Kim S, Paik R, Sugino K, Kvitsiani D, Fu Y, Lu J, Lin Y, Miyoshi G, Shima Y, Fishell G, Nelson SB, Huang ZJ (2011) A resource of Cre driver lines for genetic targeting of GABAergic neurons in cerebral cortex. Neuron 71:995-1013.

Thomson AM (1997) Neuroscience. More than just frequency detectors? Science 275:179-180.

Thomson AM, Deuchars J (1997) Synaptic interactions in neocortical local circuits: dual intracellular recordings in vitro. Cereb Cortex 7:510-522.

Thomson AM, Deuchars J, West DC (1993) Single axon excitatory postsynaptic potentials in neocortical interneurons exhibit pronounced paired pulse facilitation. Neuroscience 54:347-360.

Toledo-Rodriguez M, Gupta A, Wang Y, Wu CZ, Markram H (2003) The Handbook of Brain Theory and Neural Networks. MIT Press:719-725.

Toledo-Rodriguez M, Blumenfeld B, Wu C, Luo J, Attali B, Goodman P, Markram H (2004) Correlation maps allow neuronal electrical properties to be predicted from single-cell gene expression profiles in rat neocortex. Cereb Cortex 14:1310-1327.

Trevelyan AJ (2009) The direct relationship between inhibitory currents and local field potentials. J Neurosci 29:15299-15307.

Trevelyan AJ, Watkinson O (2005) Does inhibition balance excitation in neocortex? Prog Biophys Mol Biol 87:109-143.

Tsumoto T, Eckart W, Creutzfeldt OD (1979) Modification of orientation sensitivity of cat visual cortex neurons by removal of GABA-mediated inhibition. Exp Brain Res 34:351-363.

Varga Z, Jia H, Sakmann B, Konnerth A (2011) Dendritic coding of multiple sensory inputs in single cortical neurons in vivo. Proc Natl Acad Sci U S A 108:15420-15425.

Wahle P (1993) Differential regulation of substance P and somatostatin in Martinotti cells of the developing cat visual cortex. J Comp Neurol 329:519-538.

Wahlsten D, Rustay NR, Metten P, Crabbe JC (2003) In search of a better mouse test. Trends Neurosci 26:132-136.

Wang SS, Augustine GJ (1995) Confocal imaging and local photolysis of caged compounds: dual probes of synaptic function. Neuron 15:755-760.

Wang Y, Gupta A, Markram H (1999) Anatomical and functional differentiation of glutamatergic synaptic innervation in the neocortex. J Physiol Paris 93:305-317.

Wang Y, Gupta A, Toledo-Rodriguez M, Wu CZ, Markram H (2002) Anatomical, physiological, molecular and circuit properties of nest basket cells in the developing somatosensory cortex. Cereb Cortex 12:395-410.

Wang Y, Toledo-Rodriguez M, Gupta A, Wu C, Silberberg G, Luo J, Markram H (2004) Anatomical, physiological and molecular properties of Martinotti cells in the somatosensory cortex of the juvenile rat. J Physiol 561:65-90.

Waterston RH et al. (2002) Initial sequencing and comparative analysis of the mouse genome. Nature 420:520-562.

White EL (1989) Cortical Circuits. Synaptic Organization of the Cerebral Cortex. Birkhauser.

Wilson JR, Sherman SM (1976) Receptive-field characteristics of neurons in cat striate cortex: Changes with visual field eccentricity. J Neurophysiol 39:512-533.

Wilson NR, Runyan CA, Wang FL, Sur M (2012) Division and subtraction by distinct cortical inhibitory networks in vivo. Nature 488:343-348.

Xu H, Jeong HY, Tremblay R, Rudy B (2013) Neocortical somatostatin-expressing GABAergic interneurons disinhibit the thalamorecipient layer 4. Neuron 77:155-167.

Xu Q, Cobos I, De La Cruz E, Rubenstein JL, Anderson SA (2004) Origins of cortical interneuron subtypes. J Neurosci 24:2612-2622.

Xu X, Roby KD, Callaway EM (2010) Immunochemical characterization of inhibitory mouse cortical neurons: three chemically distinct classes of inhibitory cells. J Comp Neurol 518:389-404.

Yoshimura Y, Callaway EM (2005) Fine-scale specificity of cortical networks depends on inhibitory cell type and connectivity. Nat Neurosci 8:1552-1559.

Yu YC, Bultje RS, Wang X, Shi SH (2009) Specific synapses develop preferentially among sister excitatory neurons in the neocortex. Nature 458:501-504.

Yuste R (2005) Origin and classification of neocortical interneurons. Neuron 48:524-527.

Zhang F, Prigge M, Beyriere F, Tsunoda SP, Mattis J, Yizhar O, Hegemann P, Deisseroth K (2008) Red-shifted optogenetic excitation: a tool for fast neural control derived from Volvox carteri. Nat Neurosci 11:631-633.

Zhang F, Wang LP, Brauner M, Liewald JF, Kay K, Watzke N, Wood PG, Bamberg E, Nagel G, Gottschalk A, Deisseroth K (2007) Multimodal fast optical interrogation of neural circuitry. Nature 446:633-639.

Zhang ZW, Deschenes M (1998) Projections to layer VI of the posteromedial barrel field in the rat: a reappraisal of the role of corticothalamic pathways. Cereb Cortex 8:428-436.

Zhao S, Cunha C, Zhang F, Liu Q, Gloss B, Deisseroth K, Augustine GJ, Feng G (2008) Improved expression of halorhodopsin for light-induced silencing of neuronal activity. Brain Cell Biol 36:141-154.

Zhou FM, Hablitz JJ (1996) Morphological properties of intracellularly labeled layer I neurons in rat neocortex. J Comp Neurol 376:198-213.